

**DESIGN AND DEVELOPMENT OF ADAPTIVE THREE AXIS
POWER DIODE LASER CUTTER**

A PROJECT REPORT

Submitted by

SURYA PRAKASH S (RA1811018010020)

SHRIMAN RAGHAV S (RA1811018010044)

LOGESHWARAN G (RA1811018010045)

Under the guidance of

Mr. S. VASANTH M.E.

(Assistant Professor, Department of Mechatronics Engineering)

In Partial fulfilment for the degree

of

BACHELOR OF TECHNOLOGY

in

MECHATRONICS ENGINEERING

of

FACULTY OF ENGINEERING & TECHNOLOGY



SRM

INSTITUTE OF SCIENCE & TECHNOLOGY

(Deemed to be University u/s 3 of UGC Act, 1956)

S.R.M. Nagar, Kattankulathur, Kancheepuram District

May 2022

SRM INSTITUTE OF SCIENCE AND TECHNOLOGY

(Under Section 3 of UGC Act, 1956)

BONAFIDE CERTIFICATE

Certified that this project report titled "***DESIGN AND DEVELOPMENT OF ADAPTIVE THREE AXIS POWER DIODE LASER CUTTER***" is the bonafide work of "**SURYA PRAKASH S (RA1810018010020), SHRIMAN RAGHAV S (RA1811018010044)**, and **LOGESHWARAN G (RA 1811018010045)**", who carried out the project work under my supervision. Certified further, that to the best of my knowledge the work reported here in does not form any other project report or dissertation on the basis of which a degree or award was conferred on an earlier occasion on this or any other candidate.

SIGNATURE

Mr. S. VASANTH, M.E.,
PROJECT GUIDE,
Assistant Professor,
Dept. of Mechatronics Engineering.

SIGNATURE

Dr. G. MURALI, M.E., Ph.D.
PROFESSOR,
HEAD OF THE DEPARTMENT,
Dept. of Mechatronics Engineering.

Signature of Internal Examiner

Signature of External Examiner

ABSTRACT

Leather is one of the most essential commodities that has become quintessential to our everyday lives due to its usage in a wide range of items from shoes, wallets, designer bags in personal accessories sector to leather couches, seats in furniture and automotive sector. The contemporary population's need for leather and bespoke leather items necessitated the creation of a system with high production rate for quick manufacturing, cheap maintenance cost for small businesses, and adaptive controllability. Aside from conventional manual cutting, today's business offers cutting leather using non-conventional methods such as carbon dioxide (CO_2) laser and Nd:YAG laser machining, which practically matches the aforementioned specifications, but at a greater cost. These industrial methods outperform manual cutting in terms of production and efficiency. However, the significant quantity of carbonization, varied geometric errors, manual setup of input parameters, and high energy requirements make these procedures unsuitable for small-scale operations. The existing system's faults necessitate the use of Laser Beam Machining (LBM) with a laser diode by adopting self-tuned control to remove manual interference and by developing a well-organized user-interface for machining, this use of a laser-based diode overcomes the primary issue of increased economic value. As a result, the current thesis attempt is to design and fabricate a cost-effective three-axis laser-based diode leather machining system that will be effective in small-scale leather product companies. The fabricated three-axis laser diode machining system has wide range of Pulse width modulation control, self-adaptive Standoff distance (SOD) control, effective emission filters and Graphical user interface (GUI) implementation with touch display. Further experiments are conducted in cutting chrome + vegetable tanned cow leather since, cow leather is mostly used in almost all leather-related products. Analysis for **carbonization though machine vision, kerf width, Material removal rate (MRR), and emission rate** has been analysed and recorded to produce optimal input parameters.

Keywords: LBM, Leather, GUI, carbonization, kerf width, SOD, PWM, MMR.

ACKNOWLEDGEMENTS

It has been a great honour and privilege to undergo **B.Tech** in **MECHATRONICS** at **SRM Institute of Science and Technology**. We are very much thankful to the **Department of Mechatronics, SRM Institute of Science and Technology** for providing all facilities and support to meet our project requirements.

We would like to thank our Head of Department **Dr. G. MURALI, M.E., Ph.D.** and our project guide **Mr. S. VASANTH, M.E.** who gave us a big helping hand during the entire project. We'd also want to express our thanks to **Dr. MUTHURAMALINGAM T, M.E., Ph.D.** and **Dr. SANJEEV GUPTA, M.Tech., Ph.D.** of the Central Leather Research Institute (CLRI) for their invaluable assistance.

The success and final outcome of this project required a lot of guidance and assistance from many people and we are extremely fortunate that we have got this all along the completion of our project work. Whatever we have done is only due to such guidance and assistance and we would like to thank them for their kind support.

SURYA PRAKASH S

SHRIMAN RAGHAV S

LOGESHWARAN G

TABLE OF CONTENTS

CHAPTER NO.	TITLE	PAGE
	ABSTRACT	iii
	LIST OF TABLES	xi
	LIST OF FIGURES	xiii
	LIST OF EQUATIONS	xvi
	LIST OF ABBREVIATIONS	xvii
1	INTRODUCTION	1
	1.1 Laser Beam Machining and Mechanism	2
	1.2 Hierarchy Analysis	3
	1.3 Leather cutting using conventional & non-conventional methods	4
	1.4 Need for research	5
	1.5 Objectives	6
	1.6 Merits of Diode Laser Beam Machining	6
	1.7 Demerits of Diode Laser Beam Machining	6
	1.8 Applications of Diode Laser Beam Machining	6
	1.9 Organization of the thesis	7
2	LITERATURE SURVEY	8
	2.1 General	8
	2.2 Laser Cutting	8
	2.2.1 Laser cutting through water driven thermal separation mechanism	8
	2.2.2 Performance comparison between CO ₂ and diode laser on concrete cutting	8
	2.2.3 Oxygen assisted laser cutting of thick MS	8
	2.2.4 Laser cutting with elliptically polarized laser beams	9
	2.2.5 Picosecond laser machining	9
	2.2.6 Oxygen-assisted laser cutting	9
	2.2.7 Laser cutting of PMMA sheets	10
	2.2.8 Laser prepared cutting tools	10

CHAPTER NO.	TITLE	PAGE
	2.2.9 Distinguishing quality pulsed laser cutting	10
2.3	Leather	11
	2.3.1 High-value utilization of leather	11
	2.3.2 Trends and advancements in sustainable leather processing	11
2.4	Laser Diode	12
	2.4.1 Mastering cutting process through different types of lasers	12
	2.4.2 Different polarization techniques with Diode lasers	12
	2.4.3 Machinability of Titanium alloy	12
	2.4.4 Semiconductor laser diode arrays characteristics	13
	2.4.5 Transformation of surface on AISI 304 by power laser diode	13
	2.4.6 Possibilities of laser processing	13
	2.4.7 Laser diode arrays	14
	2.4.8 Laser cutting using sheets in pulsed mode	14
2.5	Output Parameters, Modelling & Optimization	14
	2.5.1 Kerf width deviation of micro-channel	14
	2.5.2 Effect on deviation in cut path	15
	2.5.3 Thickness validation of modelling tools	15
	2.5.4 Kerf width analysis and life cycle assessment of laser cutting process	15
	2.5.5 Multi-objective optimization of laser cutting	16
	2.5.6 Pulsed Nd: YAG laser cutting- Heat affected zone	16
3	MECHANICAL DESIGN	17
	3.1 CAD Model of Laser Beam Machining	17
	3.2 3D Printed CAD Models for LBM and Enclosure	18
	3.2.1 Limit switch holders	18
	3.2.2 VL6180X Time of flight sensor holder	19

CHAPTER NO.	TITLE	PAGE
3.2.3	Laser module holder	19
3.2.4	Enclosure exhaust grid and layer frames	20
3.2.5	BH1750 Lux sensor holder	20
3.3	Mechanical components	21
3.3.1	Aluminium work centre	22
3.3.2	Aluminium profile	22
3.3.3	Bakelite resin plates	23
3.3.4	Stainless steel guide rails	23
3.3.5	Lead screw and Round T-nuts	24
3.3.6	Hexagonal socket screws	24
3.3.7	Linear and Deep grove ball bearing bush	25
3.3.8	T-Nut and Nut seat	25
3.4	Experimental setup of LBM	26
3.5	LBM enclosure	26
3.5.1	Medium-density fibreboard (MDF)	27
3.5.2	Acrylic board	28
3.5.3	Sealer and Enamel paint	28
3.5.4	Emission control unit - ZWAS	28
3.6	Experimental setup of LBM enclosure	30
3.7	Iron sheets and Ferrite round magnets	31
3.8	Lead screw torque and efficiency	31
3.8.1	Efficiency of the lead screw	31
3.8.2	Torque required on the lead screws in X axis	32
3.8.3	Torque required on the lead screws in Y axis	33
3.8.4	Torque required on the lead screws in Z axis	33
3.9	Personal Protective Equipment (PPE)	34
3.9.1	Professional Laser Safety Goggles	34
3.9.2	Gloves	34
4	ELECTRONICS CONTROL UNIT	35
4.1	Block diagram	35
4.2	Electronic components	38

CHAPTER NO.	TITLE	PAGE
4.2.1 Raspberry Pi 4B	39	
4.2.2 Touch Screen	40	
4.2.3 Arduino MEGA microcontroller	40	
4.2.4 Arduino UNO R3 microcontroller	41	
4.2.5 ESP32 microcontroller	42	
4.2.6 NEJE Laser diode Module	43	
4.2.7 CNC control board	44	
4.2.8 NEMA-17 stepper Motor	45	
4.2.9 A4988 Stepper driver	46	
4.2.10 VL6180X Time of flight (tof) sensor	46	
4.2.11 GY30 BH1750 Lux meter sensor	47	
4.2.12 SCD30 CO ₂ Sensor	47	
4.2.13 Arbitrary Waveform Generator	48	
4.2.14 Mixed signal Oscilloscope	49	
4.2.15 USB Digital Microscope	50	
4.2.16 Handheld weighing scale	50	
4.2.17 Limit switches	51	
4.2.18 Cables	51	
4.2.19 Switches	52	
4.2.20 Suction fans	52	
4.2.21 LED lighting	53	
4.2.22 Power Supply Unit	53	
4.3 Control system mechanisms	54	
4.3.1 Standoff Distance adaptive closed loop mechanism	54	
4.3.2 Pulse Width Modulation control mechanism	55	
4.3.2.1 PWM using Arbitrary waveform generator	56	
4.3.2.2 PWM using ESP32 microcontroller	56	
4.4 Graphical user interface	57	
4.4.1 Analysis Graphical user interface (GUI)	57	

CHAPTER NO.	TITLE	PAGE
	4.4.2 Sensor integration Graphical User Interface	60
	4.5 Software	61
	4.5.1 Open Builds CNC control	61
	4.5.2 LaserWeb	62
	4.5.3 Virtual Studio Code	63
	4.5.4 Celestron Microcapture Pro	63
5	RESULTS AND DISCUSSION	64
	5.1 Experimental setup	64
	5.2 Parameters	64
	5.2.1 Input parameters	64
	5.2.1.1 Standoff Distance	64
	5.2.1.2 Feed rate	65
	5.2.1.3 Pulse Width Modulation	65
	5.2.1.3.1 Duty cycle	65
	5.2.1.3.2 Frequency	65
	5.2.2 Output parameters	65
	5.2.2.1 Carbonization	65
	5.2.2.2 Material removal rate	66
	5.2.2.3 Kerf width	66
	5.3 Selection of material and Geometric shapes	66
	5.4 Taguchi orthogonal array	67
	5.4.1 Analysis on chrome + vegetable tanned cow leather	68
	5.4.1.1 Analysing carbonization on chrome + vegetable tanned cow leather	68
	5.4.1.2 Analysing Kerf width on chrome + vegetable tanned cow leather	71
	5.4.1.3 Analysing Material removal rate (MRR) on chrome + vegetable tanned cow leather	74
	5.4.1.4 Analysing Emission rate on chrome + vegetable tanned cow leather	77

CHAPTER NO.	TITLE	PAGE
	5.4.1.5 Experimental samples	83
	5.4.1.6 Optimal parameters for cutting chrome + vegetable tanned cow leather.	84
	5.4.1.6.1 DEAR Methodology	85
6	CONCLUSION	88
	6.1 Conclusion	88
	6.2 Future scope	88
	REFERENCES	89
	APPENDIX	92

LIST OF TABLES

TABLE NO.	TITLE	PAGE
1.1	Comparison of existing systems and machines	4
3.1	Mechanical Components	21
4.1	Electronic Components	38
4.2	Raspberry Pi 4B Specifications	39
4.3	Arduino MEGA specifications	41
4.4	Arduino UNO R3 specifications	42
4.5	ESP32 microcontroller specifications	43
4.6	NEJE 20W specifications	44
4.7	NEMA-17 stepper motor specifications	45
4.8	VL6180X tof sensor specifications	47
4.9	Arbitrary Waveform Generator Specifications	48
4.10	MSO Specifications	49
5.1	Three factor L9 orthogonal array	67
5.2	Four factor L9 orthogonal array	67
5.3	Conventional SOD control - A cut	68
5.4	SOD control using Arduino UNO - B cut	68
5.5	PWM control using Arbitrary waveform generator – C cut	69
5.6	PWM control using ESP32 - D cut	69
5.7	SOD and PWM control using Arduino UNO and ESP32 - E cut	70
5.8	Conventional SOD control - A cut	71
5.9	SOD control using Arduino UNO - B cut	71
5.10	PWM control using Arbitrary waveform generator - C cut	72
5.11	PWM control using ESP32 - D cut	72
5.12	SOD and PWM control using Arduino UNO and ESP32 - E cut	73
5.13	Conventional SOD control - A cut	74
5.14	SOD control using Arduino UNO - B cut	74

TABLE NO.	TITLE	PAGE
5.15	PWM control using Arbitrary waveform generator - C cut	75
5.16	PWM control using ESP32 - D cut	75
5.17	SOD and PWM control using Arduino UNO and ESP32 - E cut	76
5.18	Emission rate interior value of conventional SOD control - A cut	77
5.19	Emission rate exterior value of conventional SOD control - A cut	77
5.20	Emission rate interior value of SOD control using Arduino UNO - B cut	78
5.21	Emission rate exterior value of SOD control using Arduino UNO - B cut	78
5.22	Emission rate interior value of PWM control using Arbitrary waveform generator - C cut	79
5.23	Emission rate exterior value of PWM control using Arbitrary waveform generator - C cut	79
5.24	Emission rate interior value of PWM control using ESP32 - D cut	80
5.25	Emission rate exterior value of PWM control using ESP32 - D cut	80
5.26	Emission rate interior value of SOD and PWM control using Arduino UNO and ESP32 - E cut	81
5.27	Emission rate exterior value of SOD and PWM control using Arduino UNO and ESP32 - E cut	81
5.28	Emission rate average difference	82
5.29	Carbonization and Its analysis	84
5.30	Averaged output values of cut E for DEAR analysis	85
5.31	Calculated values for Weights and MRPI	86
5.32	Optimising process parameters	87
5.33	Optimised process parameters	87

LIST OF FIGURES

FIGURE NO.	TITLE	PAGE
1.1	Hierachal selection for LBM	3
1.2	Conventional and non-conventional machines	5
3.1	Bakelite resin plates	17
3.2	CAD view of LBM setup	17
3.3	(a) X axis holders (b) Y axis holders and (c), (d) Z axis holders	18
3.4	VL6180X Time of flight sensor holder	19
3.5	Laser module holder	19
3.6	(a) Enclosure exhaust grid and (b) Layer frames	20
3.7	Lux sensor holder	20
3.8	Aluminium work centre	22
3.9	Aluminium profiles	22
3.10	Bakelite resin plates	23
3.11	Stainless-steel rods	24
3.12	Lead screws and rounded T-Nut.	24
3.13	M5 × 10 mm hexagonal socket screws.	25
3.14	Ball bearing bush	25
3.15	(a) T-Nut and (b) Nut seat	26
3.16	LBM setup	26
3.17	LBM enclosure	27
3.18	Moisture-resistant MDF board	27
3.19	Acrylic boards	28
3.20	Mystic Dream	28
3.21	Emission control unit	29
3.22	LBM Enclosure	30
3.23	Iron sheet, Ferrite magnet and Cow leather	31
3.24	EN 207 Goggles	34
3.25	EN 388 Gloves	34
4.1	CNC Block diagram	35

FIGURE NO.	TITLE	PAGE
4.2	LBM Block diagram with sensors	36
4.3	Raspberry Pi 4B	39
4.4	REES 7" LCD Display	40
4.5	Arduino MEGA	40
4.6	Arduino UNO R3	41
4.7	ESP32 microcontroller	42
4.8	NEJE 20W laser diode	43
4.9	CNC Control board	44
4.10	NEMA-17 4 pin stepper motor	45
4.11	A4988 stepper driver	46
4.12	VL6180X tof sensor	46
4.13	GY30 BH1750 sensor	47
4.14	SCD30 Sensor	48
4.15	Arbitrary Waveform Generator	48
4.16	MSO	49
4.17	USB Digital microscope	50
4.18	Handheld weighing scale	50
4.19	Limit switches	51
4.20	Cables	51
4.21	Push button and switches	52
4.22	Suction fans	52
4.23	LED Light	53
4.24	Multi-Socket adapter	53
4.25	SOD block diagram	54
4.26	Schematic diagram of the SOD loop	55
4.27	Algorithm executed on Arduino UNO	55
4.28	MSO, ESP32 and Arbitrary waveform generator Setup	56
4.29	ESP32 and laser diode schematic diagram	57
4.30	Carbonization Analyser GUI	57
4.31	Working algorithm	59

FIGURE NO.	TITLE	PAGE
4.32	PWM GUI	61
4.33	Open Builds CNC control software	62
4.34	LaserWeb CNC control software	62
4.35	VS code Software interface	63
4.36	Celestron Microcapture Pro	63
5.1	LBM setup	64
5.2	Kerf width	66
5.3	Carbonization graphical comparison	70
5.4	Kerf width graphical comparison	73
5.5	MRR graphical comparison	76
5.6	Emission rate graphical comparison	82
5.7	(a) A cut (b) B cut (c) C cut (d) D cut and (e) E cut	83

LIST OF EQUATIONS

FIGURE NO.	TITLE	PAGE
3.1	Velocity ratio of leadscrew	31
3.2	Angle of slope of threads	31
3.3	Friction angle	31
3.4	Efficiency of leadscrew	32
3.5	Mechanical advantage	32
3.6	Torque	32
3.7	Force of the load on X axis	32
3.8	Force of effort on X axis	32
3.9	Force of the load on Y axis	33
3.10	Force of effort on Y axis	33
3.11	Force of the load on Z axis	33
3.12	Force of effort on Z axis	33
4.1	Black pixels	59
4.2	Percentage of Black pixels	59
4.3	Percentage of White pixels	59
5.1	MRR	66
5.2	Multi response performance index	86
5.3	Weight of Emission rate	86
5.4	Weight of Carbonization	86
5.5	Weight of Kerf width	86
5.6	Weight of Material removal rate	86

LIST OF ABBREVIATIONS

LBM	Laser Beam Machining
SOD	Standoff Distance
PWM	Pulse Width Modulation
GUI	Graphical user interface
LASOX	Laser Assisted Oxygen Cutting
EDM	Electrical Discharge Machining
UFL	Upscaled Functional Leather
PMMA	Polymethyl methacrylate
HAZ	Heat Affected Zone
CAD	Computer Aided Designing
STL	Standard Tessellation Language
tof	Time of flight
CNC	Computer Numeric Control
G-CODE	Geometric Code
MDF	Medium-density Fibreboard
ZWAS	Zeolite Wool fibre Activated carbon Silica
ECU	Emission Control Unit
PPE	Personal Protective Equipment
MSO	Mixed Signal Oscilloscope
USART	Universal Synchronous Asynchronous Receiver Transmitter
MRR	Material Removal Rate
TGRA	Taguchi Grey Relational Analysis
DEAR	Taguchi Data Envelopment Analysis based Ranking
MCDM	Multi Criteria Decision Making
MRPI	Multi Response Performance Index

CHAPTER 1

INTRODUCTON

Leather is one of the most versatile and commonly accessible materials. The usage of leather in a wide range of industries has increased the demand for it to be cut in an efficient manner with higher production rates. In this instance, it becomes necessity to design an efficient approach for its manufacture, processing, and finishing in order to keep up with escalating demand. There are several existing systems available, which are currently in use, in the leather industry such as manual cutting, strap cutting, and die presses, but the caveat is in their efficiency and slower production rate. Following that, a novel, non-traditional approach must be pursued. Laser Beam Machining (LBM) is a widely used non-conventional machining process. Due to its high process efficiency and production rates, it has gained popularity in recent years and is now used in a variety of operations. There are numerous types of lasers available, including CO₂ lasers, Nd:YAG lasers, and Ruby lasers, among which CO₂ lasers are particularly popular in the industrial world. However, existing CO₂ laser beam machining techniques have a number of disadvantages such as extensive carbonization of leather during laser action and the requirement for a gaseous source to generate the laser beam. Also, the absence of an efficient user interface for controlling and monitoring of machining processes and lack of automation in the control aspect leading to process flow errors added to its shortcomings. Moreover, these errors are also observed in two-axis machining systems, and thus a solution is sought in the current attempt.

Therefore, an attempt has been made to design and fabricate a three-axis machining setup with a laser diode mounted on the tiller. This is because the laser diode has several advantages over other lasers, including a higher rate of production and a lower rate of carbonization. Also, the presence of another axis in the machining system enables it to perform the machining operation in a precise way by controlling the position of laser module over the leather sample. Consequently, a self-tuned system has been developed to control the Standoff distance (SOD) of laser module from the workpiece and this forms one of the primary objectives of the dissertation.

Another significant limitation of existing systems was the inability to control the effective power of the laser beam. This limitation has been resolved in the attempt by controlling the laser beam power using the pulse width modulation (PWM) technique through the variation of input parameters such as duty cycle and operating frequency. Apart these notable differences from the existing setups, an interactive touch screen has been incorporated into the system, thereby providing the capability to control and monitor the machining process, hence improving the ease of usage and along with that a Graphical user interface (GUI) has been programmed in order control and observe the machining setup. Finally, this attempt incorporates an entirely new design for the integration of all necessary components and sensors, as well as the machining system, with a separate chamber specifically designed for filtration containing panellised compartments of activated charcoal and zeolite beads to control the fumes generated during leather machining.

1.1 Laser Beam Machining and mechanism

Laser beam machining is a non-traditional form of subtractive manufacturing that involves a laser beam directed at the intended target work item. This kind of machining makes use of the pyro energy generated by the emission of the beam to execute material removal operations. Specifically, the beam is monochromatic and emits a certain colour based on its wavelengths in the visible light spectrum, and it does so at a high frequency rate. The material removal process is carried out by this laser beam by focusing the beam on a single location and removing the material via laser ablation.

Lasers can be categorised into two major types based upon their mode of beam emission,

- Continuous Mode: The output diode laser beam is nominally constant over an interval of time.
- Pulsed Mode: The output diode laser beam is pulsed, i.e.; the beam is emitted in the form of optical flashes with respect to time.

LBM begins with the action of the laser beam on the leather surface. The laser employed in this endeavour is a semiconductor-based laser diode that operates on the

principle of beam emission caused by an electron jumping from a higher energy orbital to a lower energy orbital within the atom. However, because this stage is deemed too unstable, absorption occurs, and once the absorption limit is reached, the laser beam begins transmitting continuously. This photon beam emission travels through a convex lens, which aids in accurately concentrating them on the appropriate target area. Then, when the laser beam is focused using the lens and comes into contact with the leather surface, it immediately melts the biomaterial, as indicated by the distinct foul odour emanating from the machining setup, after which the leather is cut according to the laser's input parameters and material removal is performed.

1.2 Hierarchy analysis

Laser diode selection plays a major role in effective cutting of leather, in current proposed model 450 nm laser diode has been selected which would be controlled in pulsed mode by varying Standoff distance, Feed rate, Duty cycle and Frequency.

Figure 1.1 shows the Hierarchical selection of LBM and its laser diode.

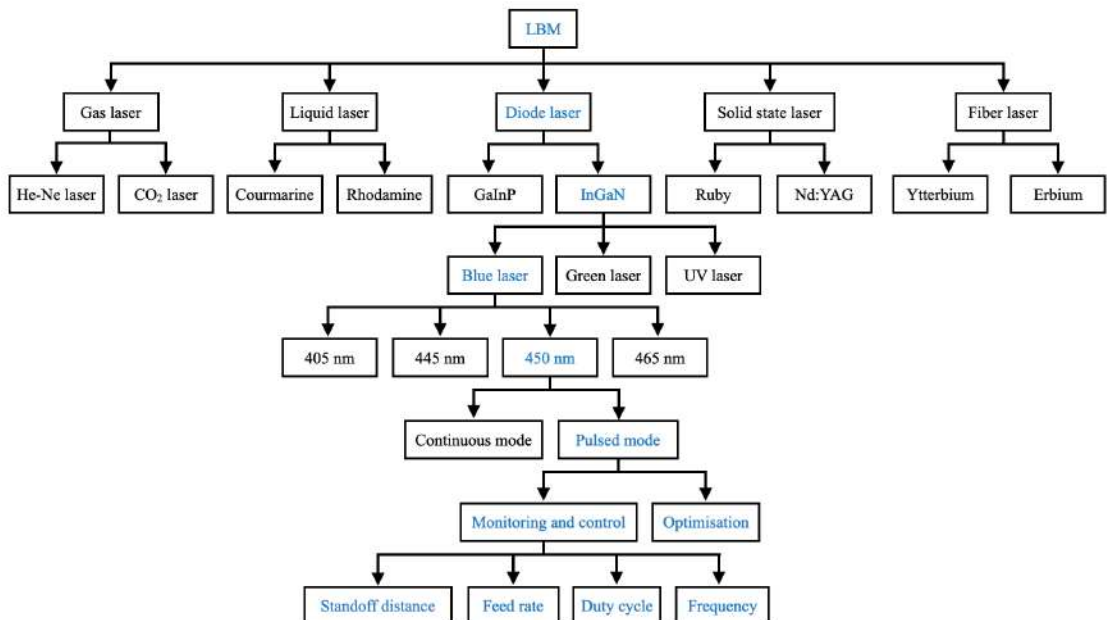


Figure 1.1 Hierarchical selection for LBM

1.3 Leather cutting using conventional and non-conventional methods

Table 1.1 compares the existing system and machines in leather cutting process.

Where Die press and Strap cutter are conventional machines, CO₂ laser and 2 Axis laser diode are non-conventional machining systems.

Table 1.1 Comparison of existing systems and machines

S. No	Requirements	Machines			
		CO ₂ Laser	2 Axis laser diode	Die Press	Strap cutter
1	Cost	Lower than Water Jet	Lower than CO ₂ Laser	Depends on Energy Used	Lower than 2 Axis Laser Diode
2	Maintenance	High	Low	Low	Low
	Workspace after work	Dross formation	Dross formation	-	-
3	Operation	Gas & Electricity	Electricity	Physical / Electricity	Electricity
	Standoff distance	-	-	-	-
4	Kerf width	Can be modified	Can be modified	-	-
5	Tools used	Nozzle	Diode	Print Rods/ Plates (Design)	Blades
6	Quality (leather)	Moderate	High than CO ₂ Laser	High	High
7	Time consumption	As per Design	As per Design / Relatively low	Less	Less
				Slow process / Need to replace	
8	Drawbacks on leather	Carbonisation / Striation	Less (carbonisation/ Striation)	press die's	Only horizontal cut



(a) CO₂ laser machine



(b) 2 axis laser diode machine



(c) Die press



(d) Strap cutter

Figure 1.2 Conventional and non-conventional machines

Figure 1.2 depicts the numerous methods of conventional and non-conventional machining that are in use in the leather cutting industry which proves to be effective but has several disadvantages like the slower production rate and excess amount of undesirable carbonization especially in the case of CO₂ laser.

1.4 Need for research

- Current small scale laser beam machining setup does not come with an integrated touch display for controlling the machining process.
- From the study of existing systems, it can be inferred that not much attention was given for filtration system when cutting leather using diode laser.
- Very few numbers of works, done in the development of Pulse width Modulation (PWM) using controllers for leather cutting.
- Very few numbers of works, done in the development of external graphical user interface (GUI) for controlling different parameters of PWM and analysis of leather contour edges.
- The energy conservation aspect of the LBM should be maximised as much as possible.

1.5 Objectives

- To design and fabricate energy efficient power diode-based Laser Beam Machining (LBM) setup.
- To optimise the standoff distance (SOD) by implementing a self-tuned control setup.
- To optimise the laser power using Pulse width Modulation (PWM)
- To control the emission of toxic gases during the machining of leather using ZWAS.
- To enhance the machinability by optimising the process parameters of LBM process.

1.6 Merits of Diode laser beam machining

- High production rate.
- Non-contact machining process.
- Machining of non-conducting materials are possible.
- Amount of carbonization is comparatively low, compared to other laser systems.
- Very low probability of the occurrence of tool wear in the machining.

1.7 Demerits of Diode laser beam machining

- Limitation in the amount of workspace available.
- Lack of metal cutting.
- Carbonization produced may sometimes provide an undesirable appearance.
- Susceptible to power surges.

1.8 Applications of Diode laser beam machining

- Micro machining and chip manufacturing.
- Critical heat treatment of materials available.
- Medical and healthcare applications.
- Wood cutting applications.

1.9 Organisation of the thesis

The project dissertation is organized in a comprehensive manner as below:

- **Chapter 1 - Introduction,** Describes about the broad contextual information of the project, existing systems and their caveats, need for a new system, comprehensive research methodology and organisation of the project report.
- **Chapter 2 - Literature Survey,** Explains about the extensive literature survey completed around the topics related to the report.
- **Chapter 3 - Mechanical Design,** Briefs about the mechanical design of the system.
- **Chapter 4 - Electronics Control Unit,** Elucidates on the electronic components and the control system present in the structure.
- **Chapter 5 - Result & Discussion,** Illuminates on the results of the experiments.
- **Chapter 6 - Conclusion & Future Scope,** Discusses the future scope of this project.
- **Chapter 7 - References,** Lists the references sought upon for this report.

CHAPTER 2

LITERATURE SURVEY

2.1 General

The literature survey has been carried out to have an encapsulation of LBM with the reference of leather processing, analysis of input variables, process parameters, material parameters and future research scopes.

2.2 Laser cutting

2.2.1 Laser cutting through water driven thermal separation mechanism

Romero et al. (2013)^[19] investigated briefly a unique form of thermal laser dicing of crystalline silicon with fluid support to improve their operational window and flexibility. A diode laser with a 1mm spot diameter and a water or glycerol layer to minimise and achieve zero kerf width with low final toughness. This method of dicing has been compared to traditional thermal cleaving by varying factors such as with and without initial stress concentrators, changes in cutting speed, and mono and multi-crystalline silicon. Thermal separations produce clean cutting edges with no damage and silicon wafer separation with no material kerf or silicon waste.

2.2.2 Performance comparison between CO₂ and diode laser on concrete cutting

Layered LBM with vitrified dross deposits are removed in between different passes is a novel non-conventional approach that has demonstrated the capacity to cut not just concrete but also other refractory materials. Philip et al. (2003)^[20] compared this machining to the capabilities of a CO₂ laser of 1.2 kW and the results were projected in a numerical model that demonstrated the result of smaller kerf width in the use of diode laser machining of 1.5kW is better when compared to the former CO₂ laser utilised. In practise, a concrete cutting technique utilising a diode laser is much preferable, instead of a CO₂ laser.

2.2.3 Oxygen assisted laser cutting of thick MS

Laser aided oxygen cutting (LASOX) is a non-traditional method of cutting thick mild steel material with thickness of 20-40 mm with combined laser of optical power

of 400W. I.Sakaev and A.A.Ishaaya (2021)^[15] cut 20mm thick mild steel samples to demonstrate the potential of low power, compact laser systems to cut substantial pieces of mild steel. The key advantage of this technology over traditional machining is the low optical power requirement in relation to the thickness of the workpiece. Occasionally, in oxy-fuel cutting, a cutting gas jet angled in the opposite direction of the cutting direction is used to increase cutting speed at the expense of cut quality.

2.2.4 Laser cutting with elliptically polarised laser beams

The effects of beam polarisation and its performance characteristics are well known in the laser machining industry, and the polarisation states of both laser and circular polarisation are widely explored in the case of CO₂ lasers, but there is only the existence of theoretical models predicting the optimal cutting performance for specific ellipse ratios but complete absence in case of experimental validation. C.Rodrigues et al. (2018)^[12] here have solved it by undertaking experiments on 2mm thick 304L stainless steel and comparing the results to a simulation model. The observed results reveal a comparable nonlinear influence on the maximum material cutting speed and validate the theoretic prediction of the best ellipse beam ratio.

2.2.5 Picosecond laser machining

C.Moorhouse (2013)^[5] investigated the benefits of picosecond laser machining for cutting-edge products, which include manufacturing relatively small, more powerful, and brighter mobile phones, as well as micro medical stents. Ultrafast industrial lasers are a crucial tool for a variety of uses, and their high repetition rates fulfil industrial throughput requirements. Fuel injection nozzles with a high aspect ratio are drilled in 1mm steel utilising picosecond pulse lasers, demonstrating superior quality with respect to present EDM technology. UV wavelength is ideal for cutting transparent polymer materials with minimum heat impacted zones.

2.2.6 Oxygen-assisted laser cutting

H.Golnabi and M.Bahar (2009)^[14] investigated the best kerf for steel and mild steel at 1 to 6 bar gas pressure. By modifying numerous parameters such as material type, thickness, and laser power, they were able to achieve an optimal power of 1 to 2mm and 0.2mm of kerf width at 67w laser power at cutting rate of 7.1mm/s. When the

same parameter is applied to mild steel, the kerf width measures to 0.3 mm. The overall average kerf width was optimised to be 0.3mm for a beam diameter of 0.27mm. The theoretical cutting speed for steel thicknesses of 1.0mm is roughly 8.07 mm/s, whereas the experimental cut rate is 1 mm/s. Simultaneously, optimal option for mild steel cutting in 67W laser power is 9.5mm/s cutting speed with oxygen pressure of 1 bar.

2.2.7 Laser cutting of PMMA Sheets

Ahmed B.Khoshaim et al. (2021)^[2] analysed laser cutting of PMMA sheets and kerf characteristics. The impact of process parameter like laser power, feed rate, gas pressure, and thickness on five parameter responses of heat impacted zone, kerf width, surface roughness, rough area and thickness was investigated. Laser technologies have shown promise in a number of manufacturing processes, including welding, cutting, and metal deposition. Due to PMMA's low thermal diffusivity and fast heating cycles, the temperature in the irradiated zone rises in the pyrolytic cutting process. The experimental design was optimised by Taguchi L18 and was carried out in a 150W CO₂ LBM.

2.2.8 Laser prepared cutting tools

The features of new materials to be treated have become complex, particularly their mechanical characteristics hardness, wear resistance, and so on. Wegener Konrad et al. (2012)^[23] investigated several parameters involved in the production of cutting tools made from such newer materials. This has been seen to be possible if the accuracy and life time requirements of the created work-tools meet current standards. The setup consists of three linear and two mechanical axes. The results show that by utilising a laser to touch dress a grinding wheel significantly reduces shear cutting pressures, hence improving its operating lifetime.

2.2.9 Distinguishing quality of pulsed laser cutting

A comparative study of laser blind cut on Incomel 625 was carried out by N.Roy et al. (2021)^[18] under a number of different conditions. As an alternative to surface reactions, this article focuses on sensitivity analysis, to explore the effect of the environment on controlling input parameters. During laser blind cuts, gas is fed to

the machining zone through the laser beams nozzle, and water maintained at a static pressure is utilised to cut through the material. It has been discovered that increasing air pressure increases depth more favourably than growing water column height, and that increasing water column height decreases depth more positively than increasing air pressure.

2.3 Leather

2.3.1 High-value utilisation of leather

Youyou Wang et al. (2021)^[24] revised the advanced nano-fibres based on functional bio-composites for high value utilisation of leather. The conventional tannery industry, is facing a consequential sustainability challenges, as such little value addition and high contamination in the work field. Upscaled functional leather (UFL) take over all of the inherent characteristics of leather and associate them with extra cross-domain functionalities, earning it widespread recognition as a sophisticated functional bio-based material. In a nutshell, this review illustrates the multi-hierarchical structure and concludes the characteristics of leather as a biomass.

2.3.2 Trends and advancements in sustainable leather processing

J.Kanagaraj et al. (2020)^[16] updated the trends and benefits of sustainable leather processing. The global leather trade is estimated to be worth \$150 billion USD per year. The sector's solid, liquid, and gaseous pollutants, on the other hand, have a negative impact on the environment. Despite ongoing research, there is a significant gap between anticipated and achieved goals for sustainable leather technology. At this point, the analysis presents a number of greener, more sustainable options that cover all critical unit functions in the leather manufacturing process. Phyto-based preservation solutions for raw skins and hides that reduce total dissolved solids and chlorides by up to 70% are being researched as an alternative to conventional preservation.

2.4 Laser diode

2.4.1 Mastering cutting process through different types of lasers

In response to the advent of fibre lasers, Dirk Petring et. al. (2012)^[9] conducted an investigation on the factors that influence the use of other newer laser systems such as disc and diode lasers, as well as other older laser systems such as CO₂ lasers. A model and simulation of the research were carried out in the well-known Cal-Cut simulation, with process parameters and 4mm stainless steel as the workpiece being used. Cal-Cut validity range has been established by testing the calculations with experimental modifications of input parameters such as laser power intensity, feed rate, focal length and location, and polarisation.

2.4.2 Different polarisation techniques with Diode lasers

Costa Rodrigues and J.R.Duflou (2016)^[11] investigated the use of a diode-based direct laser to perform cutting on, S355 stainless steel by balancing the low beam quality with a tactical use of laser polarisation in their dissertation. Depending on the inclination angle, the laser polarisation changes, resulting in different polarisation such as linear, radial, cross, and azimuthal polarisation. Cutting is direction-dependent and is known to have a positive effect on cutting speed in the direction of polarisation. To avoid this dependence and obtain homogeneous cuts, a phase retarder mirror is typically used to obtain circular polarisation, which is axisymmetric by nature.

2.4.3 Machinability of Titanium alloy

In agreement with the general opinion on titanium machinability, which is a challenge in and itself, due to its low thermal conductance and high chemical reactance, as well as high stresses at the end of cutting tools, there is a need for an effective method for its machining. Dong Hyeon Kim and Choon Man Lee (2021)^[10] presented an experimental examination on the machinability of titanium alloy Ti 6Al 4V using laser assisted end milling, where the absorptivity of Ti was evaluated through pre-heating studies using a high-power laser diode with a wavelength of 940-980nm. The results were evaluated based on surface roughness, tool wear, and cutting force and compared to a typical simultaneous technique.

2.4.4 Semiconductor laser diode arrays characterisations

Laser diode arrays and their applications have grown in popularity in recent years, leading to their use in material cutting, welding, diagnostics, and processing. As a result, controlling the beam quality becomes critical because it influences the dependability of the finished output. Luigi Zeni et al. (2001)^[17] proposed two essential ways to assessment of laser diode array beam quality, the first being measurements of intensity on planes that are orthogonal to the beam propagation route and the latter being measurement of the array's global quality factor. The basic principle is to treat the blended beam as a coherent laser and to measure its spot laser size and angle of divergence as if it were a single laser beam.

2.4.5 Transformation of surface on AISI 304 by power laser diode

Finishing morphology is crucial in the machining industry because it influences the visual appearance as well as the operating performance characteristics of diverse end products. A.Gisario et al. (2011)^[1] investigated irradiation milling of AISI 304 in order to analyse the changes in surface morphology through experiments. The milling operation was conducted by varying feed rates, and the laser finishing was carried out by varying, laser intensity and scan speed. The results were examined using 3D profilometry and SEM analysis, and it has been concluded that laser is bound to affect surface morphology and hence obtain good quality surface textures.

2.4.6 Possibilities of laser processing

Alexander Stepanov et al. (2015)^[3] investigated the possibilities of using a laser technique on paper. Aside from laser processing of metallic materials, laser processing of non-metallic materials has several industrial applications, including laser transmission welding of polymers, laser engraving of glass, and laser cutting of wood-based materials. Paper can be successfully sliced with CO₂ or diode lasers. In order to improve the wavelength absorption of a diode laser, ink must be put on the diode laser. Lasers are capable of achieving high cutting speeds with ease. This demonstrates that lasers may be used to replace traditional cutting procedures in the papermaking industry, such as water jet cutting and blade tools.

2.4.7 Laser diode arrays

Zhenfu Wang et al. (2017)^[25] discovered continuous mode diode laser array with great efficiency at 808nm wavelength. It has been proved that an asymmetric waveguide epitaxial structure with an extremely low internal optical loss of 0.5cm can be created. At a heatsink temperature of 25 degrees Celsius, 808 nm diode laser arrays with an unusually high power efficiency of 68% were seen to operate at 100W. Until now, this has been the most efficient power efficiency that have been seen at a 50% fill factor array that have been encountered. Through 1.5mm to 3mm, the inverse external differential efficiency quantum increased.

2.4.8 Laser cutting of sheets in pulsed mode

C.Bagger and F.O.Olsen (2001)^[6] describes how to optimise the laser cutting process that can cut sheet in laser using customised weld blanks. The influence of feed rate, gas purity, laser intensity, and energy pulse was studied in a series of systematic experimental studies. The properties of geometry, coarseness, and dross attachment of laser cut were intended for quality testing. Steel GA 260 of thickness 1.8mm was employed in all experiments. It has been inferred in this study that the geometry of a cut may be used for parameter optimisation. The feed rate was increased 10 times during the test, and was evaluated with the assist of gas pressures of 10, 13, 16, and up to 20 bar.

2.5 Output parameters, Modelling & optimisation

2.5.1 Kerf width deviation of micro-channel

One of the most important aspects of micro-machining is the investigation of kerf width characteristics, and S.Biswas et al. (2019)^[21] have carried out an experimental investigation of the kerf width of the micro channels on the cuts done on polymethyl methacrylate (PMMA) in a partially submerged condition. The cut was made with a diode pump laser fibre with a wavelength of 1064 nm, and the effects of varied media on kerf width were investigated after the cut was finished. Additionally, the parametric analysis discovered that when parameters are set to a lower value, kerf width is greater while machining in the air, but decreases when process variables are set to a higher value.

2.5.2 Effect on deviation in cut path.

Thermal stresses generate cracks along with which the materials are split when controlled fracture techniques are used in laser cleaving procedures. The key difference in this technique is the deviation in cut path, which Salman Nisar et al. (2010)^[22] investigated by adjusting a number of factors such as material thickness, laser intensity, and material cutting speed. The acquired results are additionally validated using finite element modelling to replicate the moving beam effect and to understand the process mechanics. It has been noted that an increase in the thickness of the glass for same power and cutting parameters. Despite the use of a laser to cut glass, the cut could not be made because, sufficient energy is not obtained for crack propagation, ramification in crack arrest.

2.5.3 Thickness validation of modelling tools

Cutting metallic sheet using a laser medium is a well-established procedure; however, a number of new entrants and changes in the process due to the introduction of new technologies have resulted in the need for considerably higher validation of the techniques being used. Costa Rodrigues et al. (2019)^[13] examined and confirmed this critical feature of a laser cutting model assumptions for thicker materials. The material in question is stainless steel 304L with thicknesses ranging from 2 to 10 mm. According to the data acquired through the experimental approach, the trend accuracy declines as the thickness of the materials increases.

2.5.4 Kerf width analysis and life cycle assessment of laser cutting process

Cutting sheet metals with a laser medium has proven to be more advantageous than traditional cutting methods in terms of precision, speed of processing, and cheap cost of execution. As a result, Bekir Sami Yibas et al. (2017)^[4] performed several cuts on various materials such as Ti 6Al 4V alloy, steel 304, and Inconel 625 to study the kerf width fluctuations in the cross-section of the cut. In addition, a life cycle assessment was employed to ascertain the ecological footprint of laser cutting in terms of material wasted during the process. According to the findings, the fluctuation in kerf width is related to the rise in laser output power, but this tendency reverses when the feed rate increases.

2.5.5 Multi-objective optimisation of laser cutting

Semiconductor backend packaging is a critical component of the silicon industry, which serves as the foundation for today's technological breakthroughs. These packages provide a layer of protection for IC chips against chemical contaminants and moisture, but they are produced using a traditional laser slow technique, necessitating the development of a newer, faster process. Chun-Hao Li and Ming-Jong Tsai (2008)^[8] created a novel non-traditional technique for optimising this slow procedure for particularly designed electronic circuit boards with multiple performance criteria found via grey relational analysis. Laser parameters were improved, and eight experiments were carried out, with the results revealing the parameter relevance and optimal parameter combinations for the laser cutting for identification.

2.5.6 Pulsed Nd: YAG laser cutting-Heat affected zone

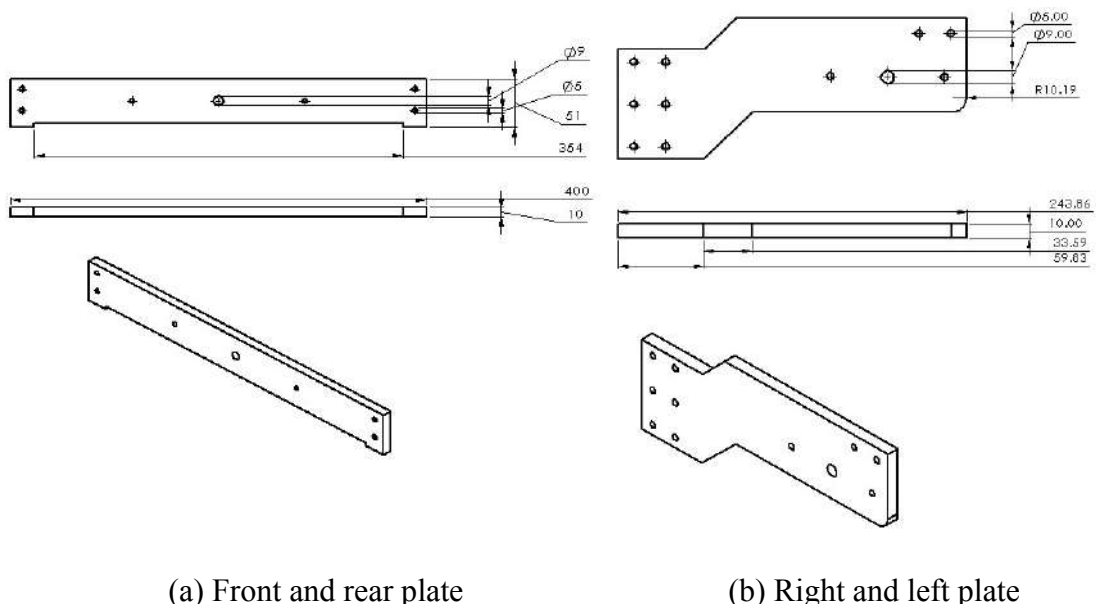
C.Leone and S.Genna (2017)^[7] explored the extension of heat affected zone (HAZ) in Nd:YAG laser cutting based on thermal interaction, resulting in thermal damage to both the matrix and the fibres. The extension of HAZ is relied on the laser and the operational factors. The experimental investigation on the laser of the CFRP plate 150W Nd:YAG laser in thickness of 1mm the kerf and HAZ were analysed using process parameters pulse energy and pulse length. The experiment demonstrates that the laser used, cuts the CFRP plate with precise process settings to obtain the highest cutting speed and HAZ. It was revealed that there is a link between HAZ extension and process parameters.

CHAPTER 3

MECHANICAL DESIGN

3.1 CAD Model of Laser Beam Machining

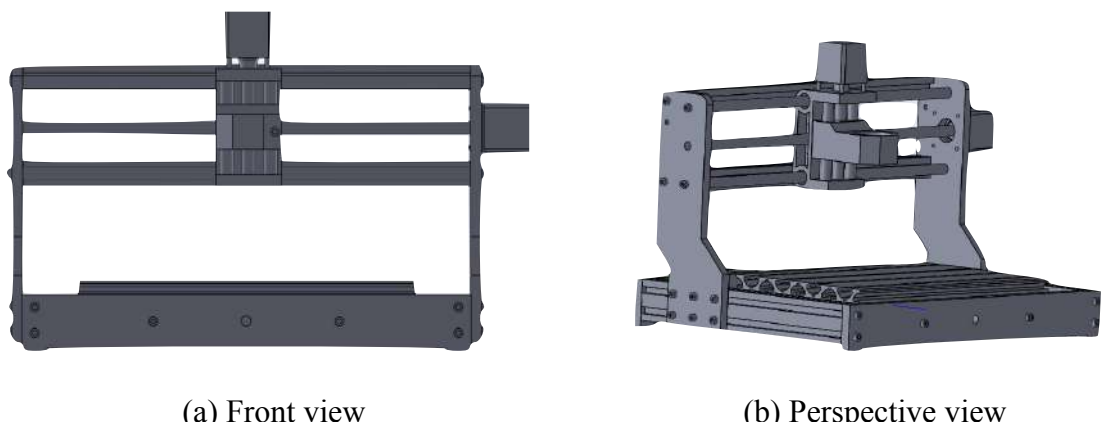
The customised Laser Beam Machining (LBM) design was created utilising SolidWorks 2021 (Academic edition) and a component-by-part technique, with each part having precise dimensions. All measurements are in millimetres (mm). Figure 3.1 illustrates the bakelite resin-designed plates with their respective sides. Figure 3.2 displays the whole LBM design in different projections.



(a) Front and rear plate

(b) Right and left plate

Figure 3.1 Bakelite resin plates



(a) Front view

(b) Perspective view

Figure 3.2 CAD view of LBM setup

The frame spans to $400 \times 330 \times 243$ mm. The LBM setup features a work area of size $300 \times 180 \times 40$ mm. The laser diode module and the work centre have a minimum depth of 10 mm.

3.2 3D Printed CAD Models for LBM and Enclosure

All components were printed on ENDER 3 3D printer using the Polylactic Acid (PLA) Pro material, which is a vegetable-based plastic. Additionally, it is suitable for printing at low temperatures and does not require a heated bed. The Standard Tessellation Language (STL) file is converted to G-code for 3D printing using Ultimaker CURA 4.9.1.

3.2.1 Limit switch holders

The present design of the LBM includes a limit switch to indicate the X-Z axis laser diode holder and Y axis Aluminium work centre at the end of their axis path. Figure 3.3 shows the limit switch holder design.

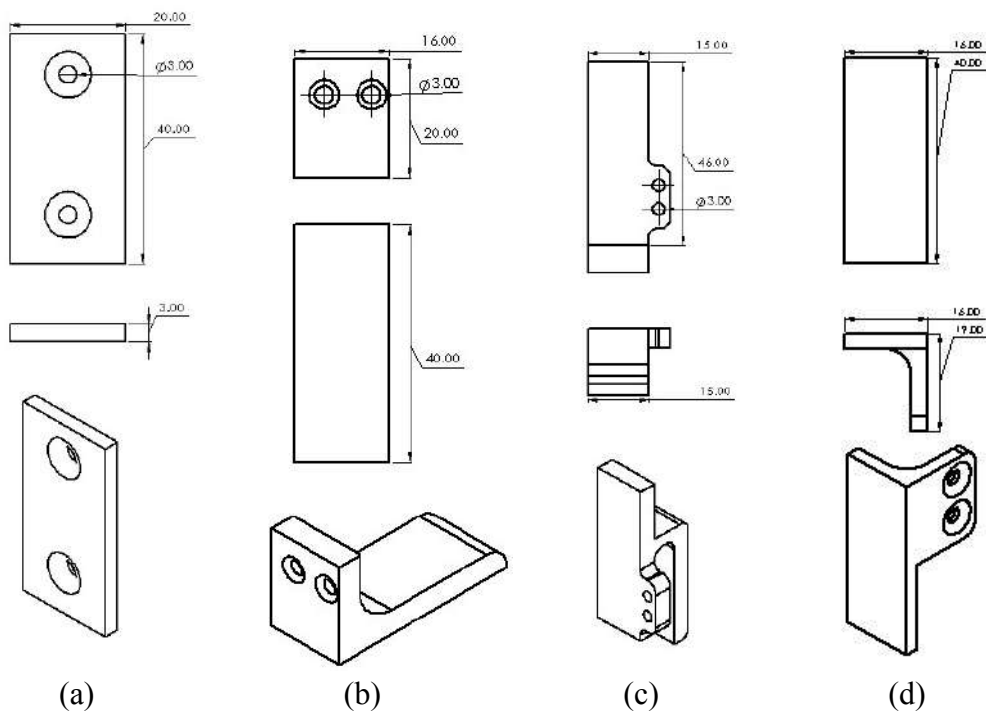


Figure 3.3 (a) X axis holders (b) Y axis holders and (c), (d) are z axis holders

In Figure 3.3 the CAD model of (a) and (b) are 3D printed twice for (X_1, X_2) and (Y_1, Y_2).

3.2.2 VL6180X Time of flight sensor holder

A VL6180X time of flight (tof) sensor is used to measure and adjust the Standoff Distance (SOD) of laser module with respect to work centre in Z axis. The VL6180X holder is shown in Figure 3.4.

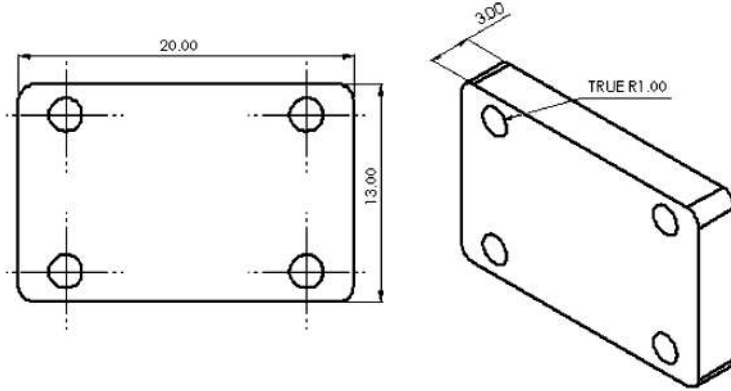


Figure 3.4 VL6180X Time of flight sensor holder

As such, an external holder is designed with dimensions $13 \times 20 \times 3$ mm and 3D printed.

3.2.3 Laser module holder

A 20W NEJE laser diode module of dimension 40×85 mm is utilised to cut and engrave the leather which is to be placed on the Z axis. The laser module holder is shown in Figure 3.5.

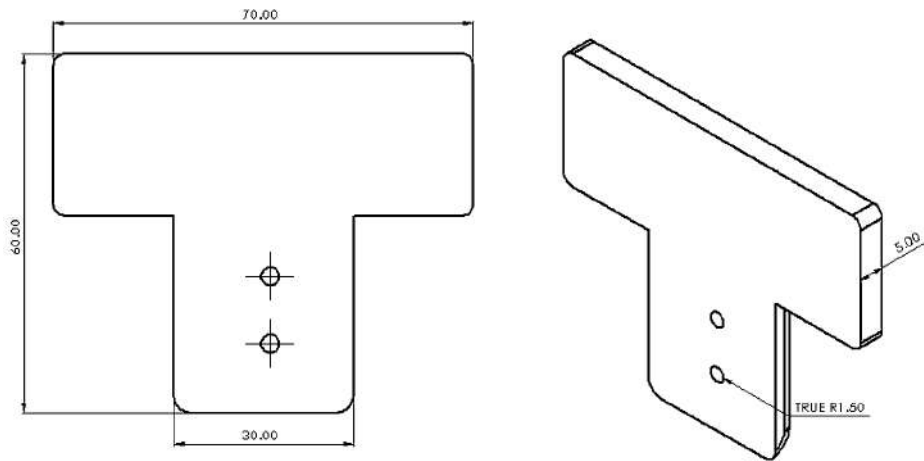


Figure 3.5 Laser module holder

As such, a holder is designed with dimensions $60 \times 70 \times 5$ mm and 3D printed.

3.2.4 Enclosure exhaust grid and layer frames

The LBM setup enclosure incorporates an exhaust system that filters the fumes while machining. The exhaust grid and layer frames has been designed to affix the filter wool with dimensions $108 \times 87 \times 12$ mm and with dimensions $80 \times 60 \times 4$ mm respectively and 3D printed. The layer frames are 3D printed twice. Figure 3.6 shows the exhaust grid and layer frames.

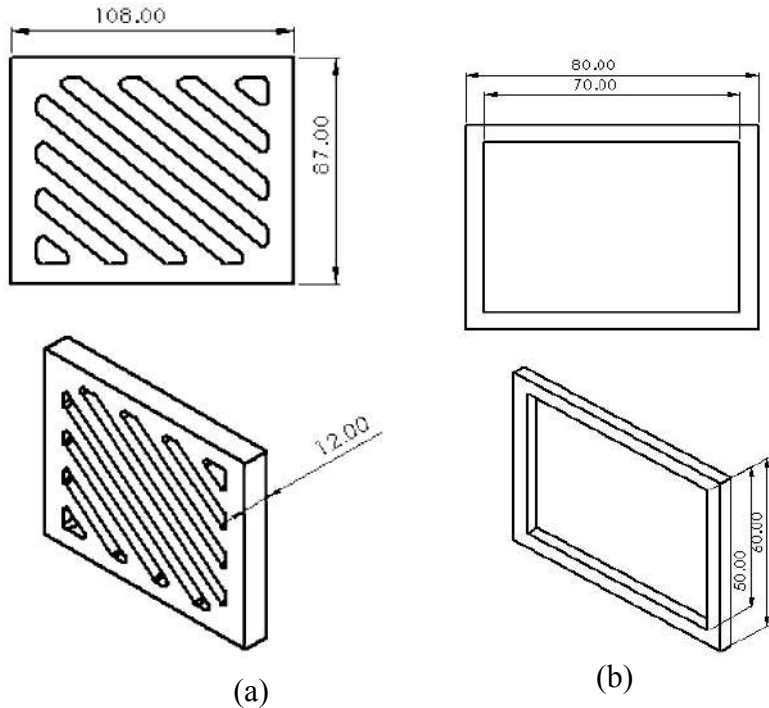


Figure 3.6 (a) Enclosure exhaust grid and (b) Layer frames

3.2.5 BH1750 Lux sensor holder

An 135-degree holder is intended to support the BH1750 Lux sensor, which is used to detect the lux value of the laser diode module, such that the sensor has an isometric viewpoint with respect to the output laser. The holder has a dimension of $15 \times 15 \times 3$ mm and 3D printed. Figure 3.7 shows the exhaust grid and layer frames.

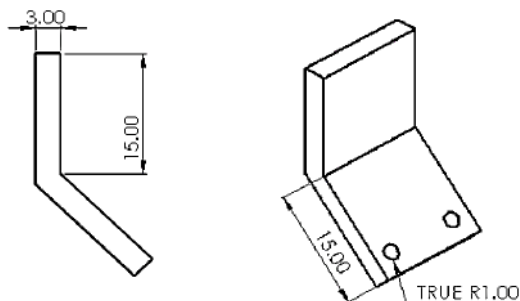


Figure 3.7 Lux sensor holder

3.3 Mechanical components

Table 3.1 Mechanical Components

S.No	Materials	Dimensions	Quantity
1	Aluminium work centre	300 × 180 mm	1
2	Aluminium profile 1	20 × 380 mm	2
3	Aluminium profile 2	40 × 300 mm	2
4	Bakelite resin plate (front and rear)	360 × 50 × 10 mm	2
5	Bakelite resin plate (right and left)	243 × 10 mm	2
6	Stainless steel guide rail 1	Ø10 × 380 mm	2
7	Stainless steel guide rail 2	Ø10 × 300 mm	2
8	Stainless steel guide rail 3	Ø10 × 12 mm	2
9	Lead screw 1	T8 × 390 mm	1
10	Lead screw 2	T8 × 305 mm	1
11	Lead screw 3	T8 × 100 mm	1
12	Hexagon Socket Screw 1	M3 × 14 mm	8
13	Hexagon Socket Screw 2	M5 × 10 mm	4
14	Hexagon Socket Screw 3	M5 × 16 mm	34
15	T-Nut 1	30M5 mm	10
16	T-Nut 2	20M5 mm	16
17	Copper Nut	Pitch 2 mm	2
18	Nut Seat	T8 mm	1
19	Linear ball bearings bush (LM10UU)	Ø10 mm inner	2
20	Deep groove ball bearing bush	Ø10 mm inner	3
21	Coupling and set screw	Ø10 mm inner 25 × 16 mm	3
22	PLA Pro+ (for 3D print)	-	500g
23	316 SS coated wood screws	25.4 mm	25
24	308 SS coated wood screws	12.7 mm	30

3.3.1 Aluminium work centre

The Aluminium work centre is attached to the Y axis lead screw 2, along with four sliders. Due to the reflective nature of Aluminium in 450 nm wavelength, it is impervious to be damaged from the high-intensity laser diode. Figure 3.8 shows the Aluminium work centre.

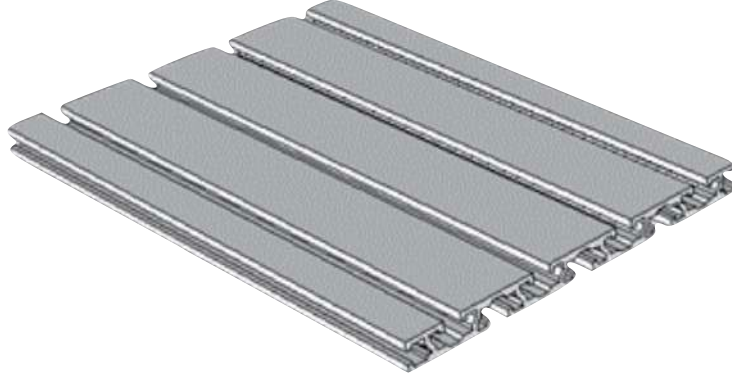


Figure 3.8 Aluminium work centre

The work centre comes with T-slots to accommodate the sliding nuts used to secure the leather piece. The dimension of the Aluminium work centre is 300×180 mm.

3.3.2 Aluminium profile

It is essentially an extruded Aluminium metal profile with T-slots. Although these profiles are lightweight, they are incredibly robust and adaptable. They are used to secure the bottom and side plates in horizontal positions. Figure 3.9 shows the Aluminium profile

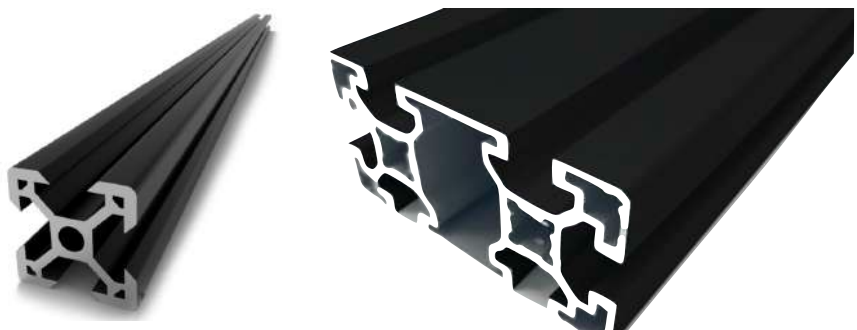


Figure 3.9 Aluminium profiles

Aluminium profile are coated with matte black spray to absorb a significant quantity of heat generated by the laser and other electrical components. The dimensions of

these Aluminium profile are 20×380 mm in two-piece set and 40×300 in two-piece sets.

3.3.3 Bakelite resin plates

Bakelite sheet is a thick, rigid material that is produced by heating and pressing layers of paper or glass cloth coated with phenolic resin. Bakelite resin is used to construct the LBM's bottom and side plates, which form the complete framework. The bottom (horizontal) is composed of two plates with dimensions $360 \times 50 \times 10$ mm, while the side (vertical) is composed of two plates with dimension of 243×10 mm. Figure 3.10 shows the bakelite resin plates.



Figure 3.10 Bakelite resin plates

One of the key characteristics of bakelite resin sheet is its ability to be easily shaped while retaining its smoothness. Additionally, it is resistant to heat and water damage.

3.3.4 Stainless steel guide rails

The stainless steel rods serve as a guide rail for the Y axis Aluminium work centre and X-Z axis holder. Without these guide rails, the work centre and the X-Z holder vibrates which may result in improper cutting of leather shapes. Figure 3.11 shows a model of the stainless-steel rod.



Figure 3.11 Stainless-steel rods

The guide rail is of 10 mm in diameter and are cut in two sets of 12 mm, 300 mm, 380 mm in length.

3.3.5 Lead screw and Round T-nuts

Lead screws are critical in the conversion of rotational motion to translational motion. It is frequently used in conjunction with a stepper motor that is linked through a coupler. Figure 3.12 shows the Lead screw and rounded T-Nut.



Figure 3.12 Lead screws and rounded T-Nut.

The brass T-Nut is used to secure the Z axis holder and the Aluminium work bed with Y axis. The dimensions of the lead screws are T8 × 305 mm, T8 × 390 mm and T8 × 100 mm. The T-Nut is equipped with a helical spring that secures the Lead screw with nut seat. The dimensions of the rounded T-Nut are Pitch 2 with 8mm diameter.

3.3.6 Hexagonal socket screws

Socket screws are used as fasteners. They are made of stainless steel, which is highly resistant to corrosion, and the threading will not readily wear away. These are used to hold the profiles, stepper motors and guide rails. Figure 3.13 shows the M5 × 10 mm hexagonal socket screws. Allen wrenches are required to tighten and loosen these socket screws.



Figure 3.13 M5 × 10 mm Hexagonal socket screws.

The dimensions of the Hexagonal socket screws are M3 × 14 mm, M5 × 10 mm, and M5 × 16 mm of quantity 8, 4 and 34 respectively.

3.3.7 Linear and Deep groove ball bearing bush

Bearing bushes are used to ensure that guide rails slide smoothly in a linear direction and can rotate without any constraints. Additionally, they provide support to the guide rails to hold the X-Z axis holder and Y axis Aluminium work centre. Figure 3.14 shows the bearing bush used.



(a) Linear LM10UU Bearing bush (b) Deep groove bearing bush

Figure 3.14 Ball bearing bush

The LM10UU bearing of two piece is required for Z axis holder and deep groove ball bearing of three quantity is required for three lead screws.

3.3.8 T-Nut and Nut seat

T-nut are used to securely fasten profiles and plates using socket screws, they prevent the profiles and plates from moving when tightened. They are especially well-suited to be used in the grooves of the profiles. Figure 3.15 shows the T-Nut and Nut seat.



Figure 3.15 (a) T-Nut and (b) Nut seat

Nut seat is used to hold the Aluminium work bed.

3.4 Experimental setup of LBM

The machining setup has been assembled in accordance with the CAD model. To operate the LBM setup, a CNC control board was utilised, for more information on board, refer Chapter 4 (4.2.7). The key goal of the present design is to control the SOD using a VL6180X tof sensor and to implement a PWM controller which in turn optimises the cutting parameters of leather. Figure 3.16 illustrates the LBM setup without an enclosing shell.



Figure 3.16 LBM setup

3.5 LBM enclosure

Fumes will be emitted while operating in LBM, particularly with leather-related materials. An enclosure is designed and developed to filter the fumes emitted into the environment and to safeguard our eyes from visible laser. This enclosure features a

REES 7" LCD touch display that enables the machine to be controlled without the usage of laptops or computers. The entire enclosure is designed using SolidWorks 2021 (Academic edition). Figure 3.17 shows the CAD model of the enclosure

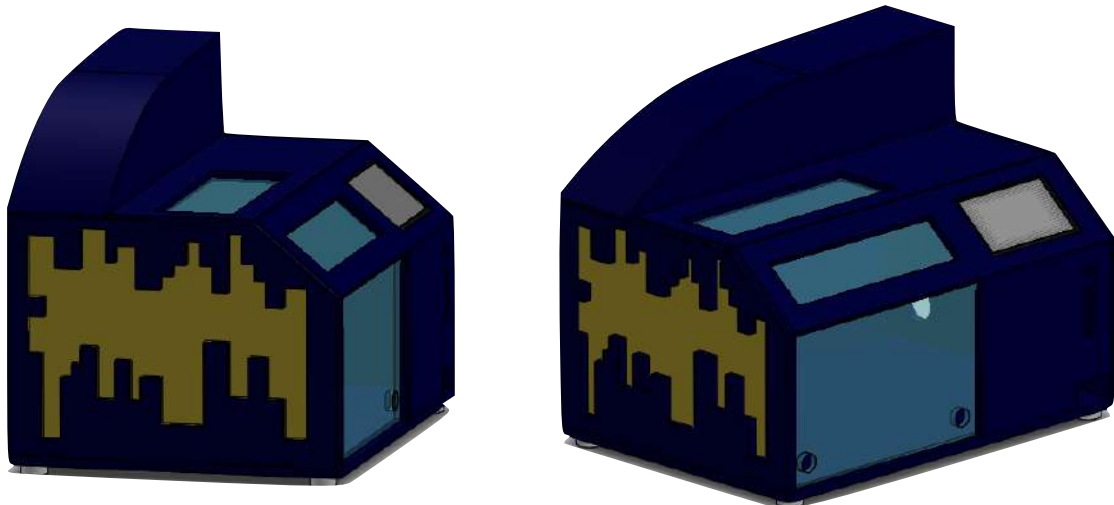


Figure 3.17 LBM enclosure

To make it visible from the outside, an LED tube light has been attached with ON/OFF switch. Two fans with dimensions 80×80 mm have been installed in the top groove of the outer exhaust to expel the fumes.

3.5.1 Medium-density fibreboard (MDF)

MDF board, commonly known as moisture-resistant MDF, was utilised to waterproof the whole enclosure. MDF is more sturdy and durable than plywood and has a longer life span. Additionally, it is simpler to paint. A 12 mm thickness MDF board is utilised to fabricate the enclosure. Figure 3.18 shows the moisture-resistant MDF board.



Figure 3.18 Moisture-resistant MDF board

3.5.2 Acrylic board

Given the strength and durability of acrylic, two types of acrylic boards are incorporated in the enclosure: one is mango gold of 2 mm in thickness, while the other is a blue transparent board measuring 6 mm in thickness. The second type is used to view the inside of the enclosure. Figure 3.19 shows the acrylic boards used.



Figure 3.19 Acrylic boards

3.5.3 Sealer and Enamel paint

Sealers are applied to the MDF board to improve the enamel's adherence to the board. Mystic Dream, code 7293 in asianpaints, is the enamel coated colour shown in figure 3.20. The coat is of matte type, which has the ability to absorb heat from the LBM.

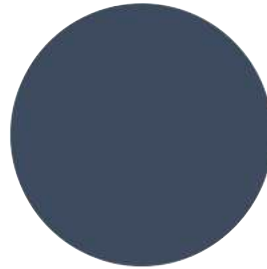


Figure 3.20 Mystic Dream

3.5.4 Emission control unit - ZWAS.

The Emission control unit (ECU) is designed and fabricated to filter the fumes and dust particles during machining process. The ECU consists of,

- **Zeolites** have the ability to provide accurate and specific gas separation, including the removal of water (H_2O), carbon dioxide (CO_2), and sulphur

dioxide (SO_2) from low-grade natural gas streams. Other separations consists of noble gases such as oxygen (O_2), Nitrogen (N_2), formaldehyde and freon.

- **Activated carbon** absorbs oil vapours, Nitrogen (N_2), and carbon dioxide (CO_2) which is being emitted while cutting leather.
- **Filter wool** enhances the absorption rate of activated carbon and also fine filters the particles present in the air.
- **Silica gels** absorbs the oil moistures and Hydrogen fluoride (HF) while cutting leather using laser diode.

Figure 3.21 shows the ECU along with the incorporated materials.



Figure 3.21 Emission control unit

3.6 Experimental setup of LBM enclosure

The final fabricated design of the LBM enclosure is shown figure 3.22. The entire dimension of the complete LBM setup is $650 \times 450 \times 420$ mm.

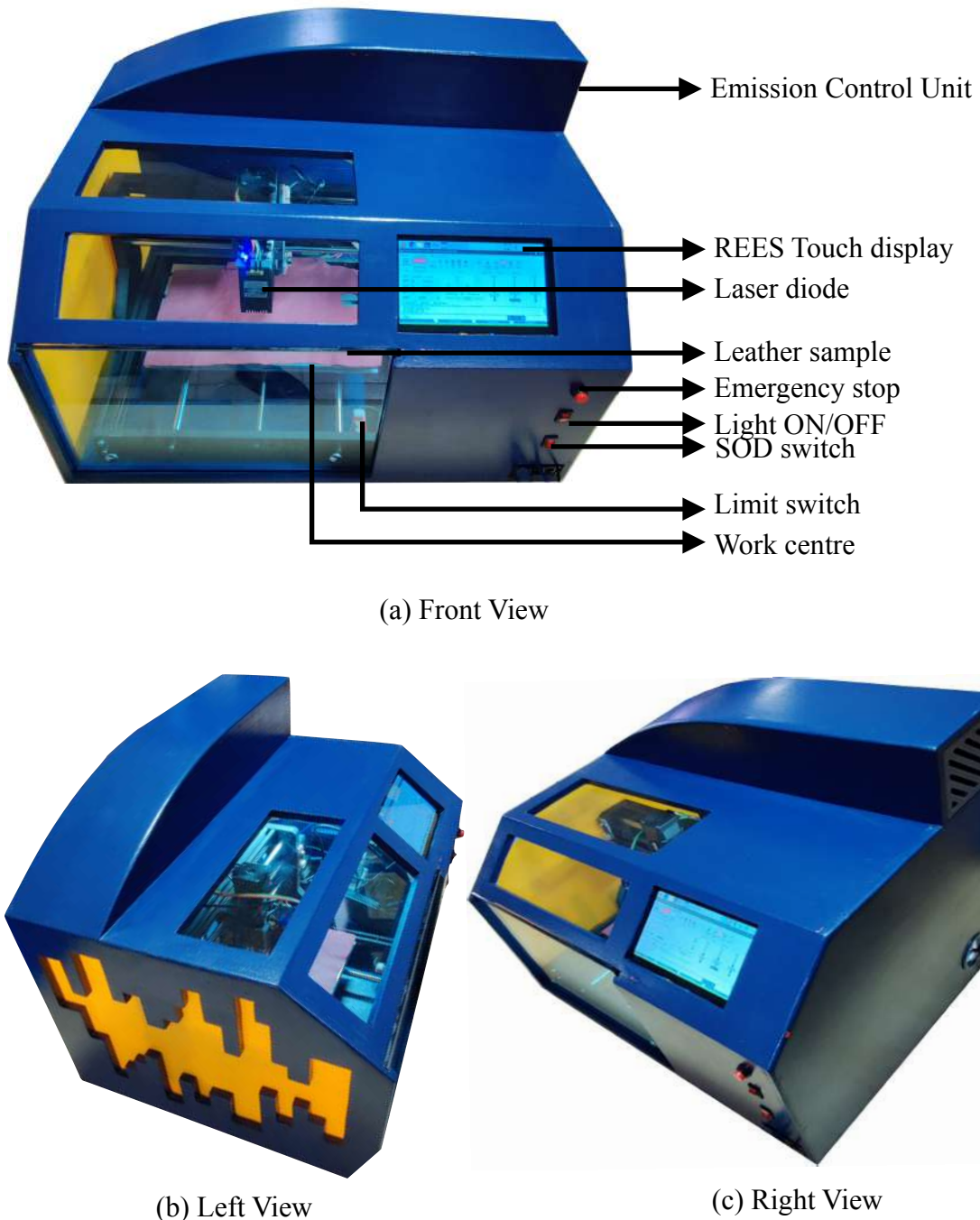


Figure 3.22 LBM Enclosure

3.7 Iron sheets and Ferrite round magnets

Iron sheet of thickness 1.5 mm and dimension 180×300 mm have been used on the surface of the Aluminium work centre which helps to attract the Ferrite round magnets which holds the leather in place during machining process. Since these magnets works as a toggle, which reduce divots in leather and thereby aides in precise cutting of the material. Figure 3.23 shows the Iron sheet and Ferrite magnet holding a leather piece.

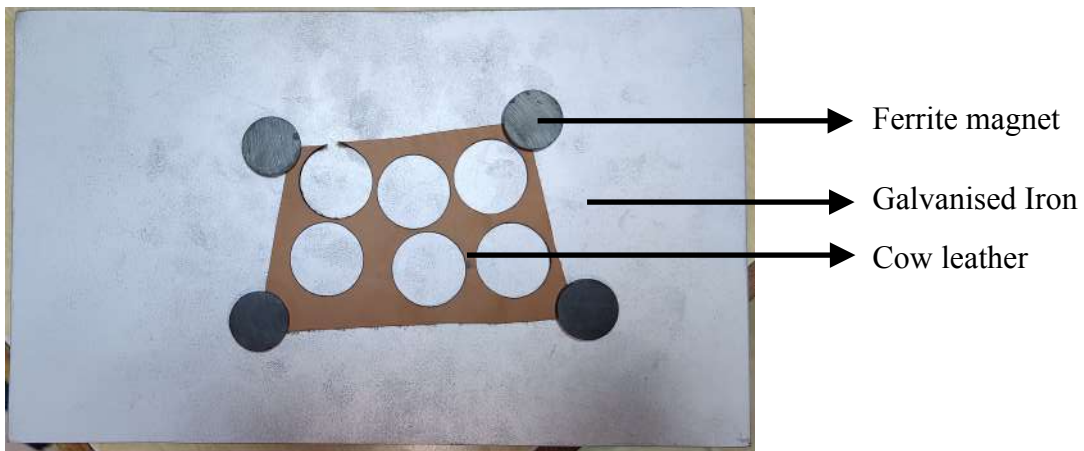


Figure 3.23 Iron sheet, Ferrite magnet and Cow leather

3.8 Lead screw torque and efficiency

The lead of the screw is essential to determine the needed torque and overall efficiency of the lead screw used. The NEMA17 stepper motor produces a torque, $\tau = 176.5197 \text{ Nmm}$.

3.8.1 Efficiency of the lead screw

$$\text{Pitch } P = 2 \text{ mm, Diameter of Lead screw } D = 8 \text{ mm.}$$

$$\text{Coefficient of friction for steel + brass nut } \mu = 0.21$$

$$\text{Velocity ratio } V_r = \frac{\pi \times D}{P} \quad (\text{Eqn. 3.1})$$

$$\text{Angle of slope of threads } \alpha = \tan^{-1}\left(\frac{1}{V_r}\right) \quad (\text{Eqn. 3.2})$$

$$\text{Friction angle } \beta = \tan^{-1}(\mu) \quad (\text{Eqn. 3.3})$$

$$\text{Efficiency } \eta = \frac{\tan(\alpha)}{\tan(\alpha + \beta)} \quad (\text{Eqn. 3.4})$$

$$V_r = \frac{\pi \times 8}{2} = 12.5663 \quad (1)$$

$$\alpha = \tan^{-1}\left(\frac{1}{12.5663}\right) = 4.5498^\circ$$

$$\beta = \tan^{-1}(0.21) = 11.8597^\circ$$

$$\eta = \frac{\tan(4.5498)}{\tan(4.5498 + 11.8597)} = 0.2702 \quad (2)$$

$$\text{Efficiency of the lead screw} = 0.2702 \times 100 = 27.02\%$$

In reference with PBC Linear Lead screw efficiencies (References) for 1mm metric lead of 10 mm diameter the efficiency is 28%. In the proposed system the efficiency of the lead screw is 27.02%.

3.8.2 Torque required on the lead screws in X axis

$$\text{Mass on X axis } m_x = 0.725 \text{ kg, Gravity } g = 9.81 \text{ m/s}^2$$

$$\text{Mechanical advantage } MA = \frac{F_l}{F_e} = V_r \times \eta \quad (\text{Eqn. 3.5})$$

$$\text{Torque } \tau = F_e \times \frac{D}{2} \quad (\text{Eqn. 3.6})$$

$$\text{Force of the load on X axis } F_{lx} = m_x \times g \quad (\text{Eqn. 3.7})$$

$$\text{Force of effort on X axis } F_{ex} = \frac{F_{lx}}{MA} \quad (\text{Eqn. 3.8})$$

From (1) and (2),

$$MA = 12.5663 \times 0.2702 = 3.3954 \quad (3)$$

$$F_{lx} = 0.725 \times 9.81 = 7.1122 \text{ kg} \cdot \text{m/s}^2$$

$$F_{ex} = \frac{7.1122}{3.3954} = 2.0946 \text{ kg} \cdot \text{m/s}^2$$

Torque required on the lead screws in X axis

$$\tau_x = 2.0946 \times \frac{8}{2} = 8.3784 \text{ Nmm} \quad (4)$$

3.8.3 Torque required on the lead screws in Y axis

Mass on Y axis $m_y = 1.66 \text{ kg}$, Gravity $g = 9.81 \text{ m/s}^2$

Force of the load on Y axis $F_{ly} = m_y \times g$ (Eqn. 3.9)

$$\text{Force of effort on Y axis } F_{ey} = \frac{F_{ly}}{MA} \quad (\text{Eqn. 3.10})$$

$$F_{ly} = 1.66 \times 9.81 = 16.2846 \text{ kg}\cdot\text{m/s}^2$$

$$\text{From (3), } F_{ey} = \frac{16.2846}{3.3954} = 4.7960 \text{ kg}\cdot\text{m/s}^2$$

Torque required on the lead screws in Y axis

$$\tau_y = 4.7960 \times \frac{8}{2} = 19.1842 \text{ Nmm} \quad (5)$$

3.8.4 Torque required on the lead screws in Z axis

Mass on Z axis $m_z = 0.33 \text{ kg}$, Gravity $g = 9.81 \text{ m/s}^2$

Force of the load on Z axis $F_{lz} = m_z \times g$ (Eqn. 3.11)

$$\text{Force of effort on Z axis } F_{ez} = \frac{F_{lz}}{MA} \quad (\text{Eqn. 3.12})$$

$$F_{lz} = 0.33 \times 9.81 = 3.2373 \text{ kg}\cdot\text{m/s}^2$$

$$\text{From (3), } F_{ez} = \frac{3.2373}{3.3954} = 0.9534 \text{ kg}\cdot\text{m/s}^2$$

Torque required on the lead screws in Z axis

$$\tau_z = 0.9534 \times \frac{8}{2} = 3.8137 \text{ Nmm} \quad (6)$$

From (4), (5) and (6) it can be inferred that the required torque for each axis is less than the rated torque of the stepper motor $\tau_x < \tau$, $\tau_y < \tau$ and $\tau_z < \tau$.

3.9 Personal Protective Equipments (PPE)

When working with machinery or doing experiments, caution is important, which is why safety equipment such as gloves and goggles are required.

3.9.1 Professional Laser Safety Goggles

450nm laser diode is classified under class D working mode in European standards, laser machining would be done using EN 207 or EN 208 goggles. Figure 3.24 shows the EN 207 Goggles.



Figure 3.24 EN 207 Goggles

3.9.2 Gloves

Gloves with European standards such as EN 388 and EN 407 should be used, where EN 388 protects against mechanical risks such as cut, tear, piercing and abrasion, and EN 407 have high heat resistance. Figure 3.25 shows the EN 388 Glove



Figure 3.25 EN 388 Glove

CHAPTER 4

ELECTRONICS CONTROL UNIT

This chapter elucidates on the various electronic components utilised and control mechanism created for achieving the objectives.

4.1 Block diagram

The complete block diagram of the Computer Numerical Control (CNC) machining setup is shown below:

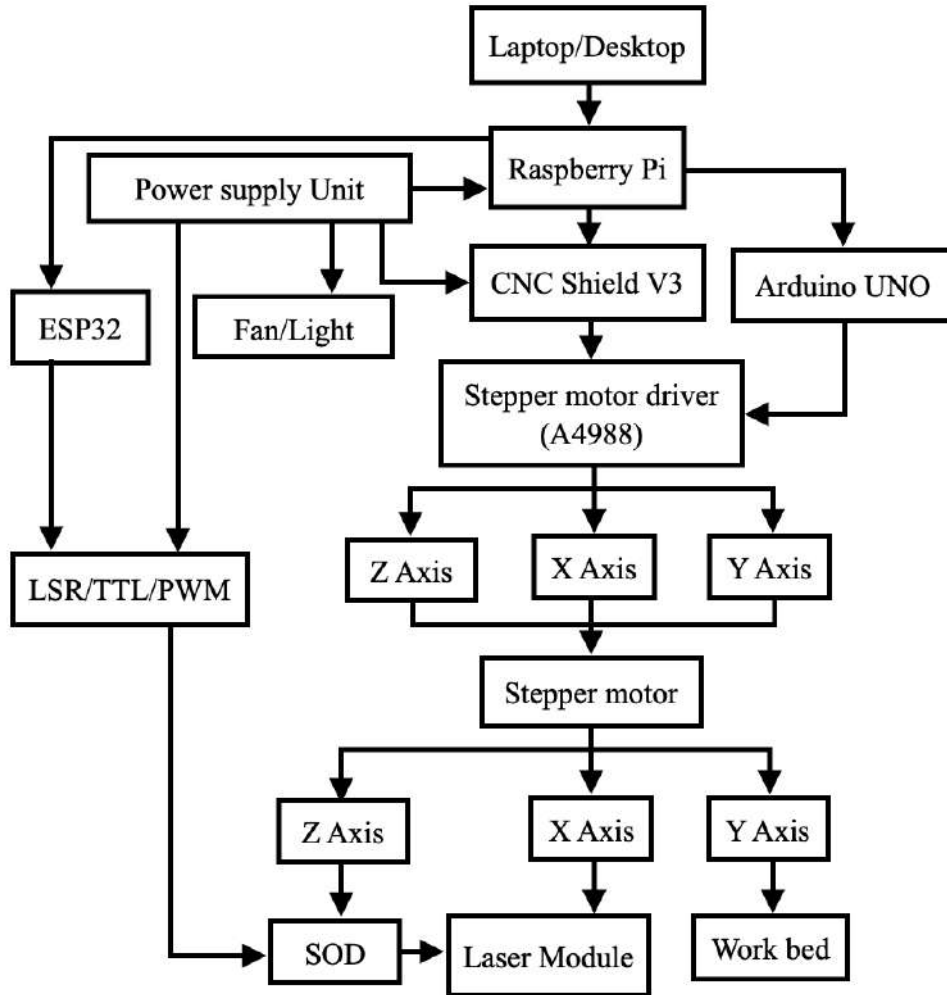


Figure 4.1 CNC Block diagram

In the Figure 4.1, it is shown that the stepper motors (Section 4.2.8) of X and Y axis are driven with the help of the CNC shield (Section 4.2.7) through a CAM software from a controlling source such as a personal computer or in this case a microcomputer - Raspberry Pi (Section 4.2.1). The drivers that have been used to

drive the stepper motor are A4988 stepper drivers (Section 4.2.9) whose usage would be briefed later in this chapter.

The block diagram of the complete system including all the microcontroller, sensors for measurements, drivers and stepper motors for actuation and the laser module integration can be shown in the Figure 4.2.

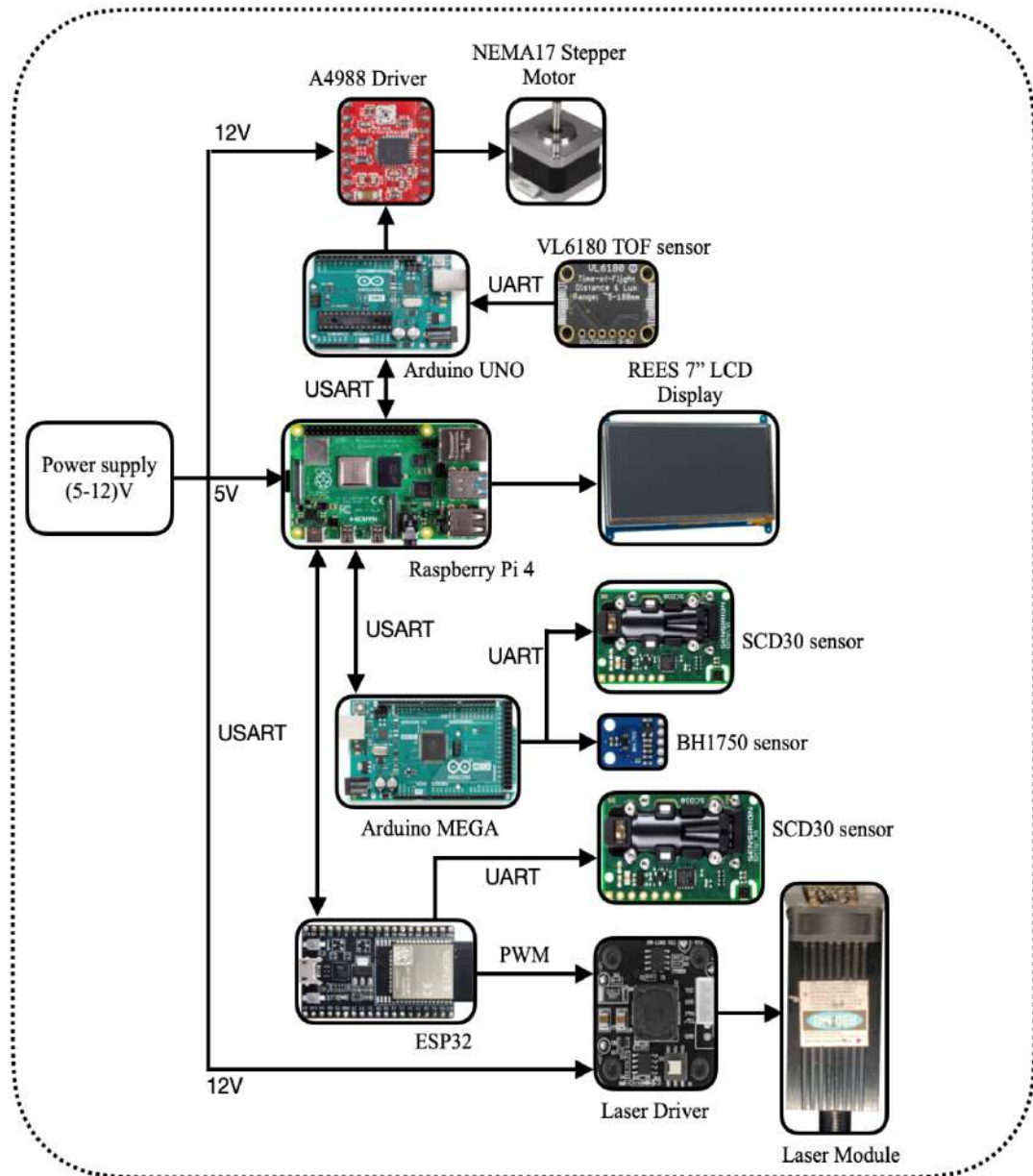


Figure 4.2 LBM Block diagram with sensors

Figure 4.2 depicts the block diagram of all the systems that are on-board the machining setup. The system's block diagram is made up of three primary branches that are interdependent on one another for distinct sets of values and readings.

The first is a 12 V supply to the laser module (Section 4.2.6), which has an input electrical power of 20 W and an average output optical power of 5.5 W.

To control the laser beam, a laser driver module is present. Another power supply branch is delivered to the A4988 Stepper driver (Section 4.2.9), which is utilised to control the NEMA-17 stepper motor (Section 4.2.8) that is used to control the machining system's X and Y axes. At a feed rate of 300 mm/min, this driver efficiently controls the stepper with precision. Finally, the power is directed to the Raspberry Pi 4B (Section 4.2.1), which is responsible for integrating all of the components and sensors available through the medium of an operating system based on the Debian Linux system architecture, and is then connected to a 7-inch touch display, allowing the user to interact with the display via touch. This raspberry Pi also includes the open-source computer-aided modelling software "Open Builds" (Section 4.6.1), which is used for effective control over the machining processes. The Raspberry Pi (Section 4.2.1) is then linked to an Arduino UNO microcontroller board, which is utilised to drive the z-axis stepper motor based on the distance from the machining centre as detected by the time-of-flight VL6180X sensor. This 3.3V sensor uses IR light irradiation technology to detect distance from the laser beam focus point to the surface of the machining centre. When directed by the Raspberry Pi, the ESP-32 microcontroller generates a pulsed signal to the laser driver linked to the laser module by altering input parameters such as the operating frequency and duty cycle (Section 4.3.3) of the pulse wave produced and thus controlling the laser power. The user can view the values from all of the microcontrollers and sensors on the touch display panel (Section 4.2.2).

4.2 Electronic components

Table 4.1 Electronic Components

S.No	Components	Specifications	Quantity
1	Raspberry Pi 4B	4GB RAM	1
2	Touch Screen	7-inch	1
3	Arduino MEGA	ATMega2560	1
4	Arduino UNO	ATMega328P	1
5	ESP-32 board	320 Kb SRAM	1
6	Laser diode module	20 W	1
7	CNC Control board	Cronos board	1
8	Stepper Motor	NEMA-17	3
9	Stepper Driver	A4988	3
10	Time of flight Sensor	VL6180x	1
11	Lux Sensor	Gy30-BH1750	1
12	CO ₂ sensor	SCD30	2
13	Arbitrary Waveform Generator	SDG1010	1
14	Mixed signal Oscilloscope	MSOX2004A	1
15	USB Digital microscope	Celestron digital microscope	1
16	Pocket Weighing machine	0.01 precision	1
17	Limit switches	-	6
18	Cables	USB A-micro-USB B	3
19	Switches	-	2
20	Suction fan	12V	2
21	Lighting	20 W Tube	1
22	Power Supply	24V-10W	1

4.2.1 Raspberry Pi 4B

Raspberry Pi is a small CPU with a 64-bit quad-cortex A72 ARM v8, Broadcom BCM2711, and a processing rate of 1.5 gigahertz. Raspberry Pi features can be summarised as follows:

- It is used to integrate machining to a touch interface, eliminating the need for a personal computer throughout the process.
- It is used to control machining with the open-source Open Builds CNC (Section 4.6.1) controller loaded on the Pi via the Raspberry Pi OS v4.
- It is used to display the readings from all of the sensors that have been connected to the Arduino microcontrollers as well as the ESP32 microcontroller which controls the PWM (Section 4.2.5).



Figure 4.3 Raspberry Pi 4B

The machining operations were configured using the interface software via the touch display on top of the setup. Table 4.2 indicates Raspberry Pi 4B Specifications.

Table 4.2 Raspberry Pi 4B Specifications

S.No	Parameters	Specifications
1	RAM	4 GB
2	CPU	Arm Cortex-A72
3	Operating Voltage	5V
4	Gpio communication	28 I/O Pins
5	Operating current	2.8 - 3 A

4.2.2 Touch Screen

Figure 4.4 shows a REES 7-inch capacitive multi-touch display that has been installed and interfaced with the Raspberry Pi 4B to display all of the data from various sensors as well as manage and monitor the machining processes.



Figure 4.4 REES 7" LCD Display

It has been connected to the Raspberry Pi via the HDMI connection port, and a USB power source that has been given to the display by the Raspberry Pi.

4.2.3 Arduino MEGA microcontroller

The Arduino MEGA 2560 is a microcontroller board that runs using the ATmega 2560 CPU. It has 54 digital I/O pins, in which 16 are analogue inputs, 4 of which are UARTs, a 16 MHz oscillator, and a DC power supply pin for power supply. Figure 4.5 shows Arduino MEGA microcontroller.

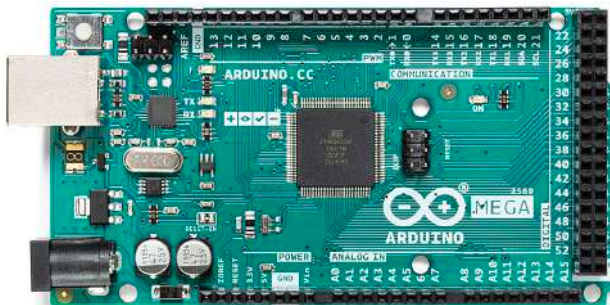


Figure 4.5 Arduino MEGA

This microcontroller is used to interface the lux meter sensor GY30-BH1750 (Section 4.2.11) along with one of the SCD30 (Section 4.2.12) sensors placed in the exterior part of the system in order to measure the CO₂ emission after filtration and

then send them to the display by attaching it to the Raspberry Pi via serial USB communication.

The specifications of the Arduino Mega is mentioned in the Table 4.3.

Table 4.3 Arduino MEGA specifications

S.No	Parameters	Specifications
1	Microcontroller	Mega 2560
2	Processor	ATmega2560
3	Analog I/O	16
4	Digital I/O	54
5	Operating Voltage	5V

In the Arduino MEGA setup, the Luxmeter sensor-GY30 is connected to SCL, SDA, VCC, GND, while SCD30 is also attached to the same SCL, SDA in a parallel connection.

4.2.4 Arduino UNO R3 microcontroller

Arduino UNO microcontroller interfaces with the VL6180X tof sensor to obtain the distance input and then controls the Z axis NEMA-17 stepper motor (Section 4.2.8) with the A44998 stepper driver (Section 4.2.9) to achieve a closed loop Standoff Distance control (SOD). Figure 4.6 shows the Arduino UNO R3.

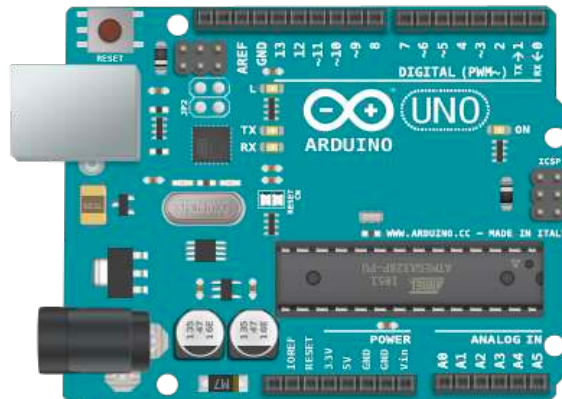


Figure 4.6 Arduino UNO R3

The specifications of Arduino Uno R3 that has been implemented are given in the Table 4.4.

Table 4.4 Arduino UNO R3 specifications

S.No	Parameters	Specifications
1	Microcontroller	Uno R3
2	Processor	ATmega328P
3	Analog I/O	14
4	Digital I/O	6
5	Operating Voltage	5V

Finally, all of the output from this Arduino is transferred to the display via serial communication with the Raspberry Pi.

4.2.5 ESP32 microcontroller

The Espressif systems ESP32 is a low-cost flexible microcontroller developer board with a large number of peripheral connectors based on the System on Chip (SoC) architecture. It also includes a WIFI and Bluetooth connection, making it easier to integrate wirelessly with a variety of devices. Figure 4.7 shows the ESP32 microcontroller.

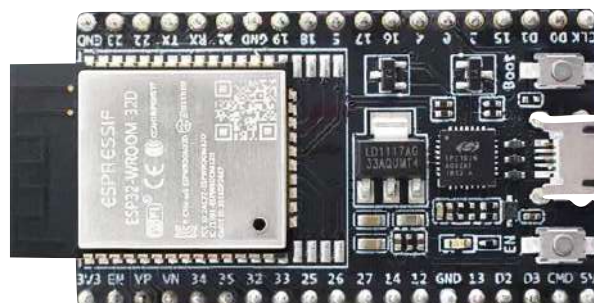


Figure 4.7 ESP32 microcontroller

Because of its broad capabilities of producing control signals of up to 80 MHz, the board was used to implement the pulse width modulation control of the laser diode. The technical specifications of the microcontroller can be observed from Table 4.5.

Table 4.5 ESP32 microcontroller specifications

S.No	Parameters	Specifications
1	Microcontroller	ESP 32
2	Processor	Xtensa LX6
3	LED PWM	16 channels
4	ADC	12-bit
5	GPIO	34 pins

In addition, one of the carbon dioxide (CO_2) emission measurement sensors SCD30 (Section 4.2.12), which is located in the system's interior, has been attached to the analogue pins of the controller, which is afterwards interfaced to the Raspberry Pi via a universal serial bus connection.

4.2.6 NEJE Laser diode Module

The laser diode is a power-driven electronic device that generates a pulsed laser beam and machines the object placed beneath it. Laser diodes are forward-biased devices that operate in the V-I curve's positive area. The length of the p-n junction found in this type of diode corresponds to the wavelength of the light beam generated by the laser. Figure 4.8 shows the NEJE 20W laser diode used in the LBM with adjustable focal length.



Figure 4.8 NEJE 20W laser diode

When an external voltage is applied to the diode, electrons begin to move, and when they recombine into available holes, photons are released. This photon then hits an atom, releasing another photon, and as the voltage increases past the breakdown

voltage, more photons are released, producing a laser beam. The general specifications of the laser has been given in the Table 4.6.

Table 4.6 NEJE 20W specifications

S.No	Parameters	Specifications
1	Laser Power	20W
2	Wavelength	450nm
3	Optical laser power	5.5W
4	Operating parameters	12V-5A
5	Color	Blue
6	Maximum Frequency	20 kHz

The laser utilised in this experiment is a 20W laser with a wavelength of 450nm, and the laser beam is blue in colour due to the wavelength being at that specific range.

4.2.7 CNC control board

The CNC control board that has been installed serves as the machining assembly's brain. It is made up of numerous resistors, capacitors, and timer circuits that are used to maintain and manage the machining process. The Arduino UNO, which is incorporated in the created Printed circuit (PCB), is the major component that connects all of the components on this board. This control board is controlled by the Raspberry Pi via a USB connection. Figure 4.9 depicts an illustration of the control board that is being used.

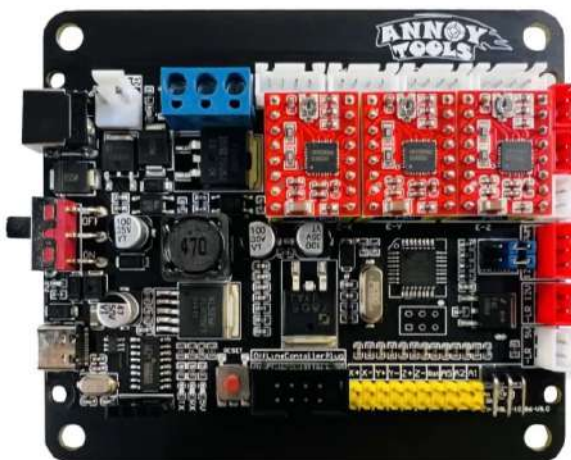


Figure 4.9 CNC Control board

In addition, an interpreter named Grbl v1.1 that transforms code from SVG to Gcode has been burned to the Arduino shield, allowing us to send Gcode and perform the machining process.

4.2.8 NEMA-17 stepper Motor

The NEMA-17 stepper motor, depicted in Figure 4.10, is a brushless stepper motor with a step angle of 1.8° and a maximum rpm of 2000.



Figure 4.10 NEMA-17 4 pin stepper motor

Along with the lead screw and linear bearing systems, three stepper motors have been utilized. Two of these stepper motors, which control the X and Y axes of the machining process, are connected to the CNC control board and interface to the display via Raspberry Pi and CNC control software, while the third stepper, which controls the Z axis, is connected separately to another Arduino UNO R3, which has the necessary code for the implementation of control loop. Table 4.7 shows the configuration of the NEMA-17 bipolar stepper that has been incorporated in the system.

Table 4.7 NEMA-17 stepper motor specifications

S.No	Parameters	Specifications
1	Model name	Nema-17 Bipolar
2	Direction	Bidirectional
3	Step angle	1.8°
4	Operating voltage	2.3V
5	Steps per revolution	200
6	Rated Current	0.8 A

4.2.9 A4988 Stepper driver

A4998 Stepper drivers are electronic circuits that are used to micro-step the stepper motor. This specification makes use of three different drivers, two of which are placed in CNC control for X and Y axes control and the third one which is connected independently to Arduino UNO R3 to control the Z axis stepper in order to achieve standoff distance control loop. Figure 4.11 shows the A4988 stepper driver.

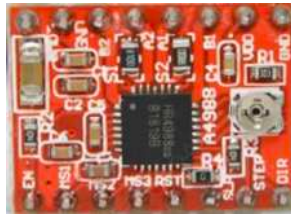


Figure 4.11 A4988 stepper driver

These drivers direct the stepper in both directions, allowing it to do accurate cutting.

4.2.10 VL6180X Time of flight (tof) sensor

The VL6180X is a sensor that can measure a target from a distance of up to 40cm using time-of-flight infrared pulses. The sensor combines proximity ranging with ambient light sensing in a single device, allowing it to precisely measure the duration between the emission of an infrared pulse and its reflection return to the sensor and properly determine distance. Figure 4.12 shows the VL6180X tof sensor.



Figure 4.12 VL6180X tof sensor

It has been employed in the implementation to calculate the standoff distance, which is the effective spacing between the diode laser unit and the machining centre. The technical specifications of the VL6180X tof sensor utilised can be observed in the Table 4.8.

Table 4.8 VL6180X tof sensor specifications

S.NO	Parameters	Specifications
1.	Sensor	VL6180X
2.	Range	Up to 40cm
3.	Resolution	1mm
4.	Operating voltage	2.7 to 5.5V
5.	Input Current	5 mA

4.2.11 GY30 BH1750 Lux meter sensor

The BH1750 is a digital light sensor with a high range of luminance values (0-65535 lx). It used to measure the intensity of ambient light in terms of lx units. This sensor has been implemented to detect the intensity of the laser beam produced by the laser diode and this sensor has been interfaced with the Arduino MEGA along with the SCD30 (Section 4.2.12) subsequently to be displayed through the display screen present. The image of this sensor used can be seen in Figure 4.13.



Figure 4.13 GY30 BH1750 sensor

4.2.12 SCD30 CO₂ Sensor

The SCD30 sensor detects the presence of carbon dioxide CO₂ in the environment. It is equipped with a very efficient type of particle detection known as Non-dispersive Infrared (NDIR) and operates on a 5V power source. The sensor was used in this venture to quantify the amount of carbon dioxide emitted in parts per million (ppm) and was positioned both within and outside the system and to determine the emission before and after filtering. Figure 4.14 shows the SCD30 sensor



Figure 4.14 SCD30 Sensor

One of the sensors is located inside the system and is linked to the ESP32, while the other is located outside the system and is connected to and interfaced with the Arduino MEGA.

4.2.13 Arbitrary Waveform Generator

An arbitrary waveform generator is an electronic test instrument which is used to produce electrical waveforms. Figure 4.15 shows the Arbitrary Waveform Generator.



Figure 4.15 Arbitrary Waveform Generator

These waveforms can be repeating or one-shot in nature, in which instance a triggering input is necessary. The technical specifications of this waveform generator can be observed from the Table 4.9.

Table 4.9 Arbitrary Waveform Generator Specifications

S.No	Parameters	Specifications
1	Bandwidth	10 MHz
2	Sampling rate	125 MSa/s
3	Resolution	14-bit
4	Channel	Dual
5	Clock Input	10 MHz

The Arbitrary waveform generator of model SDG1010 from the manufacturer Siglent has been implemented in the system in order produce pulse width modulated signal for controlling the laser power and thereby perform cuts on leather of the requisite amounts and the results have been recorded using the Taguchi orthogonal array (Refer chapter 5).

4.2.14 Mixed signal Oscilloscope

A mixed signal oscilloscope (MSO) is a special type of digital storage oscilloscope that is capable of displaying and comparing analogue and digital signals. Figure 4.16 shows the Mixed signal oscilloscope.

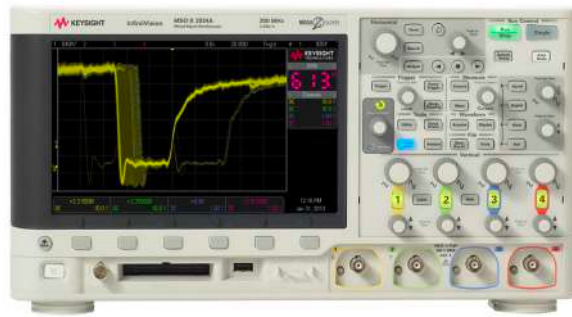


Figure 4.16 MSO

The Multi signal oscilloscope from the manufacturer Keysight technologies of the model Infivision MSOX2004A has been implemented in order to observe the signal generated by the arbitrary waveform generator and ESP32 in a simultaneous manner hence making it easier for comparison. The technical specifications of the mixed signal oscilloscope utilised is observed in Table 4.10.

Table 4.10 MSO Specifications

S.No	Parameters	Specifications
1	Bandwidth	70 MHz
2	Sampling rate	2 GSa/s
3	Memory depth	1 Mpts
4	Channel	Dual
5	Calculated rise time	5 ns

4.2.15 USB Digital Microscope

A digital microscope is a kind of a microscope that use optics and a digital camera to generate an image to a display, sometimes via computer-based software (Section 4.6.4). Figure 4.17 shows the Celestron digital microscope being used to capture the accurate image of the edge contour of the leather sample.



Figure 4.17 USB Digital microscope

The digital microscope that has been used is the Celestron Digital Microscope Pro from the manufacturer Celestron with the true 5 Megapixel image capture resolution and an optical zoom of 200X.

4.2.16 Handheld weighing scale

A handheld weighing scale with a precision of 0.01 g has been implemented in order weigh the leather samples before and after machining process thereby measuring it for determining the material removal rate (Refer Chapter 5). Figure 4.18 shows the pocket-sized weighing scale.



Figure 4.18 Handheld weighing scale

4.2.17 Limit switches

Limit switches are electromechanical devices installed in the machining equipment to define the cutting workspace suitably and to identify the end position of the moving objects. Figure 4.19 shows the Limit switches which are implemented.



Figure 4.19 Limit switches

Six limit switches are installed at each axis's extremities to regulate movement toward the ends, and they are all coupled to the resetting pins of the Arduino shield on the CNC controller unit.

4.2.18 Cables

Universal serial bus A (USB-A) serial port to Micro universal serial bus B (microUSB B) cables have been implemented in order to provide connections between different microcontroller board utilised in the system to the Raspberry PI serving a dual purpose of providing the power supply as well as establishing serial connection to the board through the Universal Synchronous Asynchronous receiver Transmitter (USART) communication protocol.



Figure 4.20 Cables

Figure 4.20 illustrates the usb cable utilised to connect the Arduino MEGA, Arduino UNO and ESP32 to the Raspberry Pi microcomputer board.

4.2.19 Switches

Multiple switches have been used in the system for various purposes namely:

- Push button : Push buttons used for the switching of laser diode and also for the emergency stop button connected directly to the machining board. Figure 4.21 shows various switches used in the system.



Figure 4.21 Push button and switches

- ON/OFF single switch: On/off switches are used to control the lighting of the system present in the interior part and also to switch between manual and adaptive modes of standoff distance control.

4.2.20 Suction fans

The suction fan is the CPU coolant fan, which operates at a voltage of 12V. These fans are used to extract gaseous fumes produced during machining process and direct them through the Emission filtering chambers (Chapter 3 3.5.4). Figure 4.22 shows various switches used in the system.



Figure 4.22 Suction fans

4.2.21 LED lighting

LED tube lighting has been used in enclosure setup for providing an aesthetic appeal to the whole project. Figure 4.23 displays the lighting tube.



Figure 4.23 LED Light

Also, this lighting helps to view the machining processes properly. It operates with a supply of 12V.

4.2.22 Power Supply Unit

The complete power supply for the entire system is drawn through a multi-socket junction box providing the voltage directly from the mains and connects to the LBM setup, the Raspberry Pi, LED Light and the suction fan placed in the enclosure setup. Figure 4.24 shows the Socket adapter.



Figure 4.24 Multi-Socket adapter

The various voltage requirement of the module and components connected to the power supply unit is listed:

- Raspberry Pi - Connected to one of the sockets drawing 5V-2A and subsequently powering the microcontrollers Arduino MEGA and ESP32 through USB connections and also the touch screen through usb connections.

- Arduino UNO - Connected to one of the sockets through a 3-pin to USB converted power supply and 5V-2A .
- CNC machining system : The CNC is connected to one of the sockets available and draws 24V-3A from the power supply unit powering the entire control board as well the laser module.

4.3 Control system mechanisms

4.3.1 Standoff Distance adaptive closed loop mechanism

Figure 4.25 shows block diagram Standoff Distance (SOD) regulator, which is coupled to the Laser Beam Machine (LBM) Z axis. The SOD control hardware consists of an Arduino UNO, which is in charge of carrying out the determined SOD utilizing the stepper control in collaboration with a stepper motor and an VL6180X tof sensor. Also, the supply is split into two parts in which one goes into the stepper driver with 12V capacitance conditioning and one into the Arduino for 5V. The VL6180X tof sensor is a STMicroelectronics type with a range of 1mm - 40cm and an operating current of 5mA. The sensor is used to determine the distance measure in between the laser module and the workbench. The distance measured is fed into the Arduino UNO microcontroller. The A4988 driver board is used to control the Stepper motor's orientation and the step degree. It operates with a 5V supply and a motor input of up to 35V, in our case 12V, with capacitance conditioning.

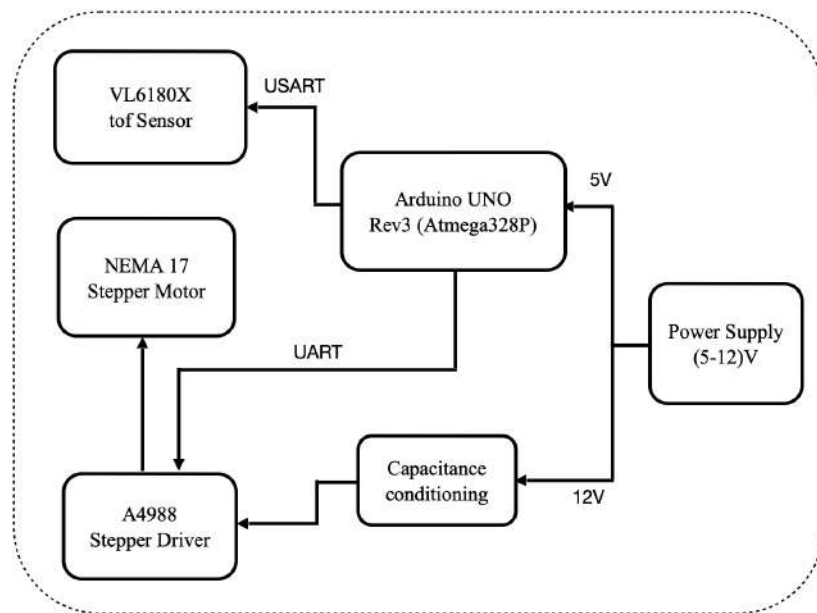


Figure 4.25 SOD block diagram

The stepper motor utilised is a NEMA-17 bipolar stepper motor with holding torque of 176 N mm and have high efficiency. Figure 4.26 depicts the schematic diagram of the standoff distance control loop.

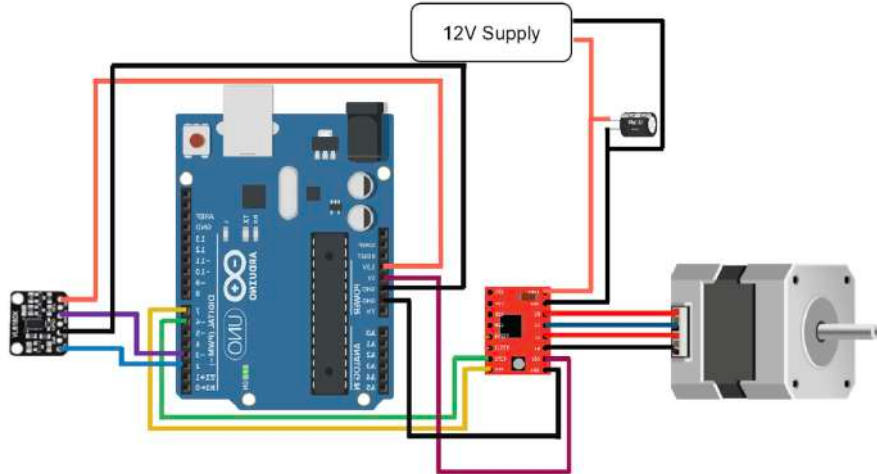


Figure 4.26 Schematic diagram of the SOD loop

Figure 4.27 portrays the main algorithms executed by the Arduino UNO R3 to set the predetermined SOD, which are divided into four parts: (i) overall hardware and communication control (Standoff computing); (ii)distance measurement (tof_exec); (iii) stepper control clockwise (stepper_ctrl_clock); and (iv) stepper control anti-clockwise (stepper_ctrl_anti). C++ is used to program and execute these algorithms in Arduino Software (IDE).

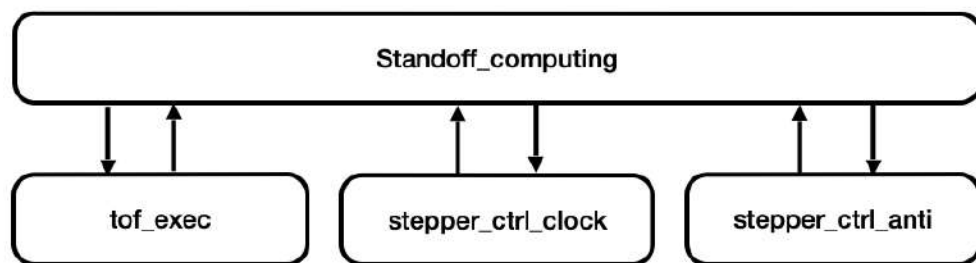


Figure 4.27 Algorithm executed on Arduino UNO

4.3.2 Pulse Width Modulation control mechanism

The Pulse Width Modulation (PWM) control system has been developed in order to control various parameters of the laser diode thereby control the laser's beam intensity. It has been carried out with the parameters of Duty cycle and Frequency

varying in three different levels each and in two different modes such as the Arbitrary waveform generator and then using ESP-32 microcontroller.

4.3.2.1 PWM using Arbitrary waveform generator

The arbitrary waveform generator is connected to the laser control board, and the duty cycle is varied manually between 70%, 75%, and 80%, as well as the operating frequency between 16KHz, 18KHz, and 20KHz. The results are recorded in the Taguchi orthogonal matrix in a L9 array (Chapter 5), with each value iterated three times for greater precision. The results of the cuts would be examined in further detail in the next upcoming chapter. The connection of the arbitrary waveform generator to the laser is seen in Figure 4.28. A multi-oscilloscope has been added to the circuit to allow viewing of the generated signal.

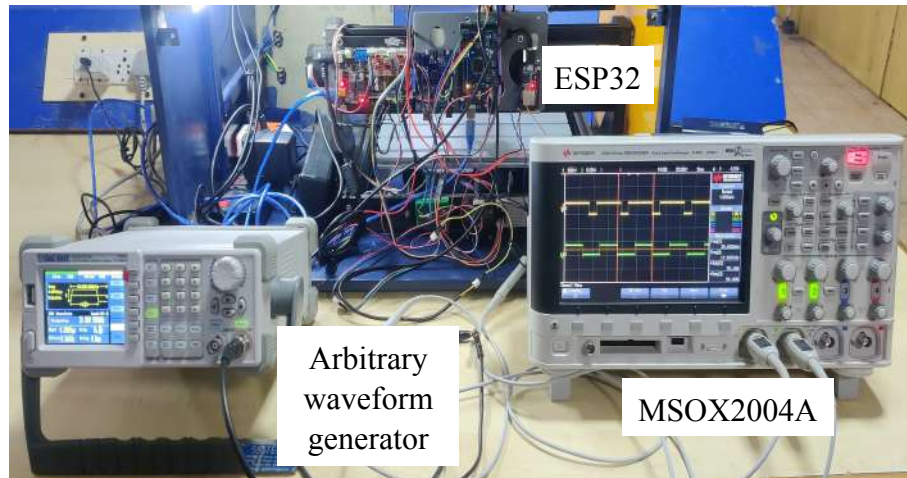


Figure 4.28 MSO, ESP32 and Arbitrary waveform generator Setup

4.3.2.2 PWM using ESP32 microcontroller

The ESP-32 is used in place of the arbitrary waveform generator to generate the pulse width modulated signal and control the laser module in the circuit. Duty cycle is varied between 70%, 75%, and 80%, while frequency is varied between 16KHz, 18KHz, and 20KHz. cuts are conducted using the Taguchi L9 orthogonal array, with each value iterated three times for more precision.

Additionally, increased and automatic control has been obtained by substituting the ESP-32 for the arbitrary waveform generator and developing a graphical user

interface that enables the user to dynamically alter the frequency and duty cycle in an intelligible manner. Figure 4.29 shows the schematic diagram of ESP32 control.

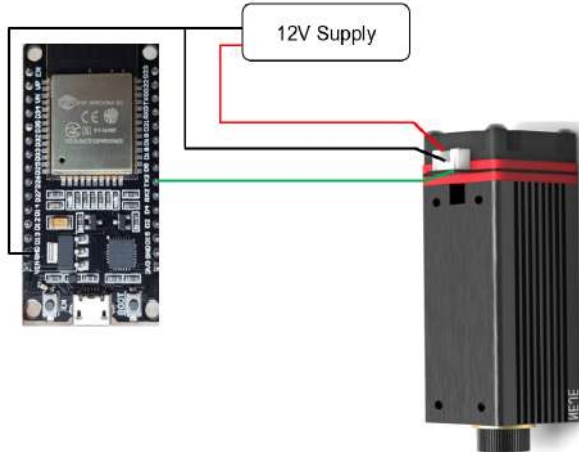


Figure 4.29 ESP32 and laser diode schematic diagram

4.4 Graphical user interface

4.4.1 Analysis Graphical user interface (GUI)

A complete software panel along with graphical user interface has been developed using python programming language thorough the tkinter library for the analysis of leather material which have been cut using laser diode and to find out the amount of carbonization. Figure 4.30 shows the GUI of Carbonization Analyser.

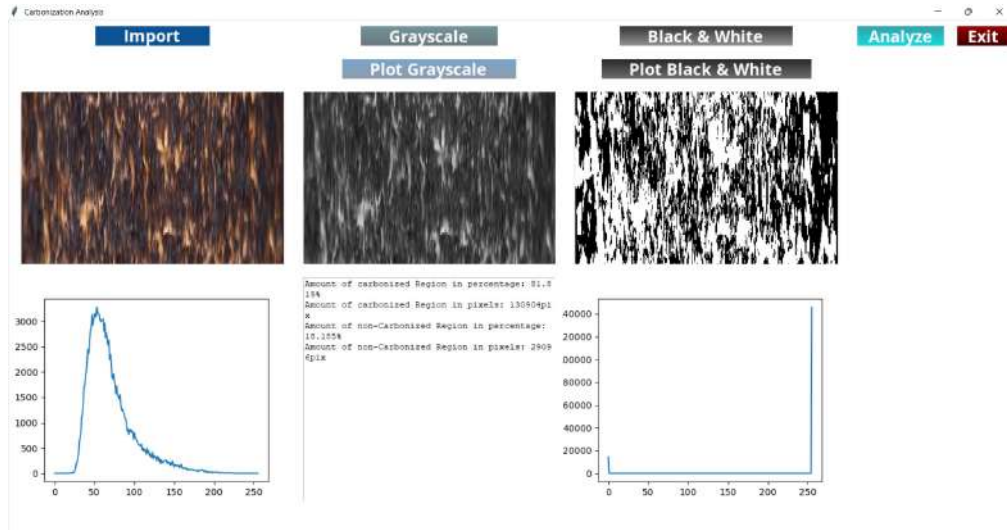


Figure 4.30 Carbonization Analyser GUI

Its functionalities are as follows:

- Import: Import button is used to import in the surface cross-section image in joint picture graphics format (JPEG) and displays it on the canvas after resizing it to 400 x 400 square.
- Grayscale: Grayscale button is used to convert the imported image into a grayscale image and displays it out on the canvas.
- Black & White: Black & White button is used to convert the grayscale image in the previous step into a black and white image for performing the analysis.
- Analyse: Analyse button is used to perform the analysis by finding out the number of black pixels subsequently finding out the amount of heat affected zone on the surface cross-section of machined leather. This analysis is then depicted directly on the canvas just below the image with details pertaining to amount of carbonized and non-carbonized region in both pixels and percentages.
- Plot Grayscale: Plot grayscale is used to plot the image histogram of the grayscale image generated when the grayscale button was pressed.
- Plot Black & White: Plot Grayscale is used to plot the image histogram of the black and white image from the black and white button after it has been pressed.
- Exit: Exit button is used to exit from the software.

The image processing algorithm that has been implemented in the graphical user interface can be elucidated briefly through the following steps:

Step 1: The execution of the program starts with import of image from the necessary path folder.

Step 2: After importing, the image is resized to predefined 400 x 400 dimensions and then it is converted to grayscale utilising the OpenCV's cv2 library function and displays to the user.

Step 3: The converted grayscale image is then converted to a black and white image through the threshold method of OpenCV library and this image is displayed to the user.

Step 4: After the thresholding process, the image is fed into the analysis part of the programming where the countNonZero method of OpenCV library counts the pixels of the image that are in white.

Step 5: The determination of amount of white pixels subsequently leads to the determination of black pixels through the formula listed.

$$Black\ pixels = Total\ pixels - White\ pixels \quad (\text{Eqn. 4.1})$$

Step 6: In similar fashion, the percentage of the black and white pixels are determined using the Eqn 4.2 and Eqn 4.3.

$$\text{Percentage of Black pixels} = \frac{\text{Black Pixels}}{\text{Total pixels}} \times 100 \quad (\text{Eqn. 4.2})$$

$$\text{Percentage of White pixels} = \frac{\text{White Pixels}}{\text{Total pixels}} \times 100 \quad (\text{Eqn. 4.3})$$

Step 7: At last, all the determined values are displayed to the user through a text box layout and the analysis is complete.

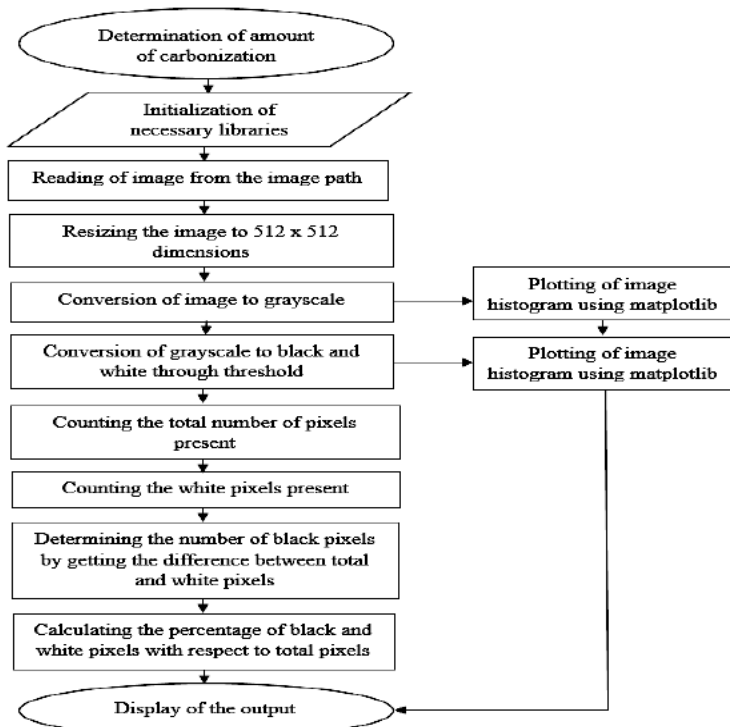


Figure 4.31 Working algorithm

4.4.2 Sensor integration Graphical User Interface

A GUI has been developed to facilitate the integration of all sensors connected to the Raspberry Pi via a USB connection. This interface enables the operator of the machining system to view the emission in parts per million and control the laser module's power in nine distinct scales via several three-level systems.

The interface's components can be explained as follows:

- Display Internal ppm: This is a tkinter library button that reads the data from the internal carbon dioxide emission sensor SCD30 linked to the ESP 32 and displays it in parts per million units in the third column.
- Display External ppm: This is a tkinter library button that reads data from the external CO₂ emission sensor SCD30 attached to the Arduino MEGA and displays it in parts per million units in the third column.
- Display Internal Lux: This is another tkinter library button that reads the output data of the BH1750 lux meter sensor and displays it in the third column of the same row in lux units.
- PWM control slider: The tkinter scale slider is configured in such a way that levels 1, 2, and 3 have the same frequency (16 KHz) but different laser powers, while levels 4, 5, and 6 have the same frequency (18 KHz) but different laser powers, and levels 7, 8, and 9 have the same frequency (20 KHz).
- Control laser power: This is a tkinter library button that interacts with all the controllers attached to the Raspberry Pi and transmits the command to control the laser power using the pulse width modulation approach.

Figure 4.32 illustrates the GUI developed and this interface is touch interactive and runs smoothly on the Raspberry Pi microcomputer board present in the system.

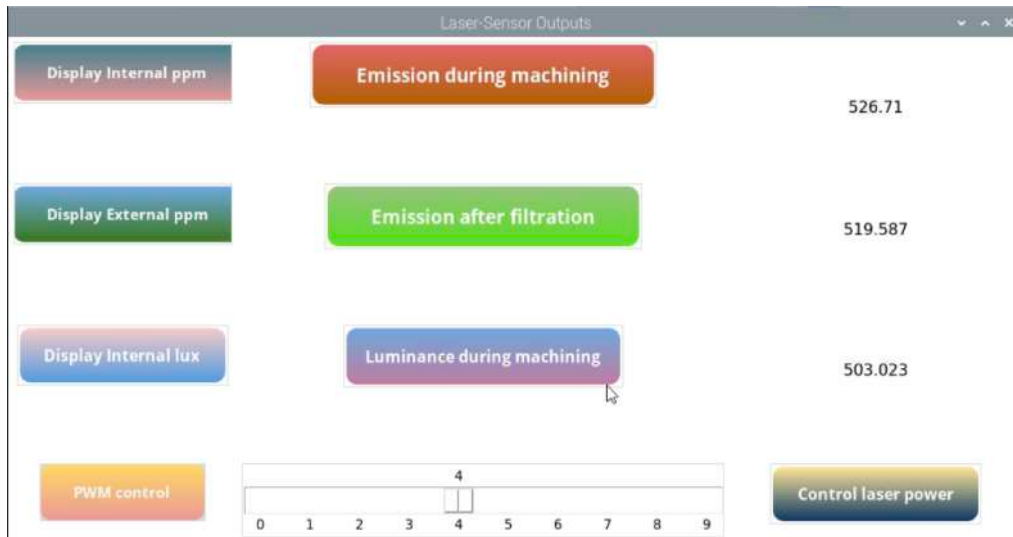


Figure 4.32 PWM GUI

4.5 Software

There are number of software that have been incorporated and are used in multiple occasions for several requirements of the system .

4.5.1 Open Builds CNC control

Open Builds CNC control is an open-source CNC machining control software that has been integrated into the processing unit of the Raspberry Pi microcomputer that is installed in the system, allowing the user to control the machining setup via an interactive touch interface, removing the need for a computer machine. The Figure 4.33 depicts the sample interface look of the software that is running on the Raspberry Pi and viewable by the user through the touch screen. Thus, this fulfils one of the important objectives of the system of eliminating the usage and requirement of a personal computer for the control of the CNC machining setup.

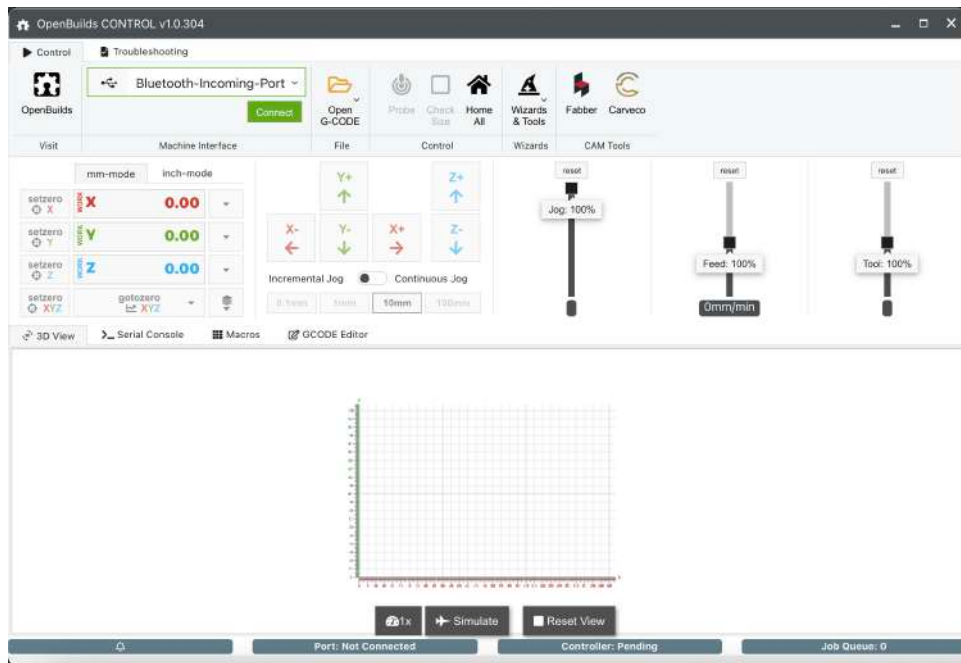


Figure 4.33 Open Builds CNC control software

4.5.2 LaserWeb

LaserWeb CNC Control is an open-source software that has been used to control the machine through a computer machine for calibrating it properly and testing purposes. One of the main advantage of the LaserWeb software is its conversion of image to Vector SVGs and then to Gcode. It can be used in Laptops and Desktops. Figure 4.34 shows the LaserWeb software.

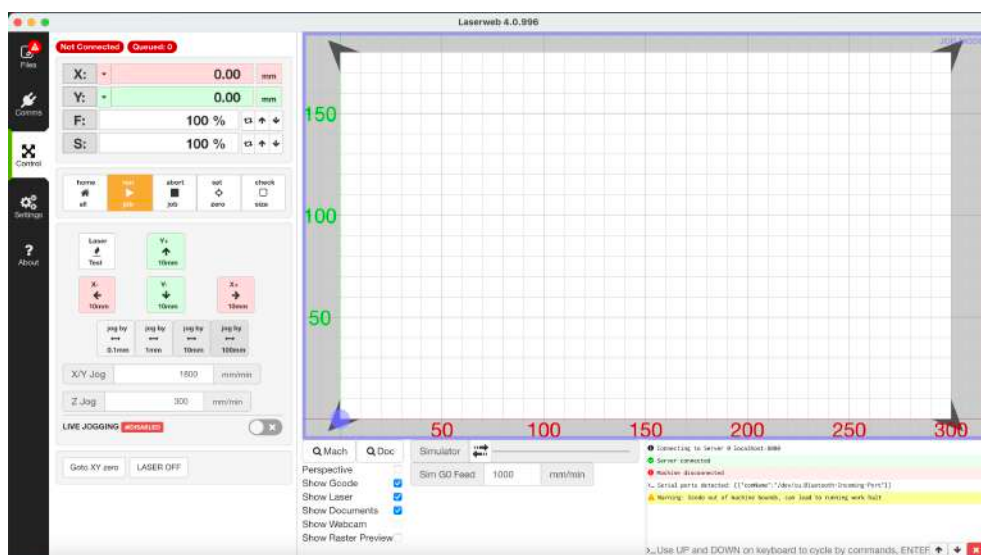


Figure 4.34 LaserWeb CNC control software

4.5.3 Virtual Studio Code

Virtual Studio (VS) Code is an open-source programming code editor software that has been used in the setup in order to program both the graphical user interfaces elucidated previously. The programming has been done in Python programming language – *PY 3.8.8 anaconda* interpreter as its base. Figure 4.35 shows the VS code interface.

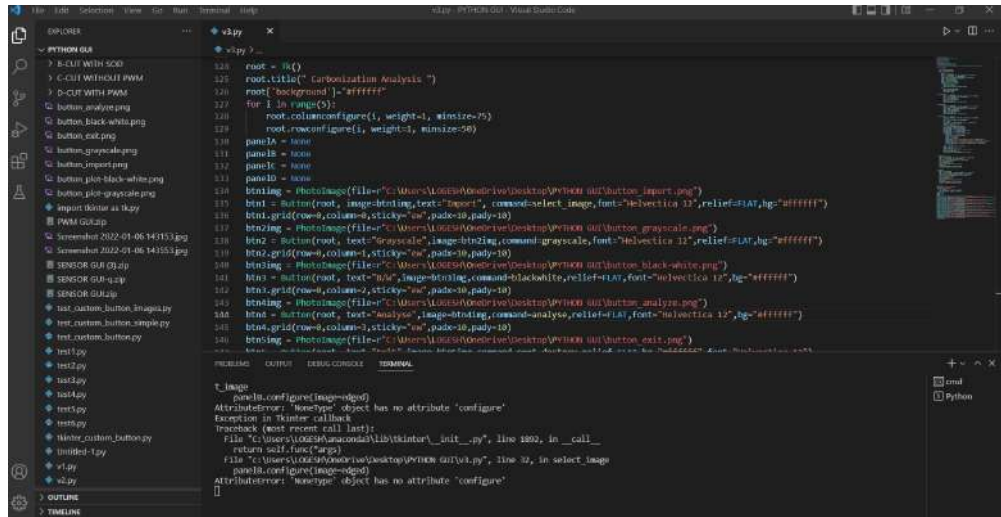


Figure 4.35 VS code Software interface

4.5.4 Celestron Microcapture Pro

Celestron's proprietary software for its digital microscope has been used in order capture the images and calculate the kerf widths of the leather samples with a magnification calibration of 58.2 scale. Figure 4.36 shows the Celestron Microcapture Pro interface.

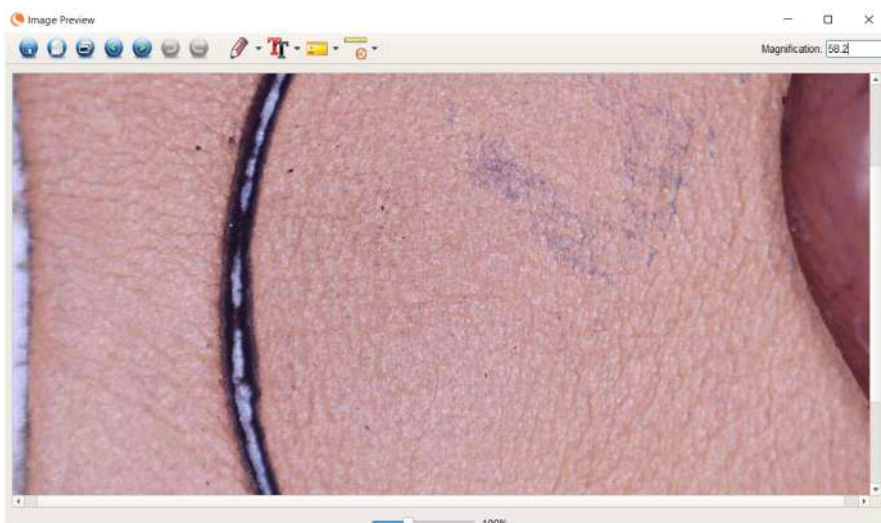


Figure 4.36 Celestron Microcapture Pro

CHAPTER 5

RESULTS AND DISCUSSION

5.1 Experimental setup

The fabricated Laser Beam Machining (LBM) setup with an enclosure, which has the laser diode as its cutting tool has been used to cut leather. Different ranges of input parameter and its output parameters have been taken into account to further modify and optimise the LBM system for leather cutting. Figure 5.1 shows the LBM setup for the experimentation.

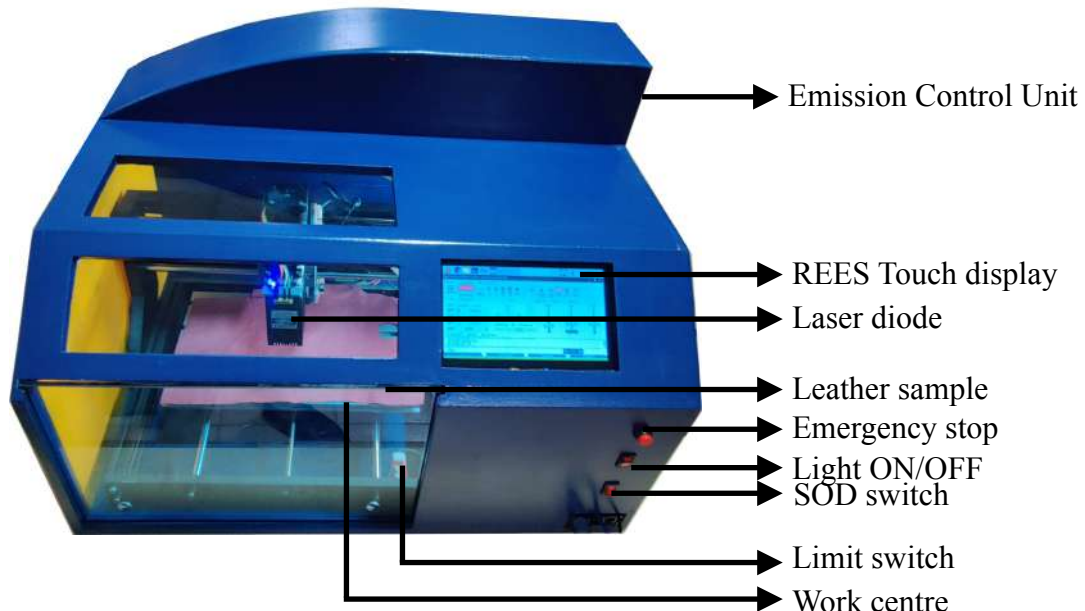


Figure 5.1 LBM setup

5.2 Parameters

Parameters are quintessential to conduct and conclude an experiment to understand the characteristics and properties, determining the particular distributions to optimise the variables.

5.2.1 Input parameters

5.2.1.1 Standoff Distance

Standoff Distance (SOD) is the distance between the laser diode nozzle and the work centre. In the forthcoming experimentation three levels of SOD values of 18 mm, 20

mm, and 22 mm have been considered to optimise the carbonization and kerf width values.

5.2.1.2 Feed rate

Feed rate is defined as the laser diode distance traveled in X-Z axis during one revolution of stepper motor. Three ranges of 200 mm/min, 250 mm/min and 300 mm/min are used in the forthcoming experimentation which could optimise the material removal rate.

5.2.1.3 Pulse Width Modulation

Pulse Width Modulation (PWM) is a technique for minimising the average power produced by an electrical signal by breaking it down into discrete components.

5.2.1.3.1 Duty cycle

Duty cycle is the percentage of laser in on mode when the pulses are emitted. This is achieved through the pulse width modulating ability of laser and therefore changing the values accordingly. The ranges that have been used here are 70%, 75% , 80% which were varied using the arbitrary waveform generator in one set of experimentation and using ESP32 PWM pin in another experiment of control system integration.

5.2.1.3.2 Frequency

Frequency of the laser module is defined as the number of laser pulses that is being emitted from the laser per second. The laser that has been used here has the maximum frequency of 20000 Hz and therefore, the ranges of 16000 Hz, 18000 Hz and 20000 Hz have been considered in order to vary and obtain the results during experimentation.

5.2.2 Output parameters

5.2.2.1 Carbonization

On leather cutting using laser ablation technique, the contour edges of the machined leather produces carbon due to the pyrolytic process, since leather is a biomaterial.

This process is known as carbonization on leather edges. In this experimentation, carbonization percentage will be identified using Carbonization Analyser GUI.

5.2.2.2 Material removal rate

Material removal rate (MRR) is considered as an output parameter to determine the leather material removed per unit time.

$$MRR = \frac{Weight\ before\ cut - weight\ after\ cut}{Time\ taken} \frac{mg}{sec} \quad (\text{Eqn. 5.1})$$

5.2.2.3 Kerf width

Kerf width (KW) is the removed material width during machining process. Figure 5.2 indicates the Kerf width in the machined leather.

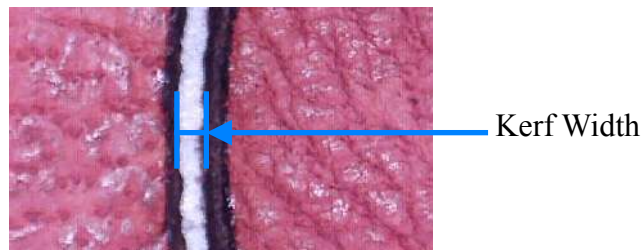


Figure 5.2 Kerf width

5.2.2.4 Emission rate

Fumes are produced during the leather cutting process. Two SCD30 sensors measures the value of carbon in parts per million (ppm) during the machining process, one inside and on at the Emission control unit.

5.3 Selection of material and Geometric shapes

Currently three major type of leather materials is being used globally namely goat, cow and buffalo leather. The forthcoming experiments are conducted on chrome + vegetable tanned cow leather of thickness 0.8mm due to its wide range of applications. Circular shape of 30 mm diameter has been selected due to its intrinsic geometry. 135 cuts have been performed in chrome + vegetable tanned cow leather. These leather cuts, output parameters are analysed and optimised.

5.4 Taguchi orthogonal array

The Taguchi orthogonal array design is a form of tabular representation and optimisation technique which consider all the necessary factors required for a process to take place and form various combinations of them in order perform experimentations. There are various design available throughout but the 9-trial experimentation design - L9 Orthogonal array has been performed in this machining process. Table 5.1 and Table 5.2 represents the L9 orthogonal array with three and four factor.

Table 5.1 Three factor L9 orthogonal array

Trial No.	Standoff distance (mm)	Feed rate (mm/min)	Duty Cycle (%)
1	18	200	70
2	18	250	75
3	18	300	80
4	20	200	75
5	20	250	80
6	20	300	70
7	22	200	80
8	22	250	70
9	22	300	75

Table 5.2 Four factor L9 orthogonal array

Trial No.	Standoff distance (mm)	Feed rate (mm/min)	Duty Cycle (%)	Frequency (kHz)
1	18	200	70	16
2	18	250	75	18
3	18	300	80	20
4	20	200	75	20
5	20	250	80	16
6	20	300	70	18
7	22	200	80	18
8	22	250	70	20
9	22	300	75	16

5.4.1 Analysis on chrome + vegetable tanned cow leather

5.4.1.1 Analysing carbonization on chrome + vegetable tanned cow leather

Table 5.3 shows the carbonization value of conventional SOD control

Table 5.3 Conventional SOD control - A cut

Trial No.	Standoff distance (mm)	Feed rate (mm/min)	Duty Cycle (%)	Carbonization (%)			
				C1	C2	C3	C avg
1	18	200	70	56.47	56.45	55.80	56.240
2	18	250	75	52.24	68.53	64.33	61.701
3	18	300	80	56.42	61.30	59.78	59.165
4	20	200	75	56.42	59.59	51.79	55.932
5	20	250	80	55.67	58.89	47.38	53.978
6	20	300	70	52.50	58.39	67.64	59.509
7	22	200	80	59.37	56.13	48.69	54.727
8	22	250	70	49.41	55.99	69.27	58.223
9	22	300	75	53.67	49.78	47.17	50.204

Table 5.4 shows the carbonization value of SOD control using Arduino UNO - B cut

Table 5.4 SOD control using Arduino UNO - B cut

Trial No.	Standoff distance (mm)	Feed rate (mm/min)	Duty Cycle (%)	Carbonization (%)			
				C1	C2	C3	C avg
1	18	200	70	57.38	57.96	51.70	55.681
2	18	250	75	59.85	53.49	67.75	60.363
3	18	300	80	45.76	47.67	66.84	53.423
4	20	200	75	57.57	45.53	54.09	52.393
5	20	250	80	57.09	51.70	49.80	52.866
6	20	300	70	35.77	57.59	67.21	53.522
7	22	200	80	64.03	54.99	34.90	51.306
8	22	250	70	51.74	53.23	50.43	51.801
9	22	300	75	59.14	48.68	40.30	49.372

Table 5.5 shows the carbonization value of PWM control using Arbitrary waveform generator - C cut

Table 5.5 PWM control using Arbitrary waveform generator - C cut

Trial No.	Standoff distance (mm)	Feed rate (mm/min)	Duty Cycle (%)	Frequency (kHz)	Carbonization (%)			
					C1	C2	C3	C avg
1	18	200	70	16	48.18	52.24	49.79	50.068
2	18	250	75	18	52.33	49.93	68.83	57.031
3	18	300	80	20	42.31	60.52	43.22	48.682
4	20	200	75	20	50.95	35.66	36.65	41.086
5	20	250	80	16	42.44	44.11	65.15	50.567
6	20	300	70	18	51.01	51.82	53.41	52.077
7	22	200	80	18	55.80	51.77	44.88	50.817
8	22	250	70	20	51.27	44.44	49.12	48.278
9	22	300	75	16	42.55	40.65	50.26	44.485

Table 5.6 shows the carbonization value of PWM control using ESP32 - D cut

Table 5.6 PWM control using ESP32 - D cut

Trial No.	Standoff distance (mm)	Feed rate (mm/min)	Duty Cycle (%)	Frequency (kHz)	Carbonization (%)			
					C1	C2	C3	C avg
1	18	200	70	16	50.98	38.41	59.98	49.788
2	18	250	75	18	50.46	45.43	42.76	46.216
3	18	300	80	20	47.55	41.25	52.08	46.963
4	20	200	75	20	39.94	40.61	41.19	40.578
5	20	250	80	16	41.86	42.52	62.45	48.942
6	20	300	70	18	52.78	52.99	42.89	49.554
7	22	200	80	18	46.90	51.88	41.04	46.605
8	22	250	70	20	40.65	39.68	56.02	45.451
9	22	300	75	16	43.63	48.25	25.14	39.006

Table 5.7 shows the carbonization value of SOD and PWM control using Arduino UNO and ESP32 - E cut

Table 5.7 SOD and PWM control using Arduino UNO and ESP32 - E cut

Trial No.	Standoff distance (mm)	Feed rate (mm/min)	Duty Cycle (%)	Frequency (kHz)	Carbonization (%)			
					C1	C2	C3	C avg
1	18	200	70	16	48.23	46.17	46.81	47.070
2	18	250	75	18	41.12	40.98	40.01	40.703
3	18	300	80	20	44.36	42.64	44.57	43.857
4	20	200	75	20	38.89	37.43	39.71	38.677
5	20	250	80	16	39.87	40.15	38.16	39.393
6	20	300	70	18	39.94	40.18	39.87	39.997
7	22	200	80	18	45.38	42.59	44.74	44.237
8	22	250	70	20	42.86	43.19	42.53	42.860
9	22	300	75	16	38.97	37.48	38.87	38.440

Figure 5.3 shows the graphical comparison of carbonization values of different cuts.

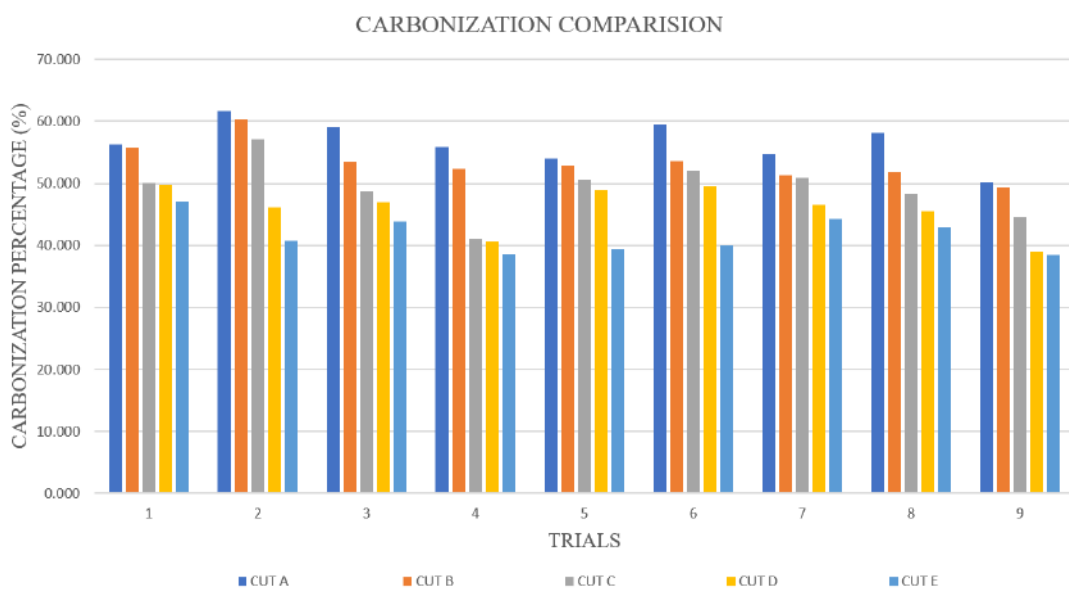


Figure 5.3 Carbonization graphical comparison

5.4.1.2 Analysing Kerf width on chrome + vegetable tanned cow leather

Table 5.8 shows the Kerf width value of conventional SOD control

Table 5.8 Conventional SOD control - A cut

Trial No.	Standoff distance (mm)	Feed rate (mm/min)	Duty Cycle (%)	Kerf Width (mm)			
				K1	K2	K3	K avg
1	18	200	70	0.125	0.107	0.121	0.118
2	18	250	75	0.117	0.124	0.121	0.121
3	18	300	80	0.109	0.124	0.124	0.119
4	20	200	75	0.120	0.122	0.114	0.119
5	20	250	80	0.122	0.129	0.124	0.125
6	20	300	70	0.123	0.118	0.114	0.118
7	22	200	80	0.122	0.114	0.126	0.121
8	22	250	70	0.122	0.120	0.121	0.121
9	22	300	75	0.124	0.124	0.125	0.124

Table 5.9 shows the Kerf width value of SOD control using Arduino UNO - B cut

Table 5.9 SOD control using Arduino UNO - B cut

Trial No.	Standoff distance (mm)	Feed rate (mm/min)	Duty Cycle (%)	Kerf Width (mm)			
				K1	K2	K3	K avg
1	18	200	70	0.124	0.105	0.121	0.117
2	18	250	75	0.117	0.124	0.12	0.120
3	18	300	80	0.108	0.123	0.122	0.118
4	20	200	75	0.121	0.121	0.113	0.118
5	20	250	80	0.121	0.126	0.124	0.124
6	20	300	70	0.123	0.117	0.115	0.118
7	22	200	80	0.123	0.113	0.123	0.120
8	22	250	70	0.12	0.121	0.119	0.120
9	22	300	75	0.124	0.124	0.122	0.123

Table 5.10 shows the Kerf width value of PWM control using Arbitrary waveform generator - C cut

Table 5.10 PWM control using Arbitrary waveform generator - C cut

Trial No.	Standoff distance (mm)	Feed rate (mm/min)	Duty Cycle (%)	Frequency (kHz)	Kerf Width (mm)			
					K1	K2	K3	K avg
1	18	200	70	16	0.117	0.111	0.107	0.112
2	18	250	75	18	0.122	0.124	0.102	0.116
3	18	300	80	20	0.124	0.105	0.119	0.116
4	20	200	75	20	0.117	0.120	0.115	0.117
5	20	250	80	16	0.117	0.117	0.115	0.116
6	20	300	70	18	0.122	0.117	0.106	0.115
7	22	200	80	18	0.118	0.118	0.118	0.118
8	22	250	70	20	0.119	0.117	0.120	0.119
9	22	300	75	16	0.121	0.122	0.114	0.119

Table 5.11 shows the Kerf width value of PWM control using ESP32 - D cut

Table 5.11 PWM control using ESP32 - D cut

Trial No.	Standoff distance (mm)	Feed rate (mm/min)	Duty Cycle (%)	Frequency (kHz)	Kerf Width (mm)			
					K1	K2	K3	K avg
1	18	200	70	16	0.115	0.104	0.114	0.111
2	18	250	75	18	0.113	0.119	0.101	0.111
3	18	300	80	20	0.117	0.115	0.114	0.115
4	20	200	75	20	0.111	0.116	0.112	0.113
5	20	250	80	16	0.113	0.109	0.123	0.115
6	20	300	70	18	0.119	0.111	0.112	0.114
7	22	200	80	18	0.115	0.119	0.119	0.118
8	22	250	70	20	0.113	0.112	0.114	0.113
9	22	300	75	16	0.117	0.117	0.115	0.116

Table 5.12 shows the Kerf width value of SOD and PWM control using Arduino UNO and ESP32 - E cut

Table 5.12 SOD and PWM control using Arduino UNO and ESP32 - E cut

Trial No.	Standoff distance (mm)	Feed rate (mm/min)	Duty Cycle (%)	Frequency (kHz)	Kerf Width (mm)			
					K1	K2	K3	K avg
1	18	200	70	16	0.110	0.111	0.110	0.110
2	18	250	75	18	0.111	0.111	0.110	0.111
3	18	300	80	20	0.113	0.111	0.113	0.112
4	20	200	75	20	0.112	0.113	0.113	0.113
5	20	250	80	16	0.115	0.113	0.115	0.114
6	20	300	70	18	0.111	0.118	0.114	0.114
7	22	200	80	18	0.118	0.115	0.117	0.117
8	22	250	70	20	0.113	0.113	0.113	0.113
9	22	300	75	16	0.115	0.117	0.115	0.116

Figure 5.4 shows the graphical comparison of Kerf width values of different cuts.

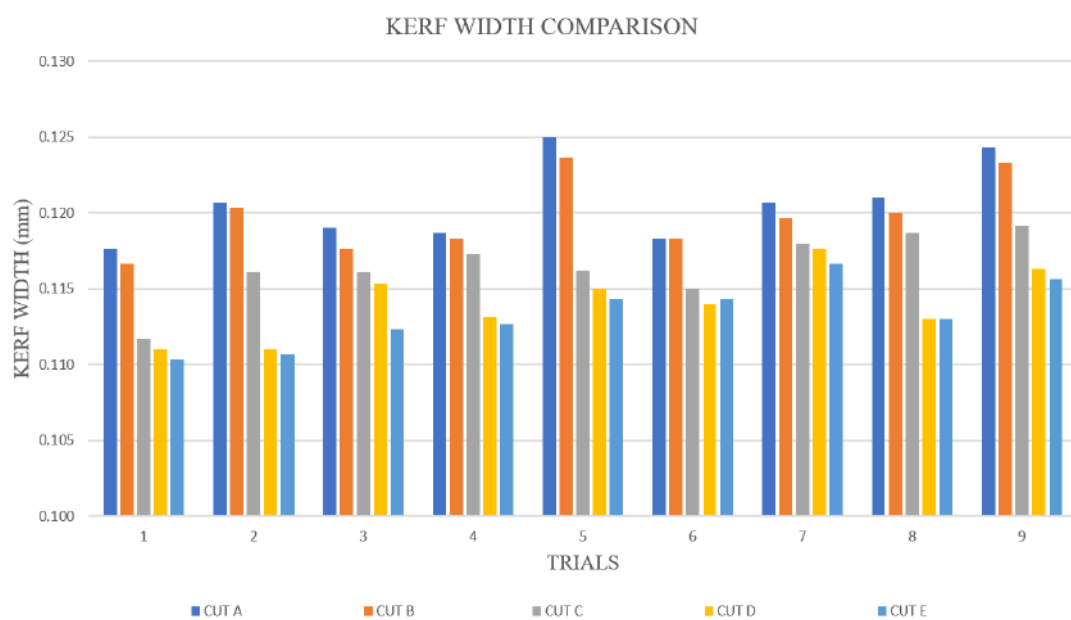


Figure 5.4 Kerf width graphical comparison

5.4.1.3 Analysing Material removal rate (MRR) on chrome + vegetable tanned cow leather

Table 5.13 shows the MRR value of conventional SOD control

Table 5.13 Conventional SOD control - A cut

Trial No.	Standoff distance (mm)	Feed rate (mm/min)	Duty Cycle (%)	Material Removal Rate			
				M1	M2	M3	M avg
1	18	200	70	0.005467	0.005310	0.005324	0.005367
2	18	250	75	0.005428	0.005383	0.005508	0.005440
3	18	300	80	0.005642	0.005597	0.005524	0.005588
4	20	200	75	0.005200	0.005206	0.005288	0.005231
5	20	250	80	0.005199	0.005254	0.005147	0.005200
6	20	300	70	0.005368	0.005387	0.005298	0.005351
7	22	200	80	0.005887	0.005798	0.005784	0.005823
8	22	250	70	0.005712	0.005787	0.005900	0.005800
9	22	300	75	0.005574	0.005517	0.005509	0.005533

Table 5.14 shows the MRR value of SOD control using Arduino UNO - B cut

Table 5.14 SOD control using Arduino UNO - B cut

Trial No.	Standoff distance (mm)	Feed rate (mm/min)	Duty Cycle (%)	Material Removal Rate			
				M1	M2	M3	M avg
1	18	200	70	0.005645	0.005806	0.005645	0.005699
2	18	250	75	0.006190	0.005714	0.005714	0.005873
3	18	300	80	0.005781	0.005469	0.005781	0.005677
4	20	200	75	0.005968	0.005806	0.006290	0.006022
5	20	250	80	0.005238	0.005873	0.006190	0.005767
6	20	300	70	0.005781	0.005938	0.006094	0.005938
7	22	200	80	0.006290	0.006290	0.006290	0.006290
8	22	250	70	0.006190	0.006032	0.006190	0.006138
9	22	300	75	0.006094	0.005938	0.005938	0.005990

Table 5.15 shows the MRR value of PWM control using Arbitrary waveform generator - C cut

Table 5.15 PWM control using Arbitrary waveform generator - C cut

Trial No.	Standoff distance (mm)	Feed rate (mm/min)	Duty Cycle (%)	Frequency (kHz)	Material Removal Rate			
					M1	M2	M3	M avg
1	18	200	70	16	0.005290	0.006290	0.005968	0.005849
2	18	250	75	18	0.006190	0.005032	0.006349	0.005857
3	18	300	80	20	0.006306	0.006150	0.006206	0.006221
4	20	200	75	20	0.006452	0.006452	0.006290	0.006398
5	20	250	80	16	0.006508	0.006349	0.006032	0.006296
6	20	300	70	18	0.006094	0.006063	0.006163	0.006106
7	22	200	80	18	0.006574	0.006252	0.006613	0.006480
8	22	250	70	20	0.006667	0.006108	0.006190	0.006322
9	22	300	75	16	0.006563	0.006094	0.006063	0.006240

Table 5.16 shows the MRR value of PWM control using ESP32 - D cut

Table 5.16 PWM control using ESP32 - D cut

Trial No.	Standoff distance (mm)	Feed rate (mm/min)	Duty Cycle (%)	Frequency (kHz)	Material Removal Rate			
					M1	M2	M3	M avg
1	18	200	70	16	0.005290	0.006452	0.006613	0.006118
2	18	250	75	18	0.006349	0.005490	0.006349	0.006063
3	18	300	80	20	0.006250	0.006094	0.006406	0.006250
4	20	200	75	20	0.006452	0.006452	0.006290	0.006398
5	20	250	80	16	0.006508	0.006508	0.006032	0.006349
6	20	300	70	18	0.006250	0.005937	0.006406	0.006198
7	22	200	80	18	0.006452	0.006290	0.006774	0.006505
8	22	250	70	20	0.006190	0.006349	0.006549	0.006363
9	22	300	75	16	0.006094	0.006406	0.006294	0.006265

Table 5.17 shows the MRR value of SOD and PWM control using Arduino UNO and ESP32 - E cut

Table 5.17 SOD and PWM control using Arduino UNO and ESP32 - E cut

Trial No.	Standoff distance (mm)	Feed rate (mm/min)	Duty Cycle (%)	Frequency (kHz)	Material Removal Rate			
					M1	M2	M3	M avg
1	18	200	70	16	0.005745	0.006613	0.006129	0.006162
2	18	250	75	18	0.006032	0.006349	0.006032	0.006138
3	18	300	80	20	0.005938	0.006694	0.006237	0.006290
4	20	200	75	20	0.006290	0.007258	0.006129	0.006559
5	20	250	80	16	0.006032	0.006649	0.006690	0.006457
6	20	300	70	18	0.005938	0.006194	0.006563	0.006232
7	22	200	80	18	0.006652	0.006590	0.006490	0.006577
8	22	250	70	20	0.006349	0.006190	0.006608	0.006382
9	22	300	75	16	0.006950	0.006000	0.006250	0.006400

Figure 5.5 shows the graphical comparison of MRR values of different cuts.

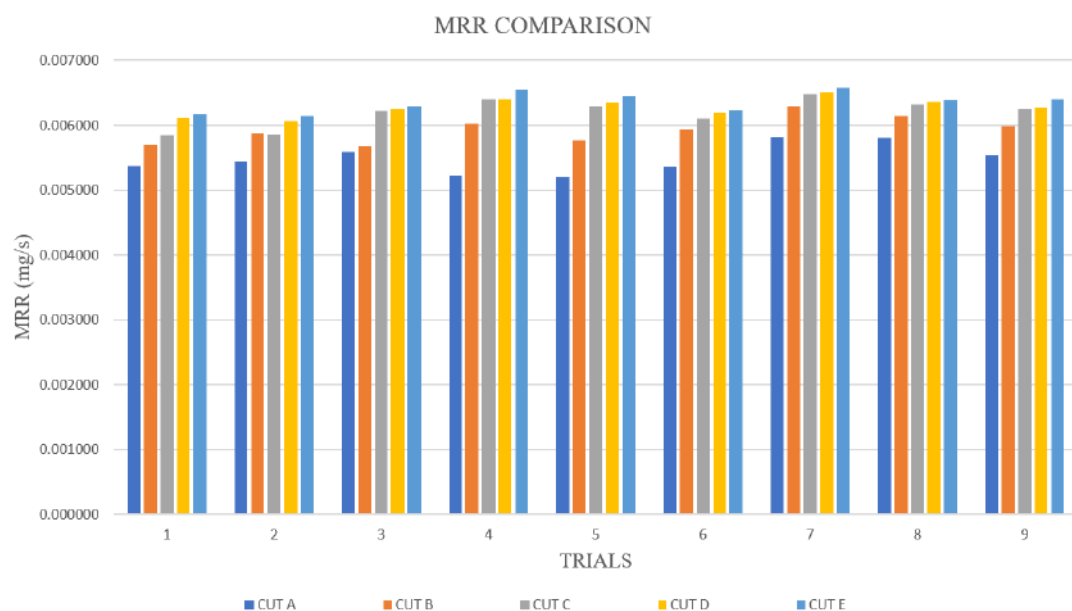


Figure 5.5 MRR graphical comparison

5.4.1.4 Analysing Emission rate on chrome + vegetable tanned cow leather

Table 5.18 shows the emission rate interior value of conventional SOD control

Table 5.18 Emission rate interior value of conventional SOD control - A cut

Trial No.	Standoff distance (mm)	Feed rate (mm/min)	Duty Cycle (%)	Emission rate - Interior (ppm)			
				E1-1	E1-2	E1-3	E1 avg
1	18	200	70	520.63	538.77	581.58	546.99
2	18	250	75	582.35	545.77	538.01	555.38
3	18	300	80	548.45	553.38	535.18	545.67
4	20	200	75	519.34	540.76	568.32	542.81
5	20	250	80	532.81	560.63	533.69	542.38
6	20	300	70	587.12	541.70	527.93	552.25
7	22	200	80	572.08	532.16	562.88	555.71
8	22	250	70	547.23	543.98	522.32	537.84
9	22	300	75	532.00	519.51	537.65	529.72

Table 5.19 shows the emission rate exterior value of conventional SOD control

Table 5.19 Emission rate exterior value of conventional SOD control - A cut

Trial No.	Standoff distance (mm)	Feed rate (mm/min)	Duty Cycle (%)	Emission rate - Exterior (ppm)			
				E2-1	E2-2	E2-3	E2 avg
1	18	200	70	429.26	462.39	495.22	462.29
2	18	250	75	490.16	451.28	461.84	467.76
3	18	300	80	478.38	469.23	441.39	463.00
4	20	200	75	427.85	446.78	494.71	456.45
5	20	250	80	445.91	471.97	442.07	453.32
6	20	300	70	482.29	475.09	466.27	474.55
7	22	200	80	493.66	451.36	461.95	468.99
8	22	250	70	461.26	441.76	441.36	448.13
9	22	300	75	442.31	434.52	450.97	442.60

Table 5.20 shows the emission rate interior value of SOD control using Arduino UNO - B cut

Table 5.20 Emission rate interior value of SOD control using Arduino UNO - B cut

Trial No.	Standoff distance (mm)	Feed rate (mm/min)	Duty Cycle (%)	Emission rate - Interior (ppm)			
				E1-1	E1-2	E1-3	E1 avg
1	18	200	70	558.76	517.16	551.79	542.57
2	18	250	75	544.66	573.14	547.32	555.04
3	18	300	80	576.62	538.51	537.33	550.82
4	20	200	75	545.33	593.79	538.85	559.32
5	20	250	80	544.78	532.25	543.27	540.10
6	20	300	70	532.48	552.24	553.68	546.13
7	22	200	80	559.63	538.46	539.94	546.01
8	22	250	70	547.32	531.28	543.07	540.56
9	22	300	75	538.83	547.21	541.45	542.50

Table 5.21 shows the emission rate exterior value of SOD control using Arduino UNO - B cut

Table 5.21 Emission rate exterior value of SOD control using Arduino UNO - B cut

Trial No.	Standoff distance (mm)	Feed rate (mm/min)	Duty Cycle (%)	Emission rate - Exterior (ppm)			
				E2-1	E2-2	E2-3	E2 avg
1	18	200	70	464.34	434.06	469.13	455.84
2	18	250	75	458.12	475.01	452.74	461.96
3	18	300	80	492.65	447.48	447.22	462.45
4	20	200	75	447.59	496.24	449.15	464.33
5	20	250	80	453.21	434.24	459.47	448.97
6	20	300	70	461.21	471.27	471.92	468.13
7	22	200	80	478.66	448.09	449.32	458.69
8	22	250	70	442.58	440.83	459.21	447.54
9	22	300	75	447.21	456.87	451.80	451.96

Table 5.22 shows the emission rate interior value of PWM control using Arbitrary waveform generator - C cut

Table 5.22 Emission rate interior value of PWM control using Arbitrary waveform generator - C cut

Trial No.	Standoff distance (mm)	Feed rate (mm/min)	Duty Cycle (%)	Emission rate - Interior (ppm)			
				E1-1	E1-2	E1-3	E1 avg
1	18	200	70	552.08	536.06	558.43	548.86
2	18	250	75	570.71	505.96	511.75	529.47
3	18	300	80	528.31	529.49	554.98	537.59
4	20	200	75	515.56	542.44	536.78	531.59
5	20	250	80	555.41	556.49	572.17	561.36
6	20	300	70	537.56	562.34	551.61	550.50
7	22	200	80	564.73	565.42	515.72	548.62
8	22	250	70	533.07	532.17	563.59	542.94
9	22	300	75	513.89	529.70	586.12	543.24

Table 5.23 shows the emission rate exterior value of PWM control using Arbitrary waveform generator - C cut

Table 5.23 Emission rate exterior value of PWM control using Arbitrary waveform generator - C cut

Trial No.	Standoff distance (mm)	Feed rate (mm/min)	Duty Cycle (%)	Emission rate - Exterior (ppm)			
				E2-1	E2-2	E2-3	E2 avg
1	18	200	70	455.20	447.83	464.21	455.75
2	18	250	75	470.39	403.17	407.28	426.95
3	18	300	80	429.59	436.09	466.73	444.14
4	20	200	75	424.99	431.68	432.69	429.79
5	20	250	80	422.94	475.90	460.98	453.27
6	20	300	70	440.44	469.39	455.54	455.12
7	22	200	80	430.97	465.47	413.78	436.74
8	22	250	70	444.04	448.81	456.17	449.67
9	22	300	75	442.87	450.63	443.76	445.75

Table 5.24 shows the emission rate interior value of PWM control using ESP32 - D cut

Table 5.24 Emission rate interior value of PWM control using ESP32 - D cut

Trial No.	Standoff distance (mm)	Feed rate (mm/min)	Duty Cycle (%)	Emission rate - Interior (ppm)			
				E1-1	E1-2	E1-3	E1 avg
1	18	200	70	535.55	514.10	541.93	530.53
2	18	250	75	516.32	547.13	556.78	540.08
3	18	300	80	518.26	568.14	548.32	544.91
4	20	200	75	588.57	562.31	598.17	583.02
5	20	250	80	561.57	577.97	599.54	579.69
6	20	300	70	581.45	566.08	523.05	556.86
7	22	200	80	594.32	528.32	527.59	550.08
8	22	250	70	575.88	524.78	582.61	561.09
9	22	300	75	587.98	578.78	579.56	582.11

Table 5.25 shows the emission rate exterior value of PWM control using ESP32 - D cut

Table 5.25 Emission rate exterior value of PWM control using ESP32 - D cut

Trial No.	Standoff distance (mm)	Feed rate (mm/min)	Duty Cycle (%)	Emission rate - Exterior (ppm)			
				E2-1	E2-2	E2-3	E2 avg
1	18	200	70	431.87	430.15	428.75	435.14
2	18	250	75	418.41	421.00	425.28	426.98
3	18	300	80	443.25	448.11	445.43	449.45
4	20	200	75	450.47	437.18	450.94	478.28
5	20	250	80	452.78	449.87	454.16	464.90
6	20	300	70	451.81	458.19	460.73	443.04
7	22	200	80	460.18	458.75	462.18	432.53
8	22	250	70	450.16	449.54	441.25	446.50
9	22	300	75	461.28	465.37	454.01	468.76

Table 5.26 shows the emission rate interior value of SOD and PWM control using Arduino UNO and ESP32 - E cut

Table 5.26 Emission rate interior value of SOD and PWM control using Arduino UNO and ESP32 - E cut

Trial No.	Standoff distance (mm)	Feed rate (mm/min)	Duty Cycle (%)	Emission rate - Interior (ppm)			
				E1-1	E1-2	E1-3	E1 avg
1	18	200	70	542.17	536.22	539.84	539.41
2	18	250	75	535.84	532.61	536.53	534.99
3	18	300	80	550.39	548.28	552.94	550.54
4	20	200	75	560.57	551.04	557.80	556.47
5	20	250	80	572.49	564.17	570.38	569.01
6	20	300	70	578.36	570.48	575.55	574.80
7	22	200	80	585.67	570.13	580.94	578.91
8	22	250	70	568.39	555.75	562.13	562.09
9	22	300	75	575.84	569.84	578.29	574.66

Table 5.27 shows the emission rate exterior value of SOD and PWM control using Arduino UNO and ESP32 - E cut

Table 5.27 Emission rate exterior value of SOD and PWM control using Arduino UNO and ESP32 - E cut

Trial No.	Standoff distance (mm)	Feed rate (mm/min)	Duty Cycle (%)	Emission rate - Exterior (ppm)			
				E2-1	E2-2	E2-3	E2 avg
1	18	200	70	431.87	430.15	428.75	430.26
2	18	250	75	418.41	421.00	425.28	421.56
3	18	300	80	443.25	448.11	445.43	445.60
4	20	200	75	450.47	437.18	450.94	446.20
5	20	250	80	452.78	449.87	454.16	452.27
6	20	300	70	451.81	458.19	460.73	456.91
7	22	200	80	460.18	458.75	462.18	460.37
8	22	250	70	450.16	449.54	441.25	446.98
9	22	300	75	461.28	465.37	454.01	460.22

Table 5.28 represents the average difference of exterior and interior in ppm

Table 5.28 Emission rate average difference

Trial No.	Emission rate: Exterior – Interior (ppm)				
	Cut A	Cut B	Cut C	Cut D	Cut E
1	84.71	86.73	93.11	95.39	109.15
2	87.62	93.08	102.53	113.10	113.43
3	82.67	88.37	93.46	95.46	104.94
4	86.36	95.00	101.81	104.74	110.27
5	89.06	91.13	108.08	114.79	116.74
6	77.70	78.00	95.38	113.82	117.89
7	86.72	87.32	111.88	117.55	118.54
8	89.72	93.02	93.27	114.59	115.11
9	87.12	90.54	97.48	113.35	114.44

Figure 5.6 shows the graphical comparison of Emission rate average difference values of different cuts.

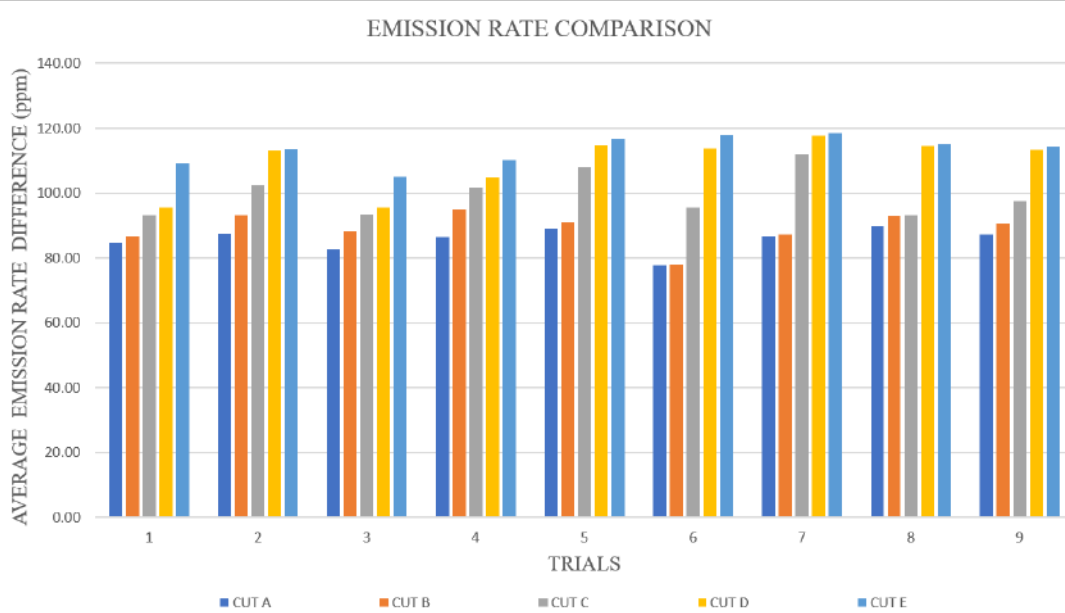


Figure 5.6 Emission rate graphical comparison

5.4.1.5 Experimental samples

Figure 5.7 shows the 135 cuts performed using chrome + vegetable tanned cow leather.

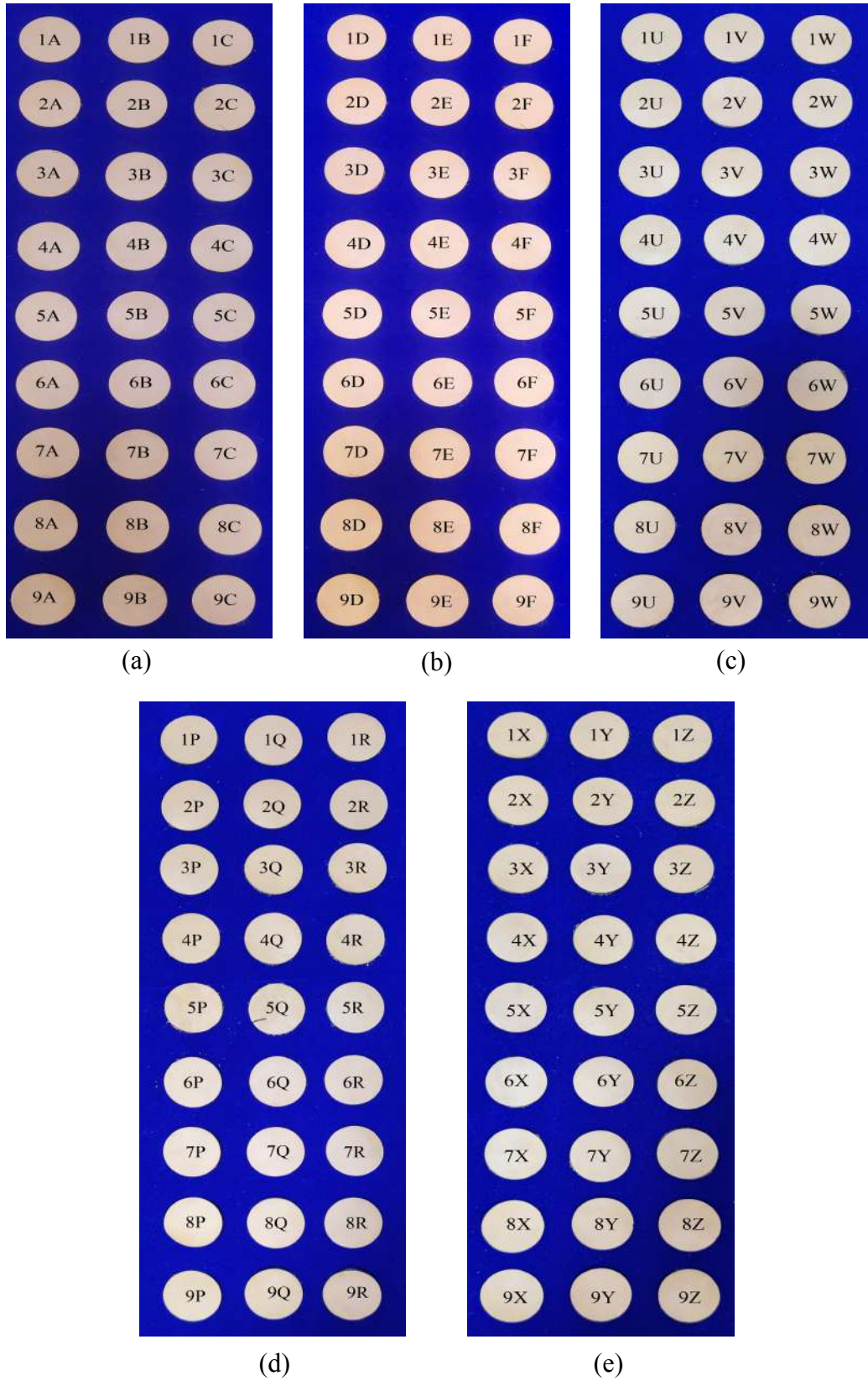


Figure 5.7 (a) A cut (b) B cut (c) C cut (d) D cut and (e) E cut

Table 5.29 shows the samples of carbonization and its analysis of E cut captured through USB microscope.

Table 5.29 Carbonization and Its analysis

Trial No.	Cut X	Analysed cut X	Cut Y	Analysed cut Y	Cut Z	Analysed cut Z
1						
2						
3						
4						
5						
6						
7						
8						
9						

5.4.1.6 Optimal parameters for cutting chrome + vegetable tanned cow leather.

Leather is one of the most adaptable and widely available materials for humans. Its use in a range of industries has increased the demand for it to be cut in an efficient manner with increasing production rates. As a result, these criteria need the use of unconventional and one-of-a-kind machining methods for its cutting mechanism, such as LBM. Implementation of direct diode lasers, in particular, due to lower operational costs and convenience of use, as compared to other types of lasers. So, an attempt has been made to perform the diode laser-based LBM and also analysed its various output factors after the machining process. Therefore, a need arises for proper and efficient methodology to record the experimentations performed. There are numerous approaches of parameter optimisations such as Artificial neural network (ANN), Response surface methodology (RSM), Taguchi grey relational analysis (TGRA), technique and much more. But, these methods of optimisations have number of caveats such as meticulous process of grey relational co-efficient selection in TGRA and requirement of higher expert knowledge in the case of RSM technique. Also, the oscillation in prediction accuracy depending upon the number of

trials in the ANN process reduces its desirability. Therefore, a more efficient yet simple process such as the Taguchi - Data envelopment analysis and ranking (DEAR) based Multi criterion decision making (MCDM) algorithm has been utilised in the dissertation. This method has been chosen to optimise the parameters of machining on leather surface particularly since it is proven to have extensive accuracy over all other mentioned techniques in the determination of optimal parameters for the process.

5.4.1.6.1 DEAR Methodology

The optimisation works with the combination of experimentation values recorded are plotted into a ratio and following steps are followed for the optimisation of parameters.

- The weights of each response are calculated by determining the dividing the fraction between responses over the sum of all the experimentation measures.
- These values are further multiplied to its own weight to get the weighted data.
- Then a ratio is found between Larger the better (LB) and smaller the better (SB) and this ratio is considered to be the MRPI.

The average values of Carbonization, Kerf width, MRR and Emission rate of cut E is taken for the DEAR analysis. Table 5.30 shows the recorded values of cut E.

Table 5.30 Averaged output values of cut E for DEAR analysis

Trial No.	Process parameters				Response variables			
	Standoff distance (mm)	Feed rate (mm/min)	Duty Cycle (%)	Frequency (kHz)	Carbonization (CZ) %	Kerf width (KW) mm	MRR mg/s	Emission Rate (ER) ppm
1	18	200	70	16	47.070	0.110	0.00616	109.15
2	18	250	75	18	40.703	0.111	0.00614	113.43
3	18	300	80	20	43.857	0.112	0.00629	104.94
4	20	200	75	20	38.677	0.113	0.00656	110.27
5	20	250	80	16	39.393	0.114	0.00646	116.74
6	20	300	70	18	39.997	0.114	0.00623	117.89
7	22	200	80	18	44.237	0.117	0.00658	118.54
8	22	250	70	20	42.860	0.113	0.00638	115.11
9	22	300	75	16	38.440	0.116	0.00640	114.44

The following equations 5.2 - 5.10 are used to calculate MRPI

$$\text{Multi response performance index } MRPI = \frac{A + D}{B + C} \quad (\text{Eqn. 5.2})$$

$$\text{Weight of Emission rate } W_{ER} = \frac{ER}{\sum ER} \quad (\text{Eqn. 5.3})$$

$$\text{Weight of Carbonization } W_{CZ} = \frac{\frac{1}{CZ}}{\sum \frac{1}{CZ}} \quad (\text{Eqn. 5.4})$$

$$\text{Weight of Kerf width } W_{KW} = \frac{\frac{1}{KW}}{\sum \frac{1}{KW}} \quad (\text{Eqn. 5.5})$$

$$\text{Weight of Material removal rate } W_{MRR} = \frac{MRR}{\sum MRR} \quad (\text{Eqn. 5.6})$$

$$A = ER \times W_{ER} \quad (\text{Eqn. 5.7})$$

$$B = CZ \times W_{CZ} \quad (\text{Eqn. 5.8})$$

$$C = KW \times W_{KW} \quad (\text{Eqn. 5.9})$$

$$D = MMR \times W_{MRR} \quad (\text{Eqn. 5.10})$$

Table 5.31 shows the MRPI Values for the cut E.

Table 5.31 Calculated values for Weights and MRPI

Trials No.	Weights				MRPI
	Emission rate (ER) ppm	Carbonization (CZ)%	Kerf width (KW) mm	MRR (mg/s)	
1	0.10696	0.097989	0.114439	0.107733	2.5243
2	0.11115	0.113317	0.113408	0.107313	2.7262
3	0.10283	0.105168	0.112395	0.109971	2.3334
4	0.10805	0.119253	0.111400	0.114674	2.5764
5	0.11439	0.117086	0.110423	0.112891	2.8876
6	0.11552	0.115318	0.110423	0.108957	2.9448
7	0.11616	0.104265	0.107592	0.114989	2.9774
8	0.11280	0.107614	0.111400	0.111579	2.8075
9	0.11214	0.119988	0.108519	0.111894	2.7750

Table 5.32 show the calculation for optimal process parameters.

Table 5.32 Optimising process parameters

Factors	Levels			Max - Min
	1	2	3	
SOD	2.5280	2.8029	2.8533	0.3253
FR	2.6927	2.8071	2.6844	0.1227
DC	2.7589	2.6925	2.7328	0.0664
Frequency	2.7290	2.8828	2.5725	0.3103

Table 5.33 show the optimised process parameters

Table 5.33 Optimised process parameters

Factors	Level	Parameter values
SOD	2	20 mm
FR	2	250 mm/min
DC	1	70 %
Frequency	2	18 kHz

From DEAR methodology it is concluded that 20 mm Standoff distance, 250 mm/min Feed rate with Duty cycle 70% and Frequency 18 KHz are optimal parameters for cutting Chrome + vegetable tanned cow leather.

CHAPTER 6

CONCLUSION

6.1 Conclusion

- Designing and developing a three-axis powers idle laser cutter is achieved through many significant fails and errors. The entire LBM setup is being controlled by CNC control board of version 1.1 Grbl. The CNC codes are modified to the requirements.
- The developed LBM has a self tuned adaptive system which controls the standoff distance (SOD) through VL6180X sensor with A4498 Stepper driver and stepper motor. The Standoff distance for perfect cut is measured through Taguchi orthogonal matrix experimental by cutting Chrome + vegetable tanned cow leather of thickness 0.8 mm.
- In the LBM, the laser diode is controlled through PWM using ESP32 which is energy efficient and has high precision throughout the cutting process.
- Finally, an enclosure has been designed and developed which controls the LBM with integrated 7" LCD touch display and that is controlled by Raspberry Pi with all the required LBM software.
- The enclosure is designed in a way that all the fumes emitted while cutting leather is controlled and reduced when exhausted outside, ZWAS emission control unit. The emission rate is measured by SCD30 sensors. The entire enclosure is made possible by water-resistant MDF boards of 12mm thickness. All the parameters which are used to enhances the machinability of the LBM is experimented and the optimal parameters are set for effective cutting process.

6.2 Future scope

- Further improvement in emission control can be achieved.
- Other types of leathers with various thickness can be experimented and analysed.
- Laser diode of wavelength and coherent beam combining can be used in LBM setup.
- Engraving and embellishing of leather can be achieved using LBM.

REFERENCES

1. A.Gisario; A.Boschetto; F.Veniali. (2011) *Surface transformation of AISI 304 stainless by high power diode laser.* Optics and lasers in engineering. Vol. 49 pp.41-51. DOI: 10.1016/j.optlaseng.2010.09.001.
2. Ahmed B.Khoshaim; Ammar H.Elsheikh; Essam B.Moustafa; Muhammad Basha; Ezzat A.Showaib. (2021) *Experimental investigation on laser cutting of PMMA sheets: Effects of process factors on kerf characteristics.* Journal of Materials Research And Technology, Vol. 11 pp.235-246. DOI: 10.1016/j.jmrt.2021.01.012.
3. Alexander Stepanov; Esa Saukkonen; Heidi Piili. (2015) *Possibilities of laser processing of paper materials.* Physics Procedia. Vol. 78 pp.138-146. DOI: 10.1016/j.phpro.2015.11.026.
4. Bekir Sami Yilbas; Mian Mobeen Shaukat; Farhan Ashraf. (2017) *Laser cutting of various materials: Kerf width size analysis and life cycle assessment of cutting process.* Optics and laser technology, Vol. 93 pp.67-73. DOI: 10.1016/j.optlastec.2017.02.014.
5. C.Moorhouse. (2013) *Advantages of picosecond laser machining for cutting-edge technologies.* Phys. Procedia. Vol. 41 pp.381-388 DOI: 10.1016/j.phpro.2013.03.091.
6. C.Bagger; F.O.Olsen. (2001) *Pulsed mode laser cutting of sheets for tailored blanks.* Journal of Materials Processing Technology. Vol. 115 pp.131-135. DOI: s0924-0136(01)00752-X.
7. C.Leone; S.Genna. (2017) *Heat affected zone extension in pulsed Nd:YAG laser cutting of CFRP.* Composites Part B (2018). DOI: 10.1016/j.compositesb.2017.12.028.
8. Chun-Hao Li and Ming-Jong Tsai. (2009) *Multi-objective optimization of laser cutting for flash memory modules with special shapes using grey relational analysis.* Optics & laser technology. Vol. 41 pp.634-642. DOI: 10.1016/j.optlastec.2008.09.009.
9. Dirk Petring; Thomas Molitor; Frank Schneider; Norbert Wolf. (2012) *Diagnostics, modeling and simulation: Three keys towards mastering the cutting process with fiber, disk and diode lasers.* Physics Procedia. Vol. 39 pp.186-196. DOI: 10.1016/j.phpro.2012.10.029.
10. Dong-Hyeon Kim and Choon-Man Lee. (2021) *Experimental Investigation on Machinability of Titanium Alloy by Laser-Assisted End Milling.* Metals (MDPI). Vol. 11 1552. DOI: 10.3390/met11101552.
11. G.Costa Rodrigues and J.R.Duflou. (2016) *Effects of different polarization strategies on laser cutting with direct diode lasers.* Physics Procedia. Vol. 83 pp.302-309. DOI: 10.1016/j.phpro.2016.08.031.

12. Goncalo C. Rodrigues; Joost R.Duflou. (2018) *Theoretical and experimental aspects of laser cutting with elliptically polarized laser beams*. Journal of Materials Processing Technology. DOI: 10.1016/j.jmatprotec.2018.09.035.
13. Gonçalo Costa Rodrigues; Nikita Levichev; Vitalii Vorkov and Joost R.Duflou. (2019) *Thickness validation of modeling tools for laser cutting applications*. Procedia Manufacturing. Vol. 29 pp.383-389. DOI:10.1016/j.promfg.2019.02.152
14. H.Golnabi and M.Bahar. (2009) *Investigation of optimum condition in oxygen gas-assisted laser cutting*. Optical & laser technology. Vol. 41 pp.454-460. DOI: 10.1016/j.optlastec.2008.08.001.
15. I.Sakaev and A.A. Ishaaya. (2021) *Diode laser assisted oxygen cutting of thick mild steel with off-axis beam delivery*. Optical & laser technology. Vol. 138. DOI: 10.1016/j.optlastec.2020.106876.
16. J.Kanagaraj; Rames C.Panda; M.Vinodh Kumar. (2020) *Trends and advancements in sustainable leather processing: Future directions and challenges -A review*. Journal of Environmental Chemical Engineering. Vol. 8. DOI: 10.1016/j.jece.2020.104379.
17. Luigi Zeni; Stefania Campopiano; Antonello Cutolo; Giuseppe D'Angelo. (2003) *Power semiconductor laser diode arrays characterization*. Optics and Lasers in Engineering. Vol. 39 pp.203-217. DOI: 10.1016/j.optlaseng.2003.39.217
18. N.Roy; D.Pramanik; A.S. Kuar. (2021) *Comparative study on quality characteristic of pulsed laser beam cutting of Inconel 625 superalloy at different environment by sensitivity analysis*. Optik- International Journal for Light and Electron Optics. Vol. 232. DOI: 10.1016/j.ijleo.2021.166516.
19. P.Romero; N.Otero; I.Coto; C.Leira; A.Gonzalez. (2013) *Experimental study of diode laser cutting of silicon by means of water assisted thermally driven separation mechanism*. Physics Procedia. Vol. 41 pp.617-626. DOI: 10.1016/j.phpro.2013.03.124.
20. Philip L.Crouse; Lin Li; Julian T.Spencer. (2004) *Performance comparison of CO₂ and diode lasers for deep-section concrete cutting*. Thin Solid Films. Vol. 453-454 pp.594-599. DOI: 10.1016/j.tsf.2003.11.142.
21. S.Biswas; K. Mandal; N.Roy; R.Biswas; A.S.Kuar. (2019) *Study on Kerf width deviation of microchannel with various medium in laser transmission cutting by diode pump fiber laser*. materials Today: Proceedings. Vol. 26 pp.804-807. DOI: 10.1016/j.matpr.2019.12.419.
22. Salman Nisar; M.A. Sheikh; Lin Li; Safdar. (2010) *The effect of material thickness, laser power and cutting speed on cut path deviation in high-power diode laser chip-free cutting of glass*. Optics & Laser technology. Vol. 42 pp.1022-1031. DOI: 10.1016/j.optlastec.2010.01.024.

23. Wegener Konrad; Dold Claus; Henerichs Marcel, Walter Christian. (2012) *Laser prepared cutting tools*. Physics Procedia. Vol. 39 pp.240-248. DOI: 10.1016/j.phpro.2012.10.035.
24. Youyou Wang; Manhui Zheng; Xinhua Liu; Ouyang Yue; Xuechuan Wang; Huie Jiang. (2021) *Advanced collagen nanofibers-based functional biocomposites for high-value utilization of leather: A review*. Journal of Science: Advanced Materials and Devices. Vol. 6 pp.153-166. DOI: 10.1016/j.jsamd.2021.02.001.
25. Zhenfu Wang; Te Li; Guowen Yang; Yunfei Song. (2017) *High power, high efficiency continuous-wave 808 nm laser diode arrays*. Optics & Laser technology. Vol. 97 pp.297-301. DOI:10.1016/j.optlastec.2017.07.015.

Engineering Your Linear Motion Solutions - What is Lead Screw Efficiency?, <https://www.pbclinear.com/Blog/2018/February/What-is-Lead-Screw-Efficiency-in-Linear-Motion>

Stepper motor torque basics - <https://www.controleng.com/articles/stepper-motor-torque-basics/>

Working with Critical Speeds and Lead Screws - <https://www.helixlinear.com/blog/lead-screws/working-with-critical-speeds-and-lead-screws/>

Using OpenCV with Tkinter - <https://www.tutorialspoint.com/using-opencv-with-tkinter>

ESP32 PWM with Arduino IDE (Analog Output) - <https://randomnerdtutorials.com/esp32-pwm-arduino-ide/>

Archived Library Examples - <https://docs.arduino.cc/library-examples/>

APPENDIX

Standoff distance control - Arduino UNO code:

```
#include <Wire.h>
#include "Adafruit_VL6180X.h"
Adafruit_VL6180X vl = Adafruit_VL6180X();
const int dirPin = 2;
const int stepPin = 3;
const int stepsPerRevolution = 200;
float range; // variable for the distance measurement
void setup()
{ Wire.begin();
  Serial.begin(115200); // // Serial Communication is starting with 115200 of
  baudrate speed
  pinMode(stepPin, OUTPUT);
  pinMode(dirPin, OUTPUT);
  vl.begin();
  delay(1000); }
int lidar_exec(){
  float range = vl.readRange();
  Serial.print("Distance measured (mm) = ");
  Serial.println(range/10);
  delay(500);
  return range/10; }
void stepper_ctrl_anti(){
  digitalWrite(dirPin, LOW);// Set motor direction counterclockwise
  for(int x = 0; x < stepsPerRevolution; x++) {
    digitalWrite(stepPin, HIGH);
    delayMicroseconds(500);
    delayMicroseconds(500); }
  delay(500); }
void stepper_ctrl_clock(){
  digitalWrite(dirPin, HIGH);//Rotates the stepper clockwise
  for(int x = 0; x >stepsPerRevolution; x++) {
```

```

digitalWrite(stepPin, HIGH);
delayMicroseconds(500);
digitalWrite(stepPin, LOW);
delayMicroseconds(500);}

delay(500);
for(;;/* empty */}

void loop(){
int dist = 0;

dist=lidar_exec();

if(dist == 10.75 || dist ==11.00 || dist ==11.50) {
    Serial.println("Stopping execution--> Reached");
} else if(dist < 11.00){
    stepper_ctrl_anti();// Change with respect to movement up or down }
else{
    stepper_ctrl_clock();// Change with respect to movement up or down}
for(;;/*Empty loop for loop stop */} }
```

SCD30 and BH1750 - Arduino MEGA code:

```

#include <Adafruit_SCD30.h>
#include <Wire.h>

#define BH_1750 0x23
#define DATA_REG_RESET 0b00000111
#define POWER_DOWN 0b00000000
#define POWER_ON 0b00000001

enum BH1750Mode {

    CHM = 0b00010000, //CHM: Continuously H-Resolution Mode
    CHM_2 = 0b00010001, //CHM_2: Continuously H-Resolution Mode2
    CLM = 0b00010011, //CLM: Continuously L-Resolution Mode
    OTH = 0b00100000, //OTH: One Time H-Resolution Mode
    OTH_2 = 0b00100001, //OTH_2: One Time H-Resolution Mode2
    OTL = 0b00100011 //OTL: One Time L-Resolution Mode
} mode;

float measuringTimeFactor;
```

```

Adafruit_SCD30 scd30;
void setup() {
    Serial.begin(115200);
    Wire.begin();
    mode = CHM;
    measuringTimeFactor = 1;
    setMode();
    setMeasuringTime();
    while (!Serial) delay(10);
    scd30.begin();
    delay(200);}
void loop() {
    delay(2000);
    getLux();
    if(scd30.dataReady()){
        if(!scd30.read()) { return; }
        Serial.println(scd30.CO2, 3);
    }else{ //...;}
    delay(500);}
void getLux(){
    uint16_t rawLux;
    float lux;
    rawLux = readBH1750();{
        lux = (rawLux/2.4)/measuringTimeFactor;    }
    else{
        lux = (rawLux/1.2)/measuringTimeFactor;    }
    Serial.print(lux);
    Serial.print(" ");
}
void powerDown(){
    writeBH1750(POWER_DOWN);}
void powerOn(){
    writeBH1750(POWER_ON);
    setMode();}

```

```

void dataRegReset(){
    writeBH1750(DATA_REG_RESET);}

void setMode(){
    writeBH1750(mode);}

void setMeasuringTime(){
    byte mt = round(measuringTimeFactor*69);
    byte highByteMT = ((mt>>5) | 0b01000000);
    byte lowByteMT = (mt & 0b01111111);
    lowByteMT |= 0b01100000;
    writeBH1750(highByteMT);
    writeBH1750(lowByteMT);}

uint16_t readBH1750(){
    uint8_t MSbyte, LSbyte;
    Wire.requestFrom(BH_1750, 2);
    if(Wire.available()){
        MSbyte=Wire.read();
        LSbyte=Wire.read(); }
    return ((MSbyte<<8) + LSbyte);}

void writeBH1750(byte val){
    Wire.beginTransmission(BH_1750);
    Wire.write(val);
    Wire.endTransmission();}

```

SCD30 and PWM - ESP32 code:

```

#include <Wire.h>

#include "SparkFun_SCD30_Arduino_Library.h"

SCD30 scd30;

const int pwm_pin =16;
const int pwm_resolution=2;
const int pwm_channel=0;
int pwm_freq = 18000;
int duty_cycle = 256; // Duty cycle at 80% by default

```

```

void setup() {
    Serial.begin(115200);
    Wire.begin();
    ledcSetup(pwm_channel,pwm_freq,pwm_resolution);
    ledcAttachPin(pwm_pin,pwm_channel);
    scd30.begin();}
void loop() {
    ledcWrite(pwm_channel,duty_cycle);
    Serial.println(scd30.getCO2());
    delay(4000);
    if (Serial.available() > 0) {
        Serial.print("Reading Serial");
        int s = Serial.read();
        switch(s){
            case '0':
                pwm_freq = 18000;
                duty_cycle =0; // 0
                ledcWrite(pwm_channel,duty_cycle);
                break;
            case '1':
                pwm_freq = 16000;
                duty_cycle =1; // 25
                ledcWrite(pwm_channel,duty_cycle);
                Serial.print("Case 1");
                Serial.println(" Freq :");
                Serial.print(pwm_freq);
                Serial.println(" Duty cycle at 70%");
                break;
            case '2':
                pwm_freq = 16000;
                duty_cycle =2; // 50
                ledcWrite(pwm_channel,duty_cycle);
                Serial.print("Case 2");
}
}

```

```

Serial.println(" Freq :");
Serial.print(pwm_freq);
Serial.println(" Duty cycle at 75%");
break;

case '3':
    pwm_freq = 16000;
    duty_cycle = 3;//75
    ledcWrite(pwm_channel,duty_cycle);
    Serial.print("Case 3");
    Serial.println(" Freq :");
    Serial.print(pwm_freq);
    Serial.println(" Duty cycle at 80%");
    break;

case '4':
    pwm_freq = 18000;
    duty_cycle =1;
    ledcWrite(pwm_channel,duty_cycle);
    Serial.print("Case 4");
    Serial.println(" Freq :");
    Serial.print(pwm_freq);
    Serial.println(" Duty cycle at 70%");
    break;

case '5':
    pwm_freq = 18000;
    duty_cycle =2;
    ledcWrite(pwm_channel,duty_cycle);
    Serial.print("Case 5");
    Serial.println(" Freq :");
    Serial.print(pwm_freq);
    Serial.println(" Duty cycle at 75%");
    break;

case '6':
    pwm_freq = 18000;

```

```

duty_cycle =3;
ledcWrite(pwm_channel,duty_cycle);
Serial.print("Case 6");
Serial.println(" Freq :");
Serial.print(pwm_freq);
Serial.println(" Duty cycle at 80%");
break;

case '7':
    pwm_freq = 20000;
    duty_cycle =1;
    ledcWrite(pwm_channel,duty_cycle);
    Serial.print("Case 7");
    Serial.println(" Freq :");
    Serial.print(pwm_freq);
    Serial.println(" Duty cycle at 70%");
    break;

case '8':
    pwm_freq = 20000;
    duty_cycle =2;
    ledcWrite(pwm_channel,duty_cycle);
    Serial.print("Case 8");
    Serial.println(" Freq :");
    Serial.print(pwm_freq);
    Serial.println(" Duty cycle at 75%");
    break;

case '9':
    pwm_freq = 20000;
    duty_cycle =3;
    ledcWrite(pwm_channel,duty_cycle);
    Serial.print("Case 9");
    Serial.println(" Freq :");
    Serial.print(pwm_freq);
    Serial.println(" Duty cycle at 80%");

```

```

break;

default:
    //Serial.print("No case running");
    ledcWrite(pwm_channel,duty_cycle); } }

```

GUI for Carbonization analyzer code in VS CODE:

```

from tkinter import *
from tkinter import filedialog as fido
from PIL import Image
from PIL import ImageTk
import cv2
from numpy import fabs
from matplotlib import pyplot as plt
from matplotlib.figure import Figure
from matplotlib.backends.backend_tkagg import
(FigureCanvasTkAgg,NavigationToolbar2Tk)
def select_image():
    global panelA, panelB,path
    path = fido.askopenfilename()

    if len(path) > 0:
        image = cv2.imread(path)
        image = cv2.resize(image, (400, 400),
interpolation=cv2.INTER_AREA)
        gray = cv2.cvtColor(image, cv2.COLOR_BGR2GRAY)
        (thresh,edged) = cv2.threshold(gray,60, 255, cv2.THRESH_BINARY)
        image = cv2.cvtColor(image, cv2.COLOR_BGR2RGB)
        image = Image.fromarray(image)
        edged = Image.fromarray(edged)
        image = ImageTk.PhotoImage(image)
        edged = ImageTk.PhotoImage(edged)
        if panelA is None:
            panelA = Label(image=image)
            panelA.image = image

```

```

        panelA.grid(row=2,column=0, padx=10, pady=10)

    else:
        panelA.configure(image=image)
        panelB.configure(image=edged)
        panelA.image = image
        panelB.image = edged

def grayscale():
    image = cv2.imread(path)
    image = cv2.resize(image, (400, 400), interpolation=cv2.INTER_AREA)
    gray = cv2.cvtColor(image, cv2.COLOR_BGR2GRAY)
    gray = Image.fromarray(gray)
    gray = ImageTk.PhotoImage(gray)
    panelB = Label(image=gray)
    panelB.image = gray
    panelB.grid(row=2,column=1, padx=10, pady=10)

def blackwhite():
    image = cv2.imread(path)
    image = cv2.resize(image, (400, 400), interpolation=cv2.INTER_AREA)
    gray = cv2.cvtColor(image, cv2.COLOR_BGR2GRAY)
    (thresh,edged) = cv2.threshold(gray,60, 255, cv2.THRESH_BINARY)
    edged = Image.fromarray(edged)
    edged = ImageTk.PhotoImage(edged)
    panelC = Label(image=edged)
    panelC.image = edged
    panelC.grid(row=2,column=2, padx=10, pady=10)

def analyse():
    image = cv2.imread(path)
    image = cv2.resize(image, (400, 400), interpolation=cv2.INTER_AREA)
    global gray
    gray = cv2.cvtColor(image, cv2.COLOR_BGR2GRAY)
    global edged
    (thresh,edged) = cv2.threshold(gray,70, 255, cv2.THRESH_BINARY)

```

```

white_pix = cv2.countNonZero(edged)
tot_pix = gray.size
black_pix = (tot_pix-white_pix)
global black_percentage,white_percentage
black_percentage = (black_pix/tot_pix)* 100
white_percentage = (100 - black_percentage)
black_percentage = float(black_percentage)
black_percentage = "{:.3f}".format(black_percentage)
white_percentage = float(white_percentage)
white_percentage = "{:.3f}".format(white_percentage)
def display_all():
    black_percent = str (black_percentage)
    white_percent = str(white_percentage)
    whitepix = str(white_pix)
    blackpix = str(black_pix)
    amountofcpers="Amount of carbonized Region in percentage:  
"+black_percent +"%"
    amountofcpix="\nAmount of carbonized Region in pixels: "+blackpix+
    "pix"
    amountofnoncpers="\nAmount of non-Carbonized Region in percentage:  
"+white_percent +"%"
    amountofnoncpix="\nAmount of non-Carbonized Region in pixels:  
"+whitepix +"pix"
    totaldisp = amountofcpers + amountofcpix + amountofnoncpers +
    amountofnoncpix
    return totaldisp

textbox = Text(root, height =30, width = 55)
panelD = Label(root)
panelD.config(font =("Times", 16))
#panelD.grid(row=2,column=1, padx=10, pady=10,sticky=EW)
display_box = display_all()
textbox.insert(END, display_box)
textbox.grid(row=3,column=1,padx=10, pady=10,sticky=S)

```

```

def plot_gray():
    image = cv2.imread(path)
    image = cv2.resize(image, (400, 400), interpolation=cv2.INTER_AREA)
    gray = cv2.cvtColor(image, cv2.COLOR_BGR2GRAY)
    histr_gray = cv2.calcHist([gray],[0],None,[256],[0,256])
    fig = Figure(figsize = (5,5))
    plot1= fig.add_subplot(111)
    plot1.plot(histr_gray)
    canvas = FigureCanvasTkAgg(fig, master=root)
    canvas.draw()
    canvas.get_tk_widget().grid(row=3,column=0)
    canvas.get_tk_widget().grid(row=3,column=0)

def plot_bw():
    image = cv2.imread(path)
    image = cv2.resize(image, (400, 400), interpolation=cv2.INTER_AREA)
    gray = cv2.cvtColor(image, cv2.COLOR_BGR2GRAY)
    (thresh,edged) = cv2.threshold(gray,40, 255, cv2.THRESH_BINARY)
    histr_bw = cv2.calcHist([edged],[0],None,[256],[0,256])
    fig = Figure(figsize = (5,5))
    plot1= fig.add_subplot(111)
    plot1.plot(histr_bw)
    canvas = FigureCanvasTkAgg(fig, master=root)
    canvas.draw()
    canvas.get_tk_widget().grid(row=3,column=2)
    canvas.get_tk_widget().grid(row=3,column=2)

root = Tk()
root.title(" Carbonization Analysis ")
root['background']="#ffffff"
for i in range(5):
    root.columnconfigure(i, weight=1, minsize=75)
    root.rowconfigure(i, weight=1, minsize=50)
panelA = None
panelB = None

```

```

panelC = None
panelD = None

btn1img = PhotoImage(file=r"C:\Users\shriman\Desktop\FINAL
PROJECT\STRAITIIONS\GUI\button_import.png")

btn1 = Button(root, image=btn1img,text="Import",
command=select_image,font="Helvetica 12",relief=FLAT,bg="#ffffff")

btn1.grid(row=0,column=0,sticky="ew",padx=10,pady=10)

btn2img = PhotoImage(file=r"C:\Users\shriman\Desktop\FINAL
PROJECT\STRAITIIONS\GUI\button_grayscale.png")

btn2 = Button(root,
text="Grayscale",image=btn2img,command=grayscale,font="Helvetica
12",relief=FLAT,bg="#ffffff")

btn2.grid(row=0,column=1,sticky="ew",padx=10,pady=10)

btn3img = PhotoImage(file=r"C:\Users\shriman\Desktop\FINAL
PROJECT\STRAITIIONS\GUI\button_black-white.png")

btn3 = Button(root, text="B/
W",image=btn3img,command=blackwhite,relief=FLAT,font="Helvetica
12",bg="#ffffff")

btn3.grid(row=0,column=2,sticky="ew",padx=10,pady=10)

btn4img = PhotoImage(file=r"C:\Users\shriman\Desktop\FINAL
PROJECT\STRAITIIONS\GUI\button_analyze.png")

btn4 = Button(root,
text="Analyse",image=btn4img,command=analyse,relief=FLAT,font="Helvetica
12",bg="#ffffff")

btn4.grid(row=0,column=3,sticky="ew",padx=10,pady=10)

btn5img = PhotoImage(file=r"C:\Users\shriman\Desktop\FINAL
PROJECT\STRAITIIONS\GUI\button_exit.png")

btn5 = Button(root,
text="Exit",image=btn5img,command=root.destroy,relief=FLAT,bg="#ffffff",font="
Helvetica 12")

btn5.grid(row=0,column=4,sticky="ew",padx=10,pady=10)

btn6img = PhotoImage(file=r"C:\Users\shriman\Desktop\FINAL
PROJECT\STRAITIIONS\GUI\button_plot-grayscale.png")

btn6 = Button(root, text="Plot
Grayscale",image=btn6img,command=plot_gray,relief=FLAT,bg="#ffffff",font="Hel
vetica 12")

btn6.grid(row=1,column=1,sticky="ew",padx=10,pady=10)

```

```

btn7img=PhotoImage(file=r"C:\Users\shriman\Desktop\FINAL
PROJECT\STRAITIIONS\GUI\button_plot-black-white.png")

btn7 = Button(root, text="Plot
BW",image=btn7img,command=plot_bw,relief=FLAT,fg="#ffffff",font="Helvetica
12")

btn7.grid(row=1,column=2,sticky="ew",padx=10,pady=10)

root.mainloop().

```

GUI for PWM level shifter and sensors code in VS CODE:

```

from tkinter import *
from PIL import Image
from PIL import ImageTk
from numpy import pad
import serial
import time
from matplotlib import pyplot as plt
from matplotlib.figure import Figure
from matplotlib.backends.backend_tkagg import
(FigureCanvasTkAgg,NavigationToolbar2Tk)
class Canvas:
    def init(self):
        self.master = Tk()
        root= self.master
        root.title("Laser - Sensor Outputs")
        root.geometry('1024x500')
        root['background'] = "#ffffff"
        for i in range(3):
            root.columnconfigure(i, weight=1, minsize=75)
            root.rowconfigure(i, weight=1, minsize=50)
        #self.ser=serial.Serial('/dev/ttyUSB0',115200,timeout=1)
        #self.ser1=serial.Serial('/dev/ttyACM0',115200,timeout=1)
        #Connect button -Btn1
        self.btn1img = PhotoImage(file=r"C:\Users\shriman\Desktop\FINAL
PROJECT\STRAITIIONS\GUI\SENSOR GUI\button_connect.png")

```

```

    self.btn1 =
Button(root,image=self.btn1img ,command=self.connect_serial,relief=FLAT,font=
"Helvetica 12",text="Enter",bg="#ffffff")
    self.btn1.grid(row=0,column=0,padx=10,pady=10)
#Display Internal data -btn2
    self.btn2img = PhotoImage(file=r"C:\Users\shriman\Desktop\FINAL
PROJECT\STRAITIIONS\GUI\SENSOR GUI\button_display-internal-pmm.png")
    self.btn2 =
Button(root,image=self.btn2img ,command=self.display_internal,relief=FLAT,font=
"Helvetica 12",text="Enter",bg="#ffffff")
    self.btn2.grid(row=0,column=1,padx=10,pady=10)
#Display External data -btn3
    self.btn3img = PhotoImage(file=r"C:\Users\shriman\Desktop\FINAL
PROJECT\STRAITIIONS\GUI\SENSOR GUI\button_display-external-pmm.png")
    self.btn3 =
Button(root,image=self.btn3img ,command=self.display_external,relief=FLAT,font=
"Helvetica 12",text="Enter",bg="#ffffff")
    self.btn3.grid(row=0,column=2,padx=10,pady=10)
#Plotting serial graph - btn4
#PWM slider levels 1 to 9
    self.pwm_label_img = PhotoImage(file=r"C:\Users\shriman\Desktop\FINAL
PROJECT\STRAITIIONS\GUI\SENSOR GUI\button_pwm-control.png")
    self.pwm_label = Label(root,text="PWM Control
slider",image=self.pwm_label_img)
    self.pwm_label.grid(row=2,column=0,padx=10,pady=10)
    self.pwm_slider = Scale(root, from_=0, to=9, orient=HORIZONTAL,
tickinterval=1,length=500,bg="#ffffff",width=25,troughcolor="#ffffff",border=1,relie
f=FLAT)
    self.pwm_slider.grid(row=2,column=1,padx=10,pady=10)
    self.pwm_btn_img = PhotoImage(file=r"C:\Users\shriman\Desktop\FINAL
PROJECT\STRAITIIONS\GUI\SENSOR GUI\button_control-laser-power.png")
    self.pwm_btn = Button(root,text="Control laser
power",image=self.pwm_btn_img,command=self.laser_pwm,font="Helvetica
12",bg="#ffffff",relief=FLAT)
    self.pwm_btn.grid(row=3,column=1,sticky="ew",padx=10,pady=10)
#Exit - btn

```

```

def connect_serial(self):
    self.ser=serial.Serial('/dev/ttyUSB0',115200,timeout=1)
    self.ser.flush()
    print("Connected to ESP32 ")
    self.ser1=serial.Serial('/dev/ttyACM0',115200,timeout=1)
    self.ser1.flush()
    print("Connected to Arduino ")

def display_internal(self):
    disp1 = self.ser.readline().decode('utf-8').rstrip()
    self.int_ppm = disp1
    display1=disp1+"ppm"
    self.panel1 =
    Label(self.master,text=display1,width=20,anchor=CENTER,justify=CENTER)
    self.panel1.config(font =("Helvetica", 12),background="#ffffff")
    self.panel1.grid(row=0,column=2,padx=5, pady=5,sticky="ew")
    self.master.after(50,self.display_internal)

def display_external(self):
    disp2 = self.ser1.readline().decode('utf-8')
    strtol = list(disp2.split(" "))
    if len(strtol) == 1:
        luxval = strtol[0]
        display2 = "Lux value:" + luxval
        self.panel3 = Label(self.master,text=display2,width=
            30,anchor=CENTER,justify=CENTER)
        self.panel3.config(font =("Helvetica",12),background="#ffffff")
        self.panel3.grid(row=2,column=2,padx=5, pady=5,sticky="ew")
    elif len(strtol) == 2:
        luxval = strtol[0]
        emval = strtol[1]
        display2 = emval+"ppm"
        self.panel2 = Label(self.master,text=display2,width=
            30,anchor=CENTER,justify=CENTER)
        self.panel2.config(font =("Helvetica",12),background="#ffffff")
        self.panel2.grid(row=1,column=2,padx=5, pady=5,sticky="ew")

```

```

    self.master.after(50,self.display_external)

def laser_pwm(self):
    self.slider_value = self.pwm_slider.get()
    print(self.slider_value)
    print(type(self.slider_value))
    if self.slider_value ==1:
        self.ser.write("1".encode())
        print("Case 1")
    elif self.slider_value ==2:
        self.ser.write("2".encode())
    elif self.slider_value ==3:
        self.ser.write("3".encode())
    elif self.slider_value ==4:
        self.ser.write("4".encode())
    elif self.slider_value ==5:
        self.ser.write("5".encode())
    elif self.slider_value ==6:
        self.ser.write("6".encode())
    elif self.slider_value ==7:
        self.ser.write("7".encode())
    elif self.slider_value ==8:
        self.ser.write("8".encode())
    elif self.slider_value ==9:
        self.ser.write("9".encode())
    elif self.slider_value ==0:
        self.ser.write("0".encode())

if __name__ =="main":
    load = Canvas()
    load.master.mainloop()

```